

HOVERING-MODE CONTROL OF THE GLIDER- TYPE UNMANNED UNDERWATER VEHICLE

**A Thesis Submitted to
the Graduate School of Engineering and Sciences of
İzmir Institute of Technology
in Partial Fulfillment of the Requirements for the Degree of**

MASTER OF SCIENCE

in Mechanical Engineering

**by
Erman Barış AYTAR**

**July 2011
İZMİR**

We approve the thesis of **Erman Barış AYTAR**

Assist. Prof. Dr. Mehmet İsmet Can DEDE
Supervisor

Assoc. Prof. Dr. Serhan ÖZDEMİR
Committee Member

Assist. Prof. Dr. Enver TATLICIOĞLU
Committee Member

06 July 2011

Prof. Dr. Metin TANOĞLU
Head of the Department of
Mechanical Engineering

Prof. Dr. Durmuş Ali DEMİR
Dean of the Graduate School of
Engineering of Sciences

ACKNOWLEDGMENTS

In the first place, I would like to thank my advisor Assist. Prof. Dr. Mehmet Ismet Can Dede for his guidance and valuable knowledge during my MSC study.

I would like to express my special thanks to Erkin Gezgin and Özgün Selvi for their valuable critics, suggestions, also for their support and eternal friendship.

I am thankful to Aylin Gazi, Ufuk Şirin and Eren Uçar for their moral support and entertainment.

Above all, I am grateful to my family for their encouragement, great patience and unconditional help. With my deepest gratitude, I dedicate this study to my family.

ABSTRACT

HOVERING-MODE CONTROL OF THE GLIDER-TYPE UNMANNED UNDERWATER VEHICLE

Research on the underwater robotics has attracted the interest of many researchers over the years. The primary reasons are the need to perform underwater intervention tasks that are dangerous for a diver and the need to perform underwater survey tasks that last for longer periods of time. Unmanned underwater vehicles can be divided into two categories. Most of the systems, today, that require a certain level of precision and dexterity are built as Remotely Operated Vehicles (ROV). On the other hand, the systems that perform repetitive tasks are configured as Autonomous Underwater Vehicles (AUV).

The objective of the thesis is to design a novel, cost-efficient, and fault-tolerant ROV that can hover and be used for shallow water investigation. In order to reduce the cost, the numbers of thrusters are minimized and internal actuators are used for steering the vehicle and stability in hovering mode. Also, the design is planned to be open for modification for further improvements that will enable the use of the vehicle for intervention tasks and studies.

In this work, previously developed unmanned underwater vehicles are reviewed. Following this, the conceptual designs are created for the underwater vehicle and internal actuator designs are developed.

Designed mechanisms are modeled in SolidWorks[®] and transferred to MATLAB[®] Simulink for hovering-mode control studies. Afterwards, to verify the simulation results, experiments are conducted with a seesaw mechanism by using LabVIEW[®] programming. Finally, results are given, discussed and future works are addressed.

ÖZET

PLANÖR-TİPİ İNSANSIZ SUALTI ARACININ ASKIDA KALMA-MODUNUN DENETLENMESİ

Denizaltı robotları uzun yıllardır arařtırmacıların ilgisini çekmektedir. Bunun başlıca sebebi denizaltı ortamında müdahale gerektiren işlerin bir dalgıç için tehlikeli olabileceđi ve uzun süreli arařtırma gerektiren işlerdir. İnsansız denizaltı araçları uzaktan kumanda edilen ve otonom olarak iki gruba bölünebilir. Uzaktan kumanda edilen araçlar belli bir seviyede becerinin ve hassasiyetin gerekli olduđu işlerde kullanılırken, otonom denizaltılar daha çok aynı işlerin tekrar edildiđi alanlarda kullanılmaktadırlar.

Bu çalışmanın amacı özgün, düşük maliyetli ve askıda kalma yetisine sahip olmasının yanı sıra oluşabilecek arızalara dayanmalı sığ sular için bir sistem tasarlamaktır. Düşük maliyetli bir sistem üretebilmek için ilk olarak itici sistem sayısı azaltıldı ve aracın yönlendirilmesi ve dengesi için içsel hareket eden kütleler kullanıldı. Bunlara ek olarak, tasarlanacak sistemin deđişikliklere açık olması ve müdahale gerektiren işler için kullanılabilir olacakdır..

Bu çalışma sırasında öncelikle daha önceden yapılmış insansız sualtı araçları incelenmiştir. Bunu takiben, insansız denizaltı aracı ve içsel eyletici için kavramsal tasarımlar sunulmuştur.

Mekanizma tasarımları SolidWorks[®] ile çizildikten sonra MATLAB[®] Simulink ortamına askıda kalma kontrol çalışmalarının yapılması için aktarılmıştır. Bundan sonrasında, simülasyon çalışmaları yapılmış ve bu simülasyon sonuçlarında LabVIEW[®] kullanarak tahterevalli mekanizması dengeleme denemeleri yapılmıştır ve simülasyon çalışmaları doğrulanmıştır. Çalışmanın son kısmında sonuçlar verilmiş ve gelecekte yapılması hedeflenen çalışmalara değinilmiştir.

TABLE OF CONTENTS

LIST OF FIGURES	ix
LIST OF TABLES.....	xiii
CHAPTER 1. INTRODUCTION	1
1.1. Underwater Vehicles.....	1
1.2. Objectives of Thesis.....	2
1.3. Outline.....	4
CHAPTER 2. LITERATURE REVIEW	5
2.1. Introduction.....	5
2.2. Classification of UUVs	5
2.2.1. Remotely Operated Vehicles	5
2.2.2. Towed Underwater Vehicles.....	7
2.2.3. Autonomous Underwater Vehicles.....	8
2.2.3.1. Underwater Gliders.....	9
2.3. Key Aspects in UUV Design	11
2.3.1. Modeling.....	11
2.3.2. Fault Tolerance	12
2.3.3. Control	12
2.3.4. Localization.....	14
2.4. Conclusion	15
CHAPTER 3. METHODOLOGY	16
3.1. Design Criteria	16
3.1.1. Previous Works.....	17
3.2. Design and Test Procedure.....	19
3.2.1. CAD Design.....	21
3.2.2. MATLAB Modeling	21
3.2.2.1. Transforming SolidWorks [®] Model to Simmechanics	23

3.2.2.2. Creating Virtual Reality Model from SolidWorks [®] Model.....	25
3.2.2.3. Integration of Virtual Reality Representation with Simmechanics Model	27
3.2.3. Experimental Set-up with Seesaw Mechanism.....	29
3.2.3.1. Seesaw Mechanism.....	29
3.2.3.2. LabVIEW [®] Programming	30
3.2.3.2.1. Integration of LabJack [®] and LabVIEW [®] system	30
3.3. Conclusion	36
 CHAPTER 4. MECHANISM DESIGN	 37
4.1. Mechanism Designs and Constraints	37
4.2. Conceptual Design for UUV	39
4.2.1. Conceptual Design - 1	39
4.2.2. Conceptual Design - 2.....	41
4.3. Conceptual Designs for Internal Moving Mass System.....	44
4.3.1. Conceptual Design - 1	44
4.3.2. Conceptual Design - 2.....	45
4.3.3. Conceptual Design - 3.....	46
4.3.4. Conceptual Design - 4.....	47
4.4. Simulation Set-up.....	49
4.4.1. Seesaw Mechanism.....	49
4.4.2. Two Degree of Freedom Mechanism.....	50
4.5. Conclusion	51
 CHAPTER 5. SIMULATION AND EXPERIMENTAL STUDIES.....	 52
5.1. Mathematical Modeling	52
5.1.1. Single DoF Seesaw System.....	52
5.1.2. Two DoF Seesaw System	55
5.2. Controller Design and Simulation Results.....	55
5.2.1. Non-linearity Cancellation.....	55
5.2.1.1. Simulation Results for Single DoF Seesaw.....	58
5.2.1.1.1. Stabilizing the System with Initial Error	59

LIST OF FIGURES

<u>Figure</u>	<u>Page</u>
Figure 1.1. Flowchart of the UUV Design.....	3
Figure 2.1. Remotely operated Vehicle	6
Figure 2.2. ROV with manipulator	6
Figure 2.3. Towed Underwater Vehicle Configuration	8
Figure 2.4. Autonomous Underwater Vehicle	9
Figure 2.5. Underwater Glider	10
Figure 2.6. Path of underwater gliders.....	11
Figure 3.1. SolidWorks [®] Motion Study.....	21
Figure 3.2. Translated Simmechanics model.....	23
Figure 3.3. Block property of translated from SolidWorks [®]	24
Figure 3.4. Revolute joint properties translated from SolidWorks [®]	25
Figure 3.5. Visual representation of a body by visualization tool	26
Figure 3.6. Visual representation of a mechanism by VR screen.....	26
Figure 3.7. VR sink block parameters window	28
Figure 3.8. VR sink block from Simulink	28
Figure 3.9. Seesaw mechanism.....	29
Figure 3.10. Potentiometers of the seesaw system	30
Figure 3.11. L293, H – bridge	32
Figure 3.12. Data flow of the experimental set-up	33
Figure 3.13. Calling LabJack via LabVIEW	34
Figure 3.14. Configuration of analog channels of LabJack	34
Figure 3.15. Converting the analog input into the meter	35
Figure 3.16. Converting the analog input into the angular position of the seesaw (in radians).....	35
Figure 3.17. Configuration of LabJack timer	36
Figure 4.1. Ray fish.....	39
Figure 4.2. SolidWorks [®] drawing of the conceptual design - 1	40
Figure 4.3. Internal moving mass system for conceptual design - 1	40
Figure 4.4. Buoyancy control of the conceptual design - 1	41
Figure 4.5. SolidWorks [®] drawing of the conceptual design - 2	42

Figure 4.6. Internal moving mass for pitch rotation for conceptual design - 2	42
Figure 4.7. Rotary mass for roll rotation for conceptual design - 2.....	43
Figure 4.8. Buoyancy control for the conceptual design - 2.....	43
Figure 4.9. Gimbal mechanism for conceptual design - 1	44
Figure 4.10. Gimbal based mechanism.....	45
Figure 4.11. x - y table based system conceptual design - 2.....	45
Figure 4.12. RR manipulator based conceptual design - 3	46
Figure 4.13. Changed center of gravity of the conceptual design - 3	47
Figure 4.14. Mobile robot based conceptual design - 4.....	48
Figure 4.15. Mobile robot based changed center of gravity of conceptual design - 4....	48
Figure 4.16. Proposed seesaw mechanism.....	50
Figure 4.17. Two degree of freedom seesaw system.....	51
Figure 5.1. Free-body diagram of the Single DoF Seesaw system.....	53
Figure 5.2. Simmechanics blocks of the seesaw system.....	58
Figure 5.3. Adding sensors and actuator to the system	58
Figure 5.4. Creating the error signal for seesaw rotation.....	59
Figure 5.5. Applied controller to the system	60
Figure 5.6. $K_p = 10$ $K_d = 0$, PD controller result	61
Figure 5.7. $K_p = 10$ $K_d = 2$, PD controller result	61
Figure 5.8. $K_p = 10$ $K_d = 8$, PD controller result	62
Figure 5.9. Cart velocity change.....	62
Figure 5.10. Cart acceleration change	63
Figure 5.11. Applied force to the cart actuator	63
Figure 5.12. LQR feedback configuration.....	64
Figure 5.13. LQR control design of the system.....	67
Figure 5.14. LQR controller test for rotation change trial-1.....	68
Figure 5.15. Applied force to the cart.....	68
Figure 5.16. LQR controller test for rotation change trial-2.....	69
Figure 5.17. Applied force to the cart.....	70
Figure 5.18. LQR controller test for rotation change trial-3 theta change with limited and unlimited force.....	70
Figure 5.19. Applied force to the cart with limited and unlimited force	71
Figure 5.20. Acceleration change of the cart with limited and unlimited force	71
Figure 5.21. Sensory data manipulation method	72

Figure 5.22. Free body diagram of the seesaw system stabilized for a given angular position set-point	73
Figure 5.23. Desired and actual orientation of the seesaw	74
Figure 5.24. Desired and actual orientation of the seesaw (focused view)	74
Figure 5.25. State input of the theta with a set point	75
Figure 5.26. Addition of disturbance to the system.....	76
Figure 5.27. Response of the system under disturbance.....	76
Figure 5.28. Schematic of state space controller using an observer	78
Figure 5.29. Mathematical model of the system.....	78
Figure 5.30. Single DoF seesaw with observer	79
Figure 5.31. Comparison of the system with and without observer	79
Figure 5.32. Kalman filter implementation to the plant	80
Figure 5.33. Comparison of the system with and without Kalman filter.....	81
Figure 5.34. Comparison of the system with and without Kalman filter under disturbance - 1	82
Figure 5.35. Comparison of the system with and without Kalman filter under disturbance - 2	83
Figure 5.36. Reaction of the controller with Kalman filter under disturbance.....	83
Figure 5.37. Position change of the cart mass under disturbance.....	84
Figure 5.38. Fixed prismatic and revolute joints	85
Figure 5.39. Rotation around Z change with a given initial condition	85
Figure 5.40. Position change of the moving mass in X direction.....	86
Figure 5.41. Applied force to the system (X)	86
Figure 5.42. Rotation around X change with a given initial condition.....	87
Figure 5.43. Position change of the moving mass in Z direction	87
Figure 5.44. Applied force to the system (Z).....	87
Figure 5.45. Theta change of the system in X and Z direction.....	88
Figure 5.46. Position change of the moving masses in X and Z direction	89
Figure 5.47. Tracking control of the 2-DoF seesaw at x-axis.....	90
Figure 5.48. Tracking control of the 2-DoF seesaw at z-axis.....	90
Figure 5.49. x-axis rotation angle change under disturbance	92
Figure 5.50. Moving mass position change at Z direction under disturbance	92
Figure 5.51. z-axis rotation angle change under disturbance	92
Figure 5.52. Moving mass position change at X direction under disturbance.....	93

Figure 5.53. Set point tracking of the system around X axis.....	94
Figure 5.54. Set point tracking of the system around Z axis	94
Figure 5.56. Creating the state vector of the system.....	96
Figure 5.56. Rotation change of the system.....	97
Figure 5.57. Cart position change of the system.....	97

LIST OF TABLES

<u>Table</u>	<u>Page</u>
Table 3.1. MATLAB [®] Simmechanics Blocks.....	22
Table 3.2. List of LabJack VIs.....	31
Table 4.1. Comparison of gliders.....	38
Table.4.2. Comparison of conceptual designs of UUV	43

CHAPTER 1

INTRODUCTION

1.1. Underwater Vehicles

“Underwater” usually used as a term to describe the natural feature of the realm below the surface of water. This realm might be ocean, sea, lake, or river. Considering that the seventy percent of the earth is covered by water, there are still lots to discover.

Although there are some underwater activities that can be achieved by humans, underwater medium is a very hazardous environment and these activities cannot be performed for a long period of time. For that reason, research efforts on underwater robotics have been increased and, underwater vehicles (UVs) are started to be used for a wide variety of tasks. General name of these vehicles are Uninhabited Underwater Vehicles or Unmanned Underwater Vehicles (UUVs).

There are mainly two types of underwater vehicles, remotely operated vehicles and autonomous underwater vehicles.

Most of the systems today that require a certain level of precision and dexterity are built as Remotely Operated Vehicles (ROVs). Whereas, the systems that perform repetitive tasks are configured as Autonomous Underwater Vehicles (AUVs).

ROVs are tethered underwater vehicles. These vehicles are usually used in deep water application such as, offshore extraction of oil, and natural gases. ROVs are highly maneuverable and operated by a person on the mother ship where communication is achieved via tether. This tether carries the electrical power and data from operator to the vehicle or vice versa. Since, the data is transferred via tether; ROVs can be controlled directly by human operator. By this way, human decision is included in the loop that enables the system to carry on precise operations in undetermined environments.

On the other hand, AUVs don't require such tether connections. Nevertheless, most survey class AUVs maintain acoustic communication with their human operator, in order to send the data and status of the vehicle. The limited bandwidth characteristic of the acoustic communication makes the live streaming of the visual information and real-time control not possible.

Both AUV and ROV systems can be modified by an addition of a robotic manipulator. These systems are called as Unmanned Vehicle Manipulator System (UVMS). It should be noted that by this addition, dexterity of the vehicle is increased while the control problems arise.

Figure 1.1 outlines the design flow of an UUV. Complying with the design criteria, after the first two decisions on inclusion of a manipulator and configuring the system as an AUV or an ROV, the design flow remains the same for all UUVs. The designer must investigate the working conditions of the system for possible additions of fault tolerance features. After the selection of sensory information, navigation and localization equipment, dynamic model of the system is developed. The dynamic model also includes the environment model with hydrodynamic effects. Later control architecture design is initiated. This design phase includes simulation studies and the verification of the developed controller and finally, examination of the system through experimental studies.

1.2. Objectives of Thesis

Various underwater vehicles are built up to this date. Most of these vehicles use thrusters for motion and steering. Usage of thrusters increases costs and because they are exposed to the sea water, they have corrosion problems.

The aim of the thesis is to design a new type of underwater vehicle which requires minimum number of thrusters. Steering of the vehicle and the stability under environmental effects are going to be provided by internal moving masses. Volume of the vehicle is going to be changed to control the depth. Internal moving masses are used to relocate the center of gravity of the vehicle, thus, the orientation of the vehicle will be changed. Change in the volume causes the change in the buoyancy and it leads to motion in heave direction.

The research in this thesis is focused on the design for internal moving masses mechanism. Conceptual designs are proposed and appropriate one is used for simulation tests to prove validity of the control for hovering stability under the influence of underwater hydrodynamic disturbance and steering.

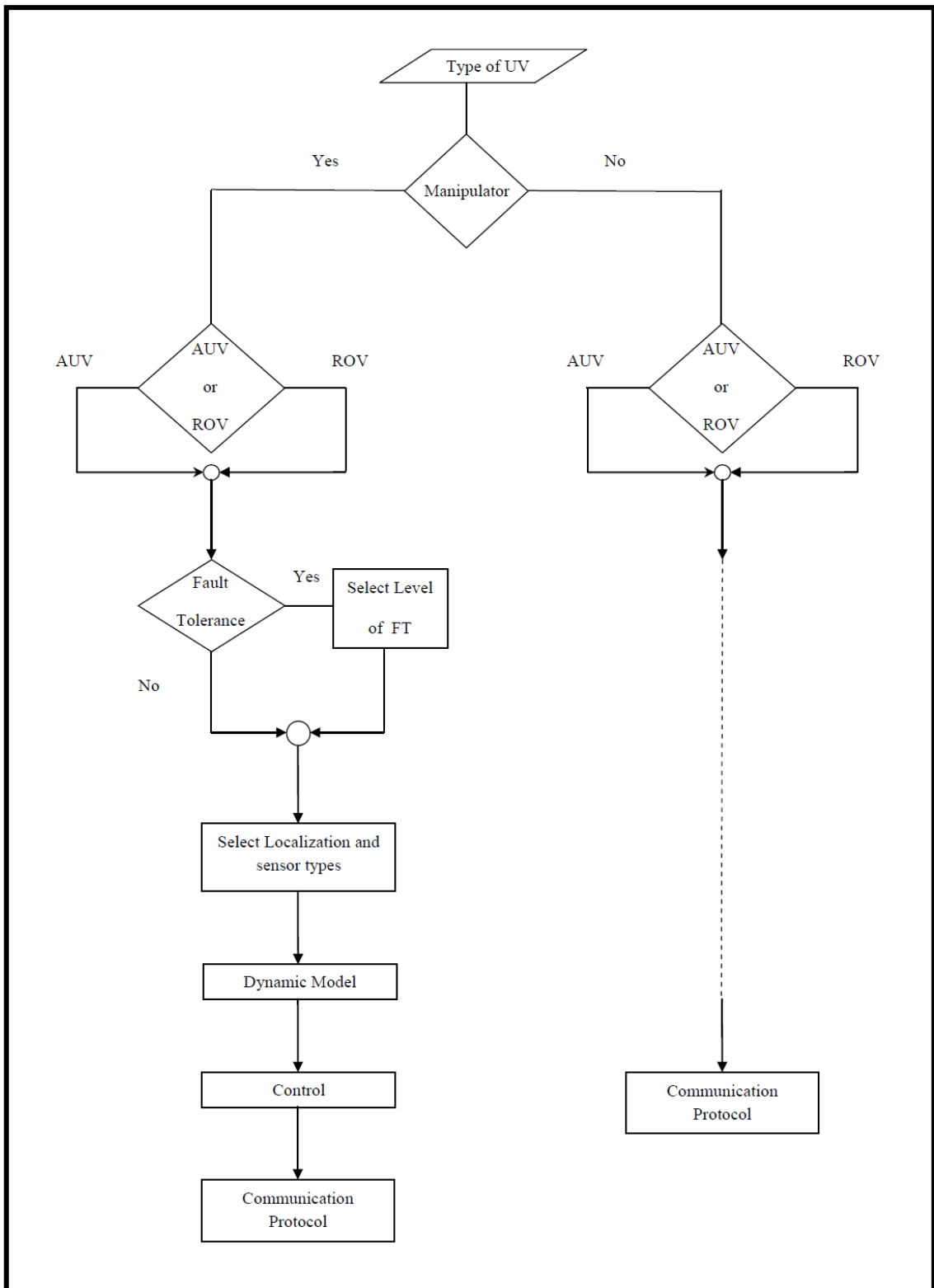


Figure 1.1. Flowchart of the UUV Design
 (Source: Aytar and Dede, 2009).

1.3. Outline

The following chapter provides three different sections of underwater vehicle classifications that are grouped with respect to their autonomy, and modification. In Chapter 3, methodology used in the thesis is explained. Software tools to model the system and to develop controls are described in this chapter. Conceptual designs of UUV and the mechanisms that are used for controlling the UUV are given in Chapter 4. Chapter 5 describes the development of control architecture and provides the simulation and experimental results. Finally, the conclusions for the study are made and discussed, and possible future studies on this work are addressed.

CHAPTER 2

LITERATURE REVIEW

2.1. Introduction

There are various types of UUVs for variety of tasks in current use. Some areas of underwater vehicle usage can be listed as the extraction of oil and gases, maintenance tasks, sea floor mapping, and measuring the concentration of elements in the water.

In this chapter, the aim is to categorize UUVs with respect to the technology used and give brief reviews of past studies on UUV technology. This section is divided into two subcategories as the classifications of UUVs and the key aspects in UUV design. At the end of this chapter, a brief conclusion is given.

2.2. Classification of UUVs

In this subsection, general definitions, areas of usage, and general properties of underwater vehicles is mentioned.

2.2.1. Remotely Operated Vehicles

The term Remotely Operated Vehicles (ROVs) resembles a physically linked (via tether as seen in Figure 2.1) underwater vehicle, to an operator who is on the submarine or the mother ship. The ROV's tether provides sensory data to the operator and sends back operator's commands to the vehicle and close the teleoperation control loop in this manner.

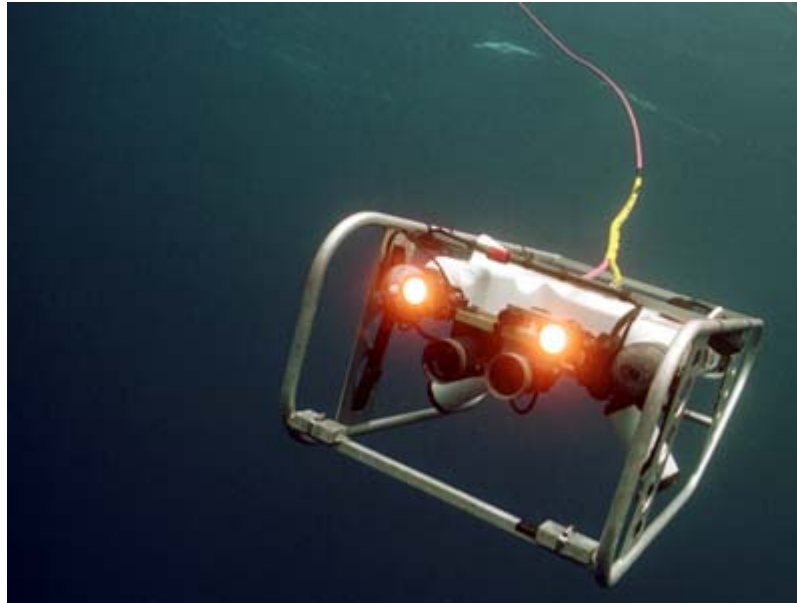


Figure 2.1. Remotely operated Vehicle
(Source: uncw, 2010)

ROVs are preferred where human dexterities and decisions are required to be included in the control loop. Since these vehicles can achieve a higher level of telepresence, it is more suitable to attach manipulators for increasing dexterity (Figure 2.2); therefore, ROVs can be used for grabbing, moving, and placing items in the sea (intervention task). ROVs are equipped with various sensors for collecting data about the ocean and sea floor. ROVs can be used in areas such as;



Figure 2.2. ROV with manipulator
(Source: Seaeye, 2010)

- Diver Observation – ensure diver safety and provide assistance
- Platform Inspection – to monitor the effects of corrosion, fouling, locating cracks, estimating biologic fouling, etc.
- Pipeline Inspection – follow underwater pipelines to check for leaks, determine overall health of the pipeline and insure the installation is acceptable
- Surveys – both visual and acoustic surveys are necessary prior to installing pipelines, cables and most offshore installations
- Drilling Support – everything from visual inspection, monitoring installation, operational support and repair when necessary using multiple manipulators
- Construction Support – a natural follow-on to drilling support. Tasks can become more complex by the use of manipulators, powered tools and cutters
- Debris Removal – offshore platforms can become a "trash dump" underwater. ROVs provide a cost effective method of keeping the area clean and safe
- Platform Cleaning – a very sophisticated task using manipulators and suction cups for positioning and systems driving brushes, water jets and other abrasive devices
- Subsea Installations - support the construction, operation, inspection, maintenance and repair of subsea installations, especially in deep water
- Telecommunications Support (Inspection, Burial or Repair) – from towed plows that bury cables for protection from trawlers and anchors to sophisticated vehicles that can locate, follow, retrieve and rebury subsea telecommunication cables
- Object Location and Recovery - Search, location, and recovery of lost objects

2.2.2. Towed Underwater Vehicles

Towed underwater vehicles have no thrusters, but actuators that are located at the fins for directing the vehicle. These vehicles are platforms that can be used to place sensors. An example of towed underwater vehicle can be seen in Figure 2.3. Depressor weight is used for reducing the disturbing effects of the cable at the vehicle.

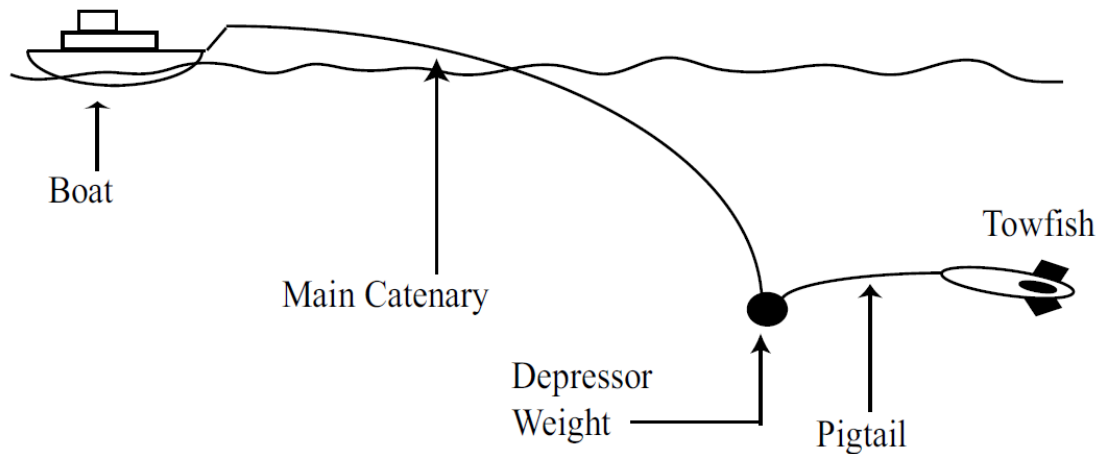


Figure 2.3. Towed Underwater Vehicle Configuration
(Source: Linklater, 2005)

2.2.3. Autonomous Underwater Vehicles

Autonomous underwater vehicles (AUVs) usually have only one thruster that is located at the backside of the vehicle. Steering of the vehicle is provided by the fins. A number of sensory systems are located on the vehicle. These sensors are inertial measurement units that contain linear acceleration and angular velocity sensors, pressure-meter to observe vehicle depth, sonar systems; front sonar to measure distance from obstacles, ground speed sonar to measure the speed of the vehicle relative to ground. Global Positioning System (GPS) is used to learn the exact location of the vehicle at the sea surface. The positioning through GPS can only be achieved when the vehicle surfaced. AUVs may also consist of acoustic systems that are used to learn the exact location of the vehicle in pre-defined areas. Also, the acoustic communication can be used for data transfer between the base station and the vehicle. AUVs are supposed to be completely autonomous, consequently relying on onboard power systems and intelligence. General view of the AUV can be seen in Figure 2.4.

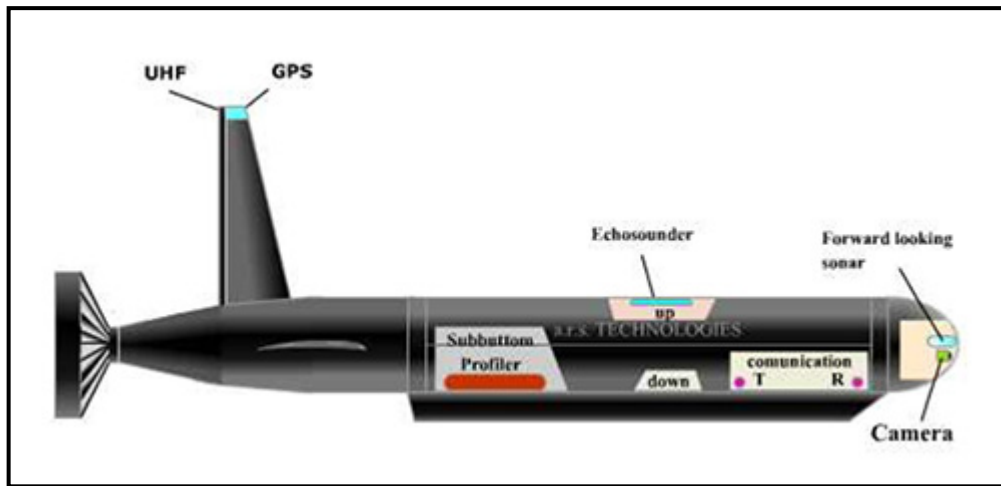


Figure 2.4. Autonomous Underwater Vehicle
(Source: Arstech 2011)

Autonomous underwater vehicles (AUVs) are like submarines, but they are small, and unmanned. First usage of AUVs was military-based mine detection and ocean mapping. In time, AUVs start to become commercially available and their usage increased significantly. AUVs have been employed for many areas such as

- Subsea Survey / Subsea Inspection
- Pipeline Inspection
- Cable Inspection
- Oceanographic Sampling
- Environmental Monitoring
- Iceberg Profiling / Under-ice Surveys
- Mine Detection and Countermeasures
- Diver Delivery / Supply Vehicles
- Downed Airplane / Shipwreck Searches
- Underwater Photography

2.2.3.1. Underwater Gliders

Underwater gliders are the type of autonomous underwater vehicles which have no thrusters and the propulsion is provided by the change of the buoyancy of the vehicle. Until now, all types of underwater vehicles have positive buoyancy. Due to the

safety reasons, if there is no force applied to the vehicle, it surfaces itself without the need of any propulsion. However, underwater gliders make use of their variable buoyancy capability during propulsion. An example of glider can be seen in Figure 2.5.

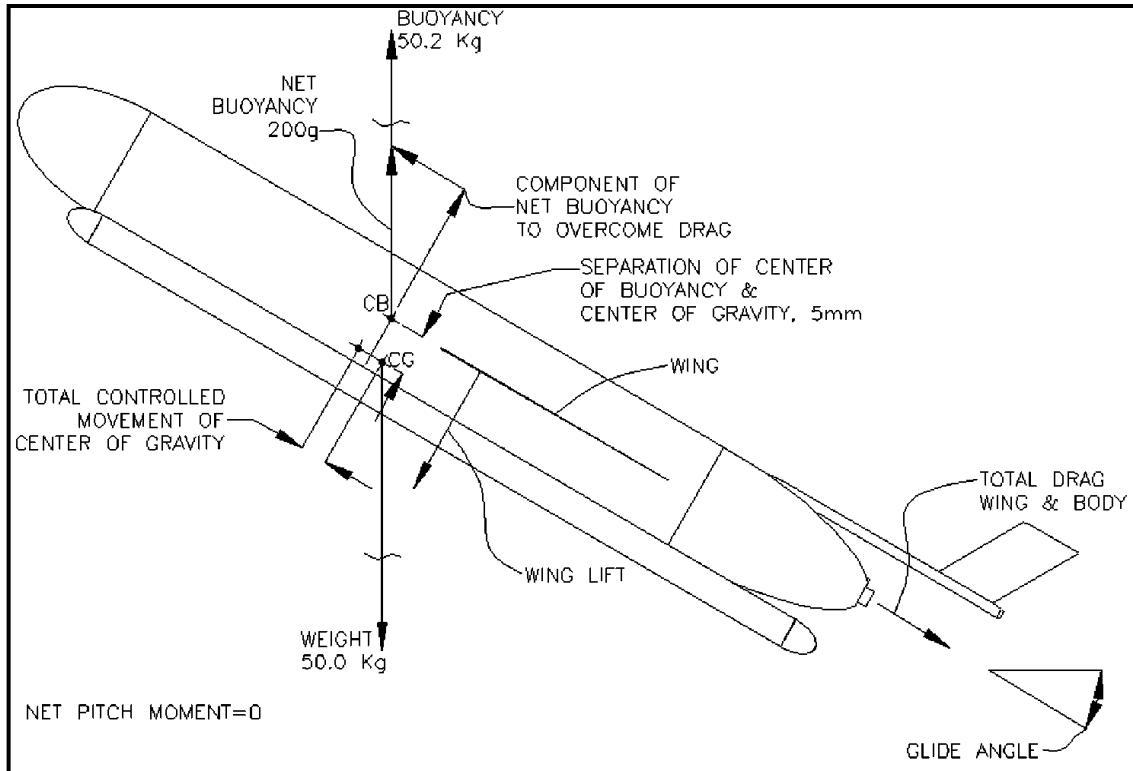


Figure 2.5. Underwater Glider
(Source: Webb, Simonetti, & Jones, 2001)

As mentioned before, working principle of the gliders is based on the change in the buoyancy. Change in the buoyancy can be achieved through changing the mass of the vehicle, or changing the volume of the vehicle. This change makes the vehicle positive buoyant or negative buoyant, which makes the vehicle dive or surface. But for propulsion, location of the center of gravity is also needed to be changed. Thus, gliders have a moving mass. Path of a glider can be seen in Figure 2.6. It resembles a saw tooth trajectory.

Gliders have a long range of operation, as they have no thrusters. They are mostly used in ocean sampling. They have various sensors for data collection. Also, they carry a GPS to send the exact position of the vehicle when they are at the sea surface.

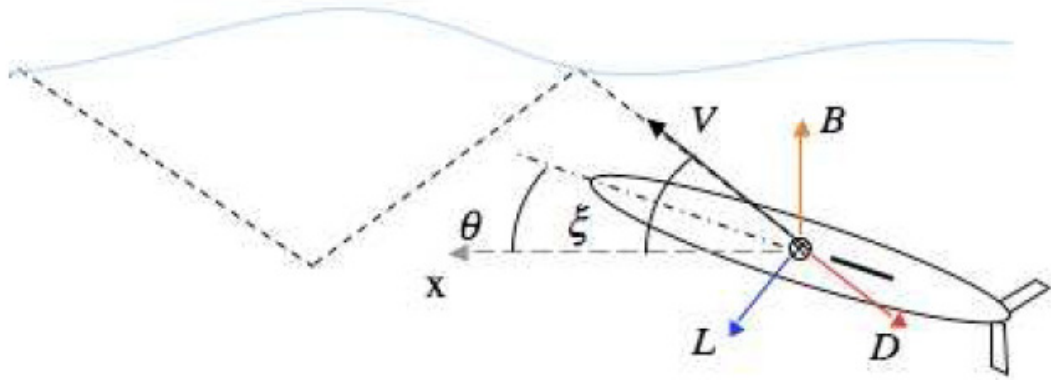


Figure 2.6. Path of underwater gliders
(Source: Bender et al. 2008)

2.3. Key Aspects in UUV Design

This section consists of earlier studies on underwater vehicle modeling, fault tolerance, control and localization.

2.3.1. Modeling

Modeling is the first phase of an UUV design regardless of selecting the UUV as an AUV or an ROV. Design criteria direct the designer whether to include a robotic manipulator to the system or not. At this point, modeling studies are initiated.

Problem of experimental identification of finite-dimensional nonlinear dynamical models for open-frame ROVs was addressed by Smallwood & Whitcomb, 2003. The results show that the development of model-based control techniques for the dynamic positioning of underwater robotic vehicles has been limited by the lack of experimentally validated plant models. In order to show that identification of small underwater vehicles can be achieved at low costs, two methods are proposed such as Least Squares (LS) and Extended Kalman Filter (EKF) (Alessandri et al., 2002).

Kane's method was utilized by Tarn et al. (1996), to develop an n-axis robot arm. External forces can directly be incorporated to the model. The provided method includes four dynamic forces. These are mass, profile drag, fluid acceleration, and buoyancy that are added to the environment model in their work. Hydrodynamic effects on a single-link arm are investigated by McLain and Rock (1998) and it was seen that

hydrodynamic forces can be large and have an important effect on the dynamic of underwater vehicle.

2.3.2. Fault Tolerance

Generally, UUVs are required to work long periods of time in unstructured environments. In such conditions, the smallest undetected failure usually results in loss of the vehicle. Even if vehicle has a fault detection system, it is clear that, in order to accomplish the mission, fault tolerant strategy must be implemented.

Fault detection is the process of monitoring the vehicle in order to identify if all systems are functional or not. Fault isolation or diagnosis is used to determine which specific sub-system has failed. On the other hand, fault tolerance is the capability to complete the mission even if failures on one or more sub-systems occur.

Fault-tolerant design of a system for the 6 degrees-of freedom ODIN AUV is described by Yang et al. (1998). Experiments focused on detection, isolation, and accommodation of thruster and sensory failures. Podder and Sarkar (2001), studied the allocation of thruster forces of an autonomous underwater vehicle under thruster faults. The allocation technique is based on the generalized inverse theory and provides the minimum norm solution to the thruster forces for a particular motion trajectory. The proposed control law allows the AUV to track the desired task space trajectory with asymptotic reduction of error in case of thruster faults. A new software and hardware architecture for AUV is presented by Barnett et al. (2002). This controller has the ability to detect failures and choose the best possibilities to keep the system working.

2.3.3. Control

Control of the underwater robots is quite challenging. It is similar to kinetic problems that arise in the control a free floating rigid body in a six dimensional space. Underwater environmental effects (hydrodynamic effects) make this control even harder. Various authors proposed several control architectures to address this problem.

Kinematics of an AUV is described by using Lyapunov-like function by Nakamura and Savant (1992). Kinematics includes six state variable and four inputs. By using this kinematic function, a nonlinear tracking control scheme is developed and

it is tested in simulation. It is declared that, this globally usable nonlinear tracking system is well fit for the non-holonomic motions. Also, it is noted that dynamics effects are needed to be considered for better results.

Yuh (1990), claimed that due to poorly unknown environment, using adaptive control was found suitable. In order to test robustness of the control system, a computer simulation was performed for a planar motion of a ROV. Simulation results showed that developed control system learns the change in the environment and adapt the output of the vehicle according to the changes. Under unknown environmental parameters, the presented adaptive control system performed well while compared to the non-adaptive control system.

Goheen and Jefferys (1990), presented a self-tuning autopilot system for ROVs. It is said that self-tuning is required due to un-deterministic characteristic of the environment and ROV. In this article, two different types of self-tuning ROV autopilot models are described. First one is based on adaptive LQG (linear-quadratic-Gaussian) formulation. The second controller combines a robust MIMO decoupling control law with an on-line recursive identification method. The results showed that this system can be used successfully for underwater autopilot systems.

Control of a six-degree of freedom underwater vehicle is presented by Antonelli et al. (2001). The authors proposed an adaptive control that can cope with poorly known time-varying underwater environment. The proposed control law adopts quaternion representation for altitude errors, and thus avoids representation singularities that occur when using Euler angles description for the orientation.

Yuh et al. (1999), proposed adaptive control system for underwater vehicles. Reason for choosing adaptive control is that the underwater robot dynamics are highly nonlinear, coupled, and subject to hydrodynamic uncertainties and external disturbances such as currents. This adaptive control system differs from usual adaptive controllers. Usually, adaptive controller's gain change by the knowledge of the dynamic model. Instead, this model changes the gain parameters according to performance of the system. It is claimed, for that reason, proposed control system is structurally simple and computationally efficient. System analyzed by the Lyapunov method proves that the tracking error can asymptotically converge to zero. Finally, the authors made field experiments which showed that controller can achieve high-performance trajectory tracking in the presence of model uncertainties, measurement noises, and external disturbance.

Another hybrid controller system was presented by Lee (2003). In proposed controller system, neuro-fuzzy controller is first trained to model the inverse dynamics of the AUV and act as a feedforward controller, and compute the trajectory of the AUV. After that, PD feedback controller computes the error compensating torque to minimize system error along the desired trajectory. Computer simulations of the proposed recurrent neuro-fuzzy control scheme and its performance comparison with some existing controllers have been conducted to validate the effectiveness of the proposed approach.

2.3.4. Localization

Most conventional systems have used a GPS system to localization purposes where they have to surface after some period of navigation. Some recent research activities have focused on developing new sensory systems and strategies to avoid this type of a procedure. The following are some examples to these efforts.

An enhanced inertial navigation system which used in Morpheus AUV is proposed by Grenon et al. (2001). The inertial measurement unit consisted of 3-axis ring laser gyros and 3-axis accelerometers and is aided with ground speed measurement by using RDI Doppler velocity sonar. In order to fuse the sensory data, extended kalman filter is used. A complementary filter was implemented to provide much smoother and stable attitude estimation. The results show that the filtering performance can be considered acceptable when the error autocorrelation function falls within a tolerable limit.

Design of a multi-rate navigation system for AUVs is presented by Oliveira and Pascoal (1998). The proposed design technique makes use of Kalman filtering theory and leads naturally to multi-rate complementary filtering structures.

De Angelis and Whitney (2000), mentioned the localization problem of the underwater vehicles. The authors claimed that currently, underwater vehicles use the inertial measurement units and Doppler velocity sonar that is fused by Kalman filtering. Nevertheless, using Kalman filter in long range operation may cause divergence from the likelihood and AUV must surface to set its position via GPS. Doing this procedure several times in a mission reduces the efficiency of the vehicle dramatically. The authors combined a database which contains sonargrammetric, terrain matching, and

image registration information with the standard navigation. The accuracy of positional estimates could be maintained over a longer duration. As a result of this adaptive calibration, it is discussed that it is no longer necessary to surface to get absolute position from GPS.

In another study, the authors provided a navigation method of an AUV for photo mosaicing of shallow vent areas where bubbles are spouting (Maki et al., 2006). Authors used the Simultaneous Localization and Mapping (SLAM) approach which enables drift free, accurate, real-time and independent navigation. This procedure is highly suitable for photo mosaicing. Authors performed a test of this system on the AUV “Tri-Dog 1” and results proved the validity of the system.

Zhou et al. (2010), proposed a scheme called Scalable Localization scheme with Mobility Prediction (SLMP) by utilizing the predictable mobility patterns of underwater objects for underwater sensor networks. In SLMP, localization is performed in a hierarchical way, and the whole localization process is divided into two parts: anchor node localization and ordinary node localization. During the localization process, every node predicts its future mobility pattern according to its past known location information, and it can estimate its future location based on its predicted mobility pattern.

2.4. Conclusion

There are a wide variety of underwater vehicle in the literature, which is mainly divided in two categories; AUVs and ROVs. AUVs are mostly preferred where repetitive tasks are performed and ROVs are used where intervention tasks that are performed in un-deterministic environments calling for increased dexterity.

One of the significant problems of the UVs is the control issue. Generally, UVs are required to be stable under the influence of uncertain conditions at a certain depth. Researchers used several methods to cope with this control issue. Some of these methods include adaptive, neural network, and fuzzy logic algorithms.

The aim of this thesis is to build a new control for UUVs which can preserve their position and depth under disturbances. Thus, proposed controllers investigated in this chapter are examined.

CHAPTER 3

METHODOLOGY

In this chapter, design criteria are determined. Conceptual designs are modeled in SolidWorks[®] complying with the design criteria. Conceptual designs are investigated in two parts; general design of the UUV and the mechanism designs for steering and stability of the vehicle. Afterwards, conceptual designs are transferred into MATLAB[®] environment for their simulation and control studies.

After simulation studies finalized, test set-up for experimental works is explained. In this part, software used for experimental studies, LabVIEW[®], general specification of the selected data acquisition system and motor driver are described.

This chapter composes of three subsections; (1) Design criteria, (2) Design and Test procedure, (3) Conclusion.

3.1. Design Criteria

During literature survey, varieties of UUVs were investigated. Underwater vehicles can be categorized in two main groups; AUVs and ROVs. Gliders, a member of AUVs, have the advantage of using no thruster system, which increases the duration of operation and decreases the cost. However, they have no ability to hover at a specific depth. On the other hand, ROVs has a relatively good maneuverability, because they have usually four or more thrusters. The cost of having several thrusters is excessive amount of power consumption and control problems.

The aim of this study to develop a novel cost efficient and fault tolerant UUV that can hover under the presence of disturbance. In order to reduce the cost of the vehicle, numbers of thrusters are minimized and internal moving masses are used for stability and steering the vehicle. Change in the volume causes the change in the buoyancy and it leads to motion in heave direction.

Design criteria decided as follows; the proposed underwater vehicle's propulsion will be provided by a thruster. The reason for that is, in gliders, propulsion is achieved by the change in buoyancy and the system it is required to always dive and surface to

propagate which results in a slower navigation. The reasons to limit the number of thrusters are their cost, energy consumptions, and their exposure to corrosion. Since, the numbers of the thrusters are limited, for steering the vehicle, internal moving masses will be used similar to the gliders. Advantage of using internal moving masses is the fact that they are not exposed to sea water (they are placed in the dry box in the system) therefore, the moving mass system will not experience corrosion or biological fouling and it consumes less energy. In addition to these, internal moving masses will be utilized in hovering-modes stability. For hovering-mode stability, internal moving masses are going to act as balancers. With respect to disturbance, internal moving masses are going to change its location and stabilize system in an un-deterministic environment.

Another feature of the vehicle is to have heave motion capability. Heave motion can be provided by changing the buoyant force that acts on the vehicle. This can be in two ways, as mentioned earlier, either by changing the total mass of the vehicle, or by changing the volume of the vehicle. This feature will give ability to vehicle dive and surface without using thrusters.

The last design criterion is to have fault tolerance in the system. Normally, underwater vehicles has positive buoyancy and incase of a lost communication or control, they are naturally surface. On the other hand, the proposed vehicle has variable buoyancy and it might not surface in case of failure. Therefore, a fault tolerant system is required. In all active sub-systems of the vehicle redundancy for the fault tolerance such as, thrusters, moving mass actuators, etc.

3.1.1. Previous Works

After design criteria is developed, similar studies/research are investigated. Survey is initiated by investigating underwater gliders. The first idea of underwater gliders was presented by Henry Stommel, named SLOCUM. The aim of this vehicle was moving by using natural energy. This is achieved by changing the applied buoyant force of the vehicle, thus, the vehicle dives or surfaces (Stommel, 1989). In order to change the buoyancy of the vehicle an energy source was needed and this energy source was chosen as thermal energy. In addition, the roll rotation of the underwater glider was provided by the help of a rudder (Webb et al., 2001). A more improved model of

SLOCUM underwater glider is Spray. The improvement was the operation range was extended and the rudder of SLOCUM was replaced with an eccentric mass (Sherman et al., 2001). Another example of underwater gliders is Seaglider. Similar to other underwater gliders, the working principle of Seaglider is based on diving and surfacing. During the process, this vehicle was able to measure sea properties, such as, temperature, salt ratio, depth, and flow rate. Also, Seaglider uses the eccentric mass for roll rotation (Eriksen et al., 2001).

In another research, it is mentioned that internal moving masses help the system to stabilize and control. In this work, internal moving masses are used for AUVs and it is claimed that the usage of internal moving masses are more effective at lower speeds when fins are useless. Besides, internal actuators are protected from the corrosion of the sea water since they are not in the water. It is also mentioned, instead of using internal moving masses, it is possible to use internal rotors create rotation during the motion (Woolsey and Leonard, 2002a, 2002b). ROGUE was yet another glider that was produced for laboratory experiments. This vehicle has two masses, one of them is fixed but variable, other one's mass is fixed but it can move. Variable mass is used to change the buoyancy of the vehicle and make it dive or surface. Second mass, movable, is used to change the dive angle of the vehicle. In addition to this, a model based feedback control algorithm is applied to the vehicle and while the vehicle is in a stable position, disturbances are rejected by changing the location of the masses and the vehicle kept in balance (Leonard and Graver, 2001). Another work on ROGUE glider is about the using a syringe system to change the buoyant force on the glider and make it dive or surface, or kept its position (Bhatta and Leonard, 2002).

There are different studies to keep in the UUV in hovering mode at a certain depth. The ROV from University of Florida uses 4 thrusters. Two of them are located vertically; two of them are located horizontally. In this work, two air tanks are located at the bottom of the vehicle for buoyancy. One of these tanks takes water inside to keep changing the buoyancy and the other tank provides air when it is wanted to surface (Novick et al., 1998; Laine et al., 1999). Another example of underwater vehicle stability and variable mass is studied by Detweiler et al. (2009). In this study, an AUV changes its weight and dynamics during a mission which is a pick and place. With respect to weight of the picked object, vehicle changes the applied buoyant force on it. By this way, it is prevented to consume excessive amount of energy. Variable buoyancy idea was also used in shallow water AUV as proposed by Tangirala and Dzielski

(2007). In this vehicle, two tubes were located inside, and these tubes were used to change the buoyancy of the vehicle and by this way, propulsion was provided without using thrusters.

Another example of hybrid gliders was presented by Alvarez et al. (2009). This underwater vehicle was named Fòlaga. In this work, the vehicle was able to move in heave direction by changing its mass. For the propulsion system, thrusters were located back side of the vehicle. The dive system was a combination of buoyant force and center of gravity change mechanisms. Internal moving mass were also used in the navigation of the vehicle. At low speeds fins are useless and the vehicle cannot make the rotation that it supposed to do. Therefore, internal moving masses were added to the vehicle and they were used at low speeds (Li, Song, and Shao, 2008).

3.2. Design and Test Procedure

According to the virtual rapid prototyping for robot controllers methodology (Dede, 2010), first step of a robot design starts with development of Computer-Aided Design (CAD) robot model. Next step is to simulation phase where kinematics and dynamics model of the vehicle and environment is used. In the simulation phase, controller for the robot is created, tested, and verified. Since all of these works are based on virtual environment, this method allows the designer to interfere anytime to modify the model according to test results and design iterations.

Currently almost any CAD software allows designers to test their design even before manufacturing them. Even though, CAD software has many capabilities such as structural and mechanism analyses, still, it is not used to design controller for a robotic system. In this thesis, integrated use of three software packages; such as, SolidWorks[®], MATLAB[®], and LabVIEW[®], will be employed for mechanism and controller design, simulation tests and experimental studies.

SolidWorks[®] is a powerful CAD tool. It can be used to design system parts and assemblies. It also has ability to animate the system motion and perform mechanism analyses by using its animation tool called SolidWorks[®] Motion.

Also, SolidWorks[®] is able to transfer to robot's data into MATLAB[®] Simulink. The visual representation of the robot is transferred to MATLAB[®] Virtual Reality

environment as VRML files. This enables the designer to view the robot in action while the simulation is running.

In order to create simulations, MATLAB[®] Simulink environment and Simmechanics blocks are used. By this way, forward kinematics and dynamics of the model of the robots can be created. In this environment, it is also possible to develop a control algorithm for the robot and perform simulation tests. MathWorks[®] released a add-on that can translate the SolidWorks[®] model into MATLAB[®] Simulink environment by making use of Simmechanis blocks to configure forward kinematics and dynamics model of the robot. Once the Simmechanics blocks are transferred, Virtual Reality (VR) model can be integrated, again, by transferring the information from SolidWorks[®].

Following the verification of the controllers in MATLAB[®] Simulink simulations, next step is the validation of the results in experimental studies. A seesaw mechanism and LabVIEW[®] software are used for experimental studies. Final part of this section is dedicated to describe experimental set-up of seesaw mechanism. LabVIEW[®] is a graphical programming environment which is commonly used for experimental studies. LabVIEW[®] has two parts as front panel and block diagram. Front panel is the graphical user interface (GUI) of the developed program. In the front panel, control and indicators allows operator to input or extract data from a running instrument. Block diagrams are used to develop controllers and GUI.

A data acquisition (DAQ) system is required for data transfer between the PC and the experimental set-up. This system acquires the sensory information and translates them into digital information that can manipulated by a computer. Also, DAQ systems send out command signals, which are regulated in a computer software such as LabVIEW[®], to the actuators of the experimental set-up. Even though, there are a variety of different DAQ systems, usually, a DAQ system includes analog to digital converters (ADC), digital to analog converters (DAC), encoder decoders, counters, timers, digital inputs and outputs.

In this work, the DAQ system was chosen as LabJack[®]. The reason to choose this DAQ is that it provides enough input and output channels and it can easily connect to a PC via USB.

3.2.1. CAD Design

SolidWorks[®] is one of the many commercially available CAD programs. Advantage of using this software is that it has an animation tool and it is possible to transform the designs into MATLAB[®].

The assembly process becomes very important if the mechanism is going to be animated. The mating process should be done carefully. The fixed or welded parts should not have any relative motion with respect to each other. On the other hand, if these parts have any relative motion with respect to each other, the joints connected these parts will be created as translational, revolute, etc. complying with the mates between these two parts.

SolidWorks[®] includes Motion Study add-on for animation of the mechanism. User can specify the motion of the mechanism and run certain analyses to extract reaction force/moment, speed, and acceleration profiles. In the Figure 3.1, a representation of the general view of this tool is shown.

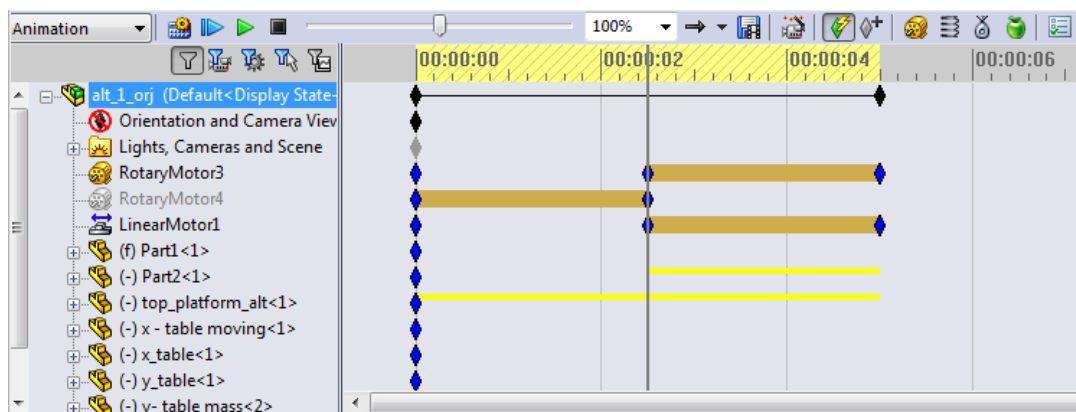


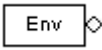
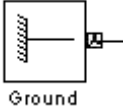

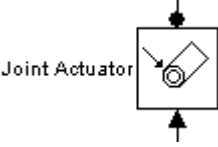
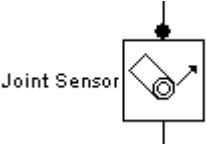
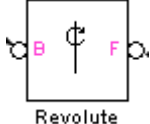
Figure 3.1. SolidWorks[®] Motion Study

3.2.2. MATLAB Modeling

MATLAB[®] models of physical systems can be created in two different ways. One of them is using M-files. M-files is a matrix-based programming language. In this method, programmers can create the model by writing the code line by line. Second method is to use Simulink environment. This tool is a graphic programming environment, there are pre-defined subroutines configured as blocks. By using these

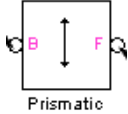
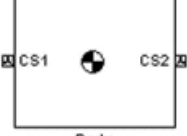
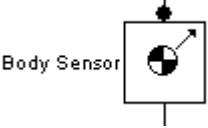
blocks, it is possible to model physical environments and simulate them. As Simulink environment became a major simulation environment for most of the researchers, the platform also evolved in time providing a variety of blocks for modeling purposes. One of these tools is Simmechanics. This blockset offers link, joint, actuator, and sensor blocks to develop the simulation model of any mechanical system that uses these components. Some of these blocks are introduced in Table 3.1.

Table 3.1. MATLAB[®] Simmechanics Blocks

	<p>The Machine Environment block allows user to view and change the mechanical environment settings for one machine in the model.</p>
	<p>A Ground block represents an immobile ground point at rest in the absolute inertial World reference frame. Connecting it to a Joint prevents one side of that Joint from moving.</p>
	<p>The Joint Initial Condition Actuator block supplies the prismatic and revolute joint primitives of a Joint block with initial value data. The initial values are the positions and velocities of the joint primitives and fully specify the initial state of motion of those primitives.</p>
	<p>The Joint Actuator block actuates a Joint block connected between two Bodies with a generalized force or a motion.</p>
	<p>The Joint Sensor block measures the position, velocity, and/or acceleration of a joint primitive in a Joint block. It also measures the reaction force and torque across the Joint.</p>
	<p>The Revolute block represents a single rotational degrees of freedom (DoF) about a specified axis between two bodies. The rotational sense is defined by the right-hand rule. A revolute joint is one of SimMechanics primitive joints, along with prismatic and spherical.</p>

(Cont. on next page)

Table 3.1 (cont.)

 <p style="text-align: center;">Prismatic</p>	<p>The Prismatic block represents single translational degrees of freedom (DoF) along a specified axis between two bodies.</p>
 <p style="text-align: center;">Body</p>	<p>The Body block represents a rigid body with properties that user can customize. These properties are; the mass and moment of inertia, center of gravity, and body coordinate systems.</p>
 <p style="text-align: center;">Body Sensor</p>	<p>The Body Sensor block senses the motion of a body represented by a Body block. Programmer can connect the Body Sensor to a Body coordinate system (CS) on the Body whose motion wants to sense. The sensor specifically measures the motion of the origin of this Body CS.</p>

3.2.2.1. Transforming SolidWorks[®] Model to Simmechanics

As mentioned above, physical model of a system can be created by using the Simmechanics blocks. The programmer has to specify the weight, inertia, orientation, center of gravity, rotation/translation axes and link lengths if he/she creates the model from scratch. This is a time consuming process.

MathWorks released a software to translate the SolidWorks[®] model to MATLAB[®]. A forward kinematics and dynamics model of the system created in MATLAB[®] Simulink as a result of this translation. The model is built by using Simmechanics blocks and all the necessary information (mass, inertia, orientation, etc.) is automatically transferred to these blocks. An example of a translated model is shown in Figure 3.2.

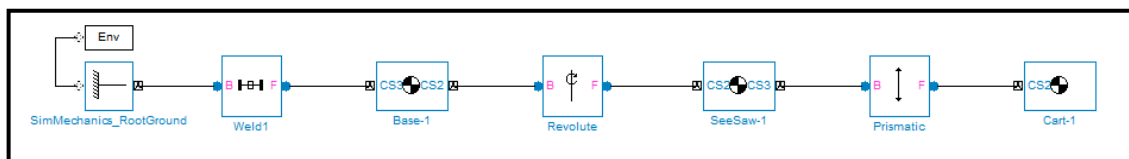


Figure 3.2. Translated Simmechanics model

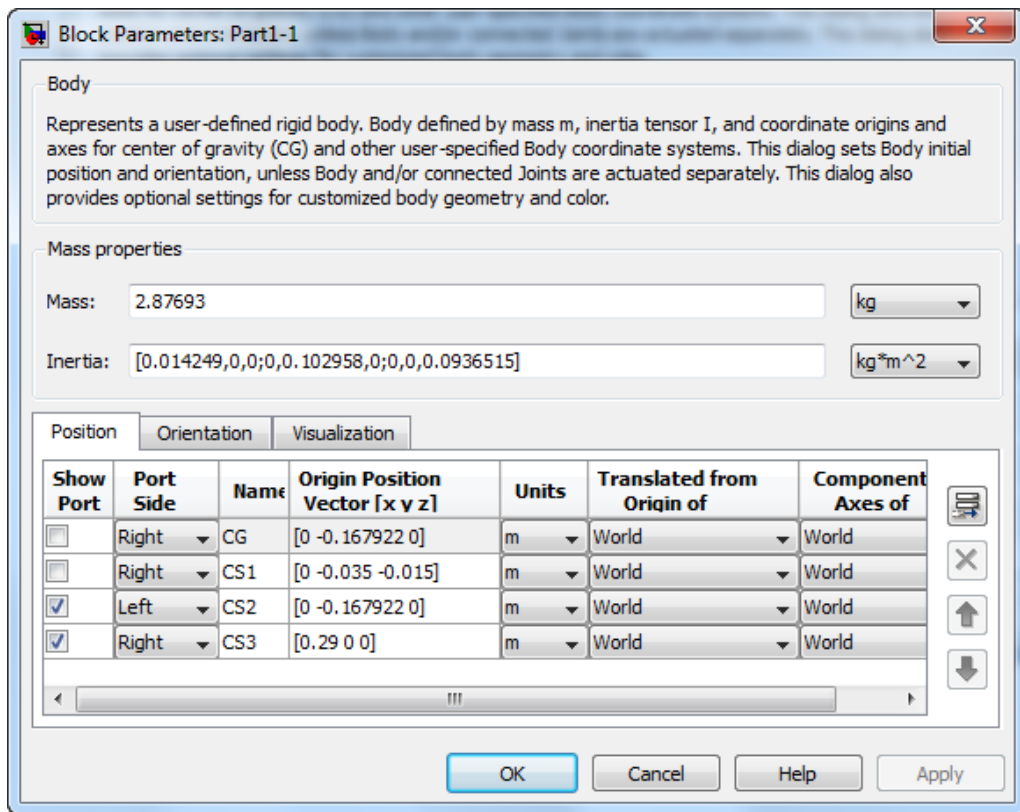


Figure 3.3. Block property of translated from SolidWorks[®]

Figure 3.3 shows the parameters of a block called as body block. All information is transformed from SolidWorks[®], such as, mass, inertia, center of gravity and length. Figure 3.4 shows the block parameters of a revolute joint, where the rotation axis defined. As it can be seen from image, it is possible to add actuator and sensor to the joint.

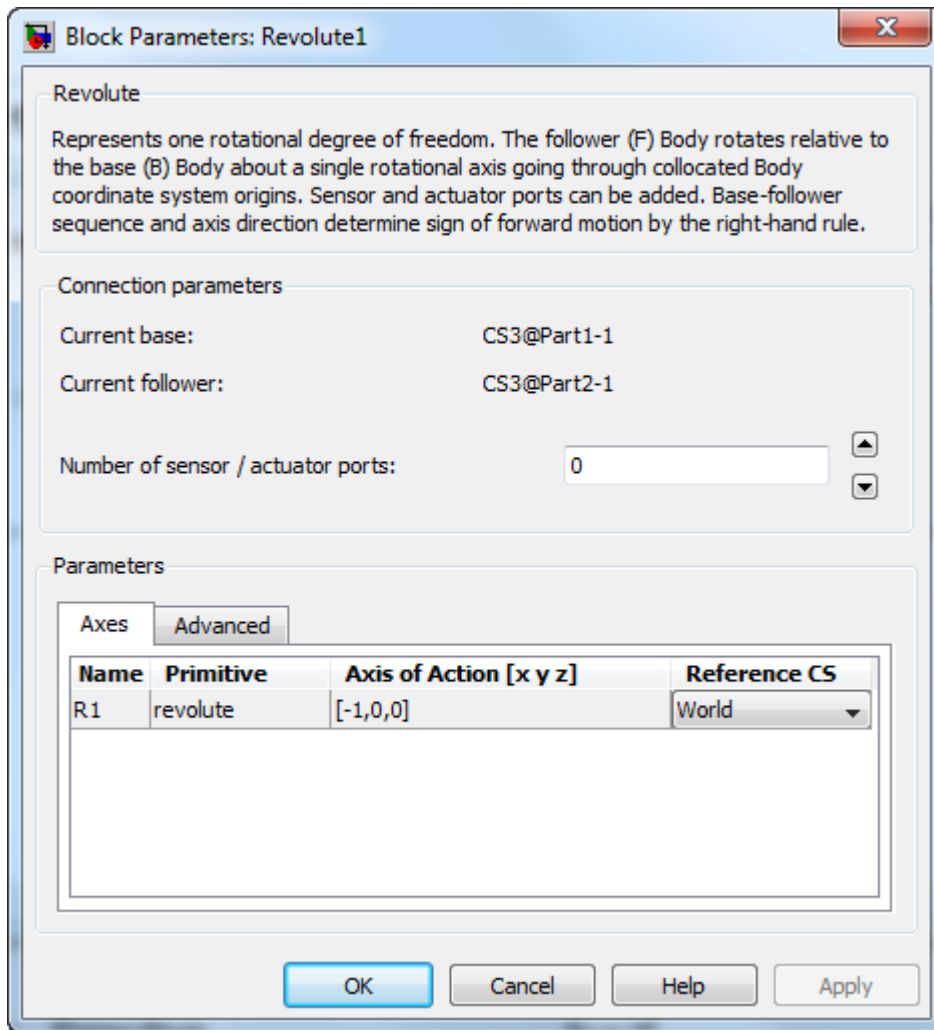


Figure 3.4. Revolute joint properties translated from SolidWorks[®]

3.2.2.2. Creating Virtual Reality Model from SolidWorks[®] Model

VR is an important tool for designers to observe the system during simulation. In MATLAB[®], this can be done in two ways. One way is using the built-in visualization tool. This tool basically, generates joints at the connection points to create the machine and also shows the center of gravity of the links. An example can be seen in Figure 3.5.

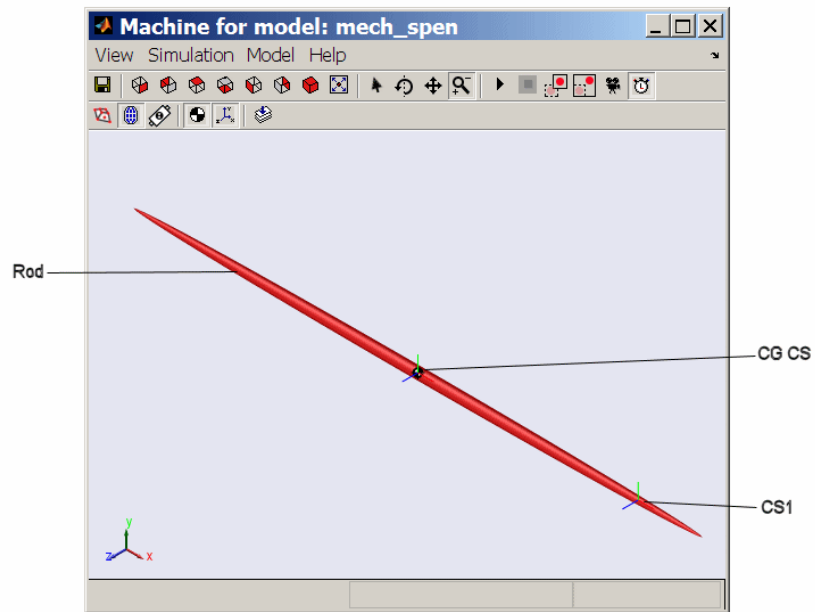


Figure 3.5. Visual representation of a body by visualization tool

Another way to create visual representation of Simulink model is to use the Virtual Reality Toolbox. Once the virtual model is created in SolidWorks[®] in VRML format by using “VR sink” block, it is possible to visualize the mechanism. This second method makes the simulation run much faster with respect to the first method. An example of VR representation can be seen in Figure 3.6.

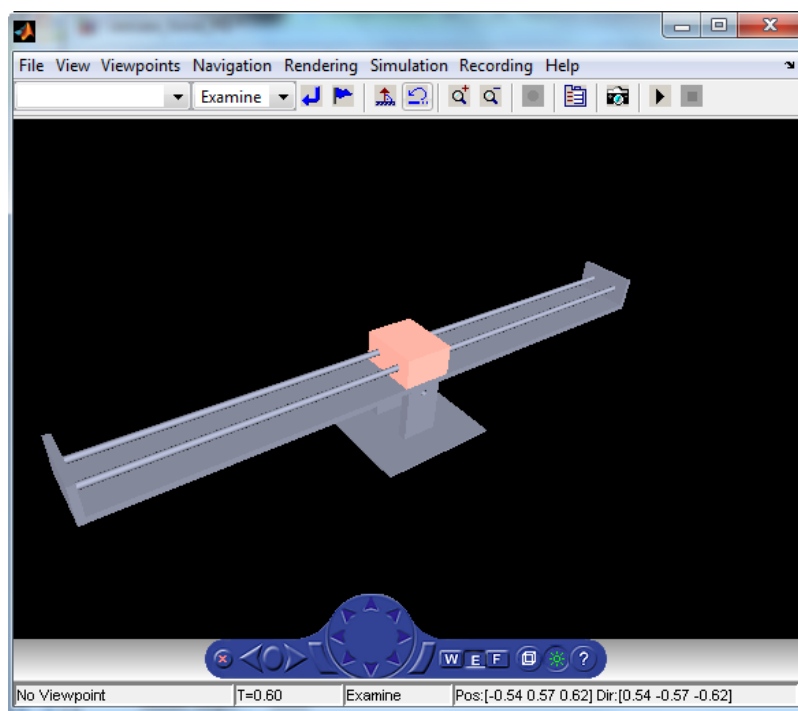


Figure 3.6. Visual representation of a mechanism by VR screen

3.2.2.3. Integration of Virtual Reality Representation with Simmechanics Model

VR representation and Simmechanics model are both created from the SolidWorks[®] model. These two need to be synchronized using Simulink blocks. In order to visualize the VR information, "VR sink" block is used. The VR information has to be edited in V-realm program to make the integration possible with the Simmechanics model (Dede, 2010).

In Figure 3.7, "VR sink" block parameter of the seesaw mechanism is presented. It can be seen that some of the boxes are checked and some of the boxes are unchecked. The checked boxes create inputs in the Simulink model and they allow programmer to send commands from these inputs as it can be seen in Figure 3.8.

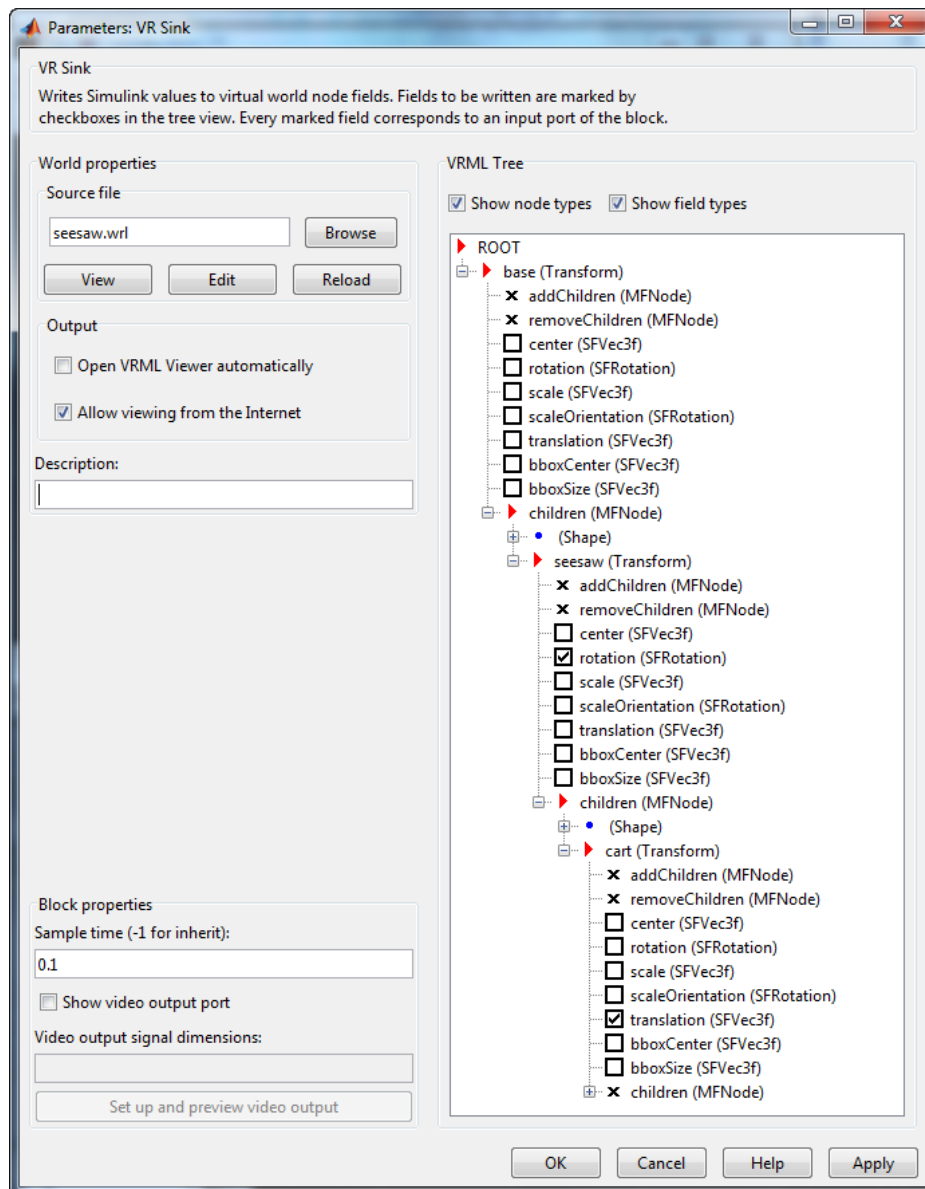


Figure 3.7. VR sink block parameters window

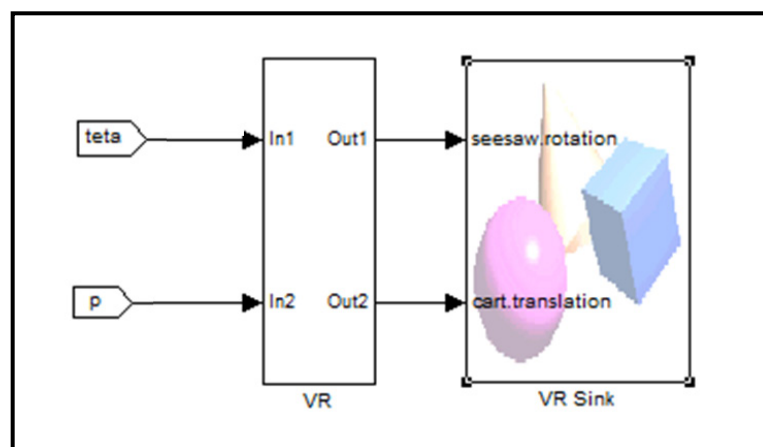


Figure 3.8. VR sink block from Simulink

3.2.3. Experimental Set-up with Seesaw Mechanism

The seesaw mechanism has one rotational degree of freedom (DoF). Experimental system includes a cart that is located on top of the seesaw which moves along the axis that is perpendicular to the rotation axis. This cart motion is utilized to keep the system at the equilibrium point. The seesaw mechanism used for the experiments can be seen in Figure 3.9.

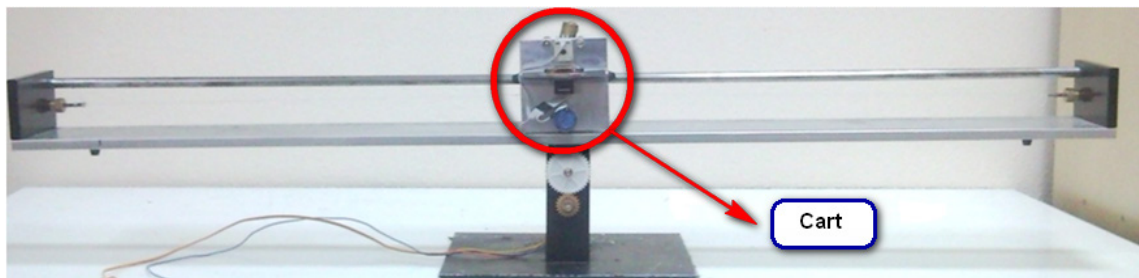


Figure 3.9. Seesaw mechanism

The mechanism, electromechanical components and electronics used to configure the system are presented in the following sub-sections.

3.2.3.1. Seesaw Mechanism

Seesaw system consists of three mechanical parts, these are;

- Base
- Seesaw
- Cart

Seesaw system has 2 analog sensors which are located at the cart to measure its position and at the center of rotation to measure the orientation of the seesaw. The position sensors are potentiometers as seen in Figure 3.10. The actuation system is a DC motor located at the cart. The rotational motion of the rotor is translated into linear motion through a capstan drive. The cart moves along its axis of translation as a result of this.

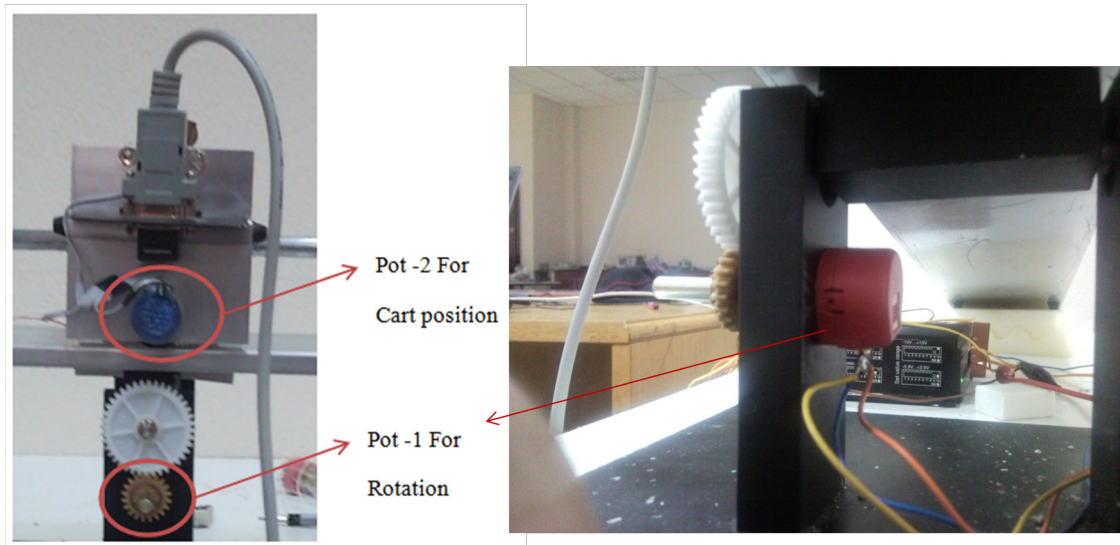


Figure 3.10. Potentiometers of the seesaw system

Specifications of the data acquisition system and motor driver are given in the Appendix A.

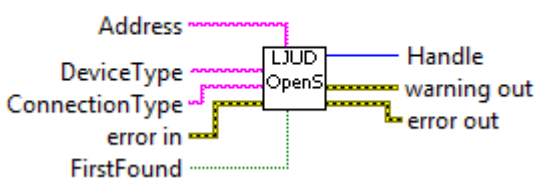
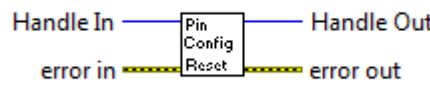
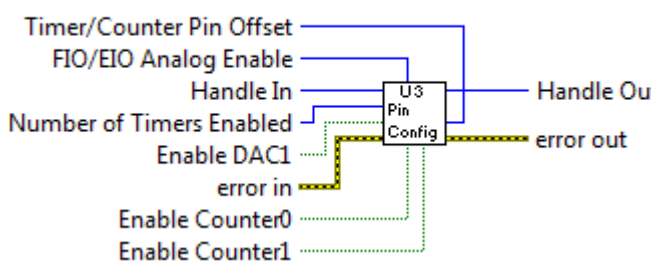
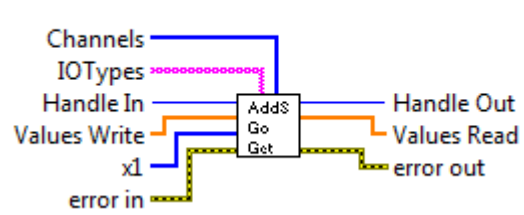
3.2.3.2. LabVIEW[®] Programming

LabVIEW[®] is a graphical programming environment. The program is used to develop measurement, test, and control systems. It uses graphical icons and wires that resemble a flow chart. The programmer calls the blocks and wires them to each other instead of writing the code line-by-line.

3.2.3.2.1. Integration of LabJack[®] and LabVIEW[®] System

A number of the essential virtual instruments (VIs), which are the blocks containing certain sub-routines, used in the integration is listed in the Table 3.2.

Table 3.2. List of LabJack VIs

<p style="text-align: center;">LJUD_OpenLabJackS.vi</p> 	<p>This VI specifies address of the LabJack and used device type with connection type. If only one LabJack is used, by choosing first found option, it is possible to skip address.</p>
<p style="text-align: center;">Pin Configuration Reset.vi</p> 	<p>Pin configuration reset VI, is used for the retuning the previous channel information on the LabJack.</p>
<p style="text-align: center;">U3 Pin Configuration.vi</p> 	<p>At pin configuration VI, programmers specifies how many analog channel is going to be used, timers, counters and extra Digital to Analog Converter (DAC) will be enabled or not and if timers enabled, which channel is going to be used for timer.</p>
<p style="text-align: center;">AddS-Go-Get.vi</p> 	<p>Adds-go-get VI is a package where programmer specifically determines the channel numbers of analog input and digital inputs and outputs. And programmer can collect the data from this VI.</p>

(Cont. on next page)

Table 3.2. (cont.)

<p>LJUD_eTCCConfigSB.vi</p> <p>Inputs: aEnableCounters, Handle In, aEnableTimers, aTimerModes, aTimerValues, error in, TCPinOffset, TimerClockBase, TimerClockDivisor.</p> <p>Outputs: Handle Out, error out.</p>	<p>This VI is used for configured to digital outputs of the LabJack, at this VI; it is possible to enable timers and counters. Determine the timer modes such as, 8-bit or 16-bit and deciding the working rate of the device.</p>
<p>LJUD_eTCValuesB.vi</p> <p>Inputs: aResetCounters, aReadCounters, Handle In, aReadTimers, aUpdateResetTimers, error in, aTimerValues Write.</p> <p>Outputs: Handle Out, aTimerValues Read, aCounterValues, error out.</p>	<p>In this VI, once configured timer values can be read. And they can be reset during the operation.</p>
<p>LJUD_ErrorToString.vi</p> <p>Input: error in.</p> <p>Output: String.</p>	<p>Finally, error output of the every VI can be returned into the string, in order to show in the front panel.</p>

The motor driver for the DC motors requires $\pm 10V$ analogue signals as inputs to drive in current mode. However, DAQ system is only able produce 5V. Therefore, an H-bridge type microchip is used between LabJack and motor driver and PWM signals from the LabJack are used to create $\pm 10V$ input signals to the motor driver. H-bridge can be seen in Figure 3.11.



Figure 3.11. L293, H – bridge
(Source: toko-robot.com)

General futures of the H – bridge system is

- Wide supply voltage range 4.5V to 36V.
- Output current is 1 A for channel.
- Peak output current is 2 A.
- Thermal shutdown.

The bilateral data flow between the PC and the seesaw mechanism is presented in Figure 3.12.

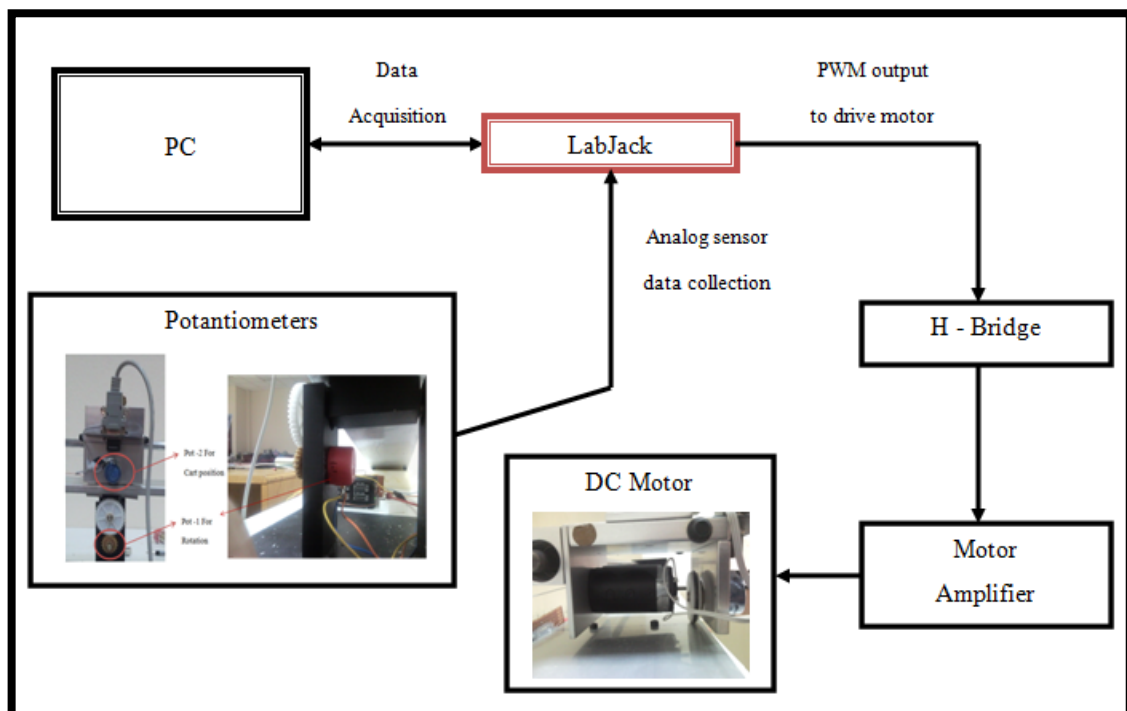


Figure 3.12. Data flow of the experimental set-up

First, data from potentiometers are acquired via LabJack, and the angular position of the seesaw and position of the cart are measured. Following this, control algorithm calculates the necessary PWM outputs to drive the motor of the cart. The PWM outputs are sent to the H-bridge, L293D. In this experiment, two output channels of the H-bridge are used to change the direction of the motor rotation. The supplied voltage to the H-bridge is 10V, thus, the signal is amplified to 10V. The motor amplifier works with $\pm 10V$ analogue signals, and H-bridge converts incoming PWM signals into $\pm 10V$ analogue signals and these signals are connected to the motor amplifier.

Integration of the LabJack[®] and LabVIEW[®] starts with placing the LabJack interface in LabVIEW[®] as seen in Figure 3.13. The model of the LabJack and connection type is needed to be specified.

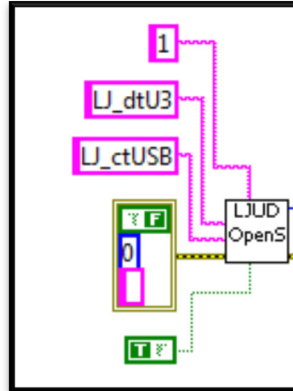


Figure 3.13. Calling LabJack via LabVIEW

After LabJack interface is added, the I/O channels are needed to be configured. The I/O channels configured in this experimental set-up are two analog inputs to acquire potentiometer measurements and two timers to create PWM output signals (Figure 3.14 and Figure 3.17).

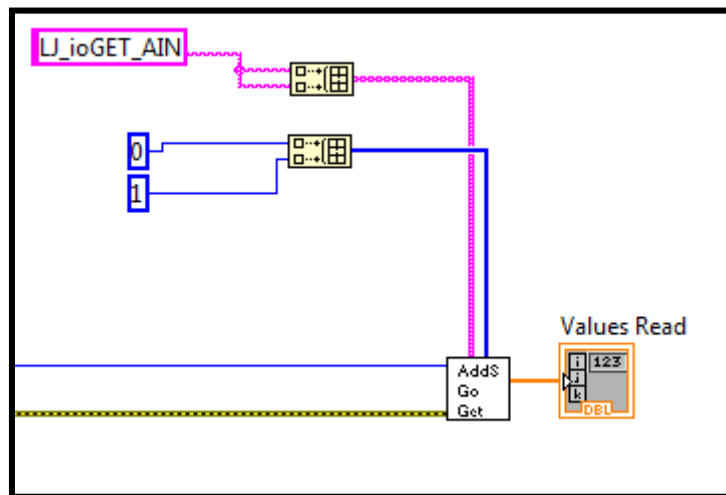


Figure 3.14. Configuration of analog channels of LabJack

Since seesaw is using only 2 analog sensors, it is sufficient to set-up first 2 channels (AIO0 & AIO1) as analog inputs. It is necessary to convert the acquired signals into meters and radians to be used in the control. Therefore, maximum and minimum values of the potentiometers and the limits of the system were measured.

Total distance that can be travelled by the cart is 0.90 meters and the maximum rotation amount of the seesaw is ± 12 degrees. Then, the range of the potentiometers of the system for rotation and position change is measured. Calculation for the cart position and the rotation amount of the seesaw are shown in Figure 3.15 and 3.16 respectively.

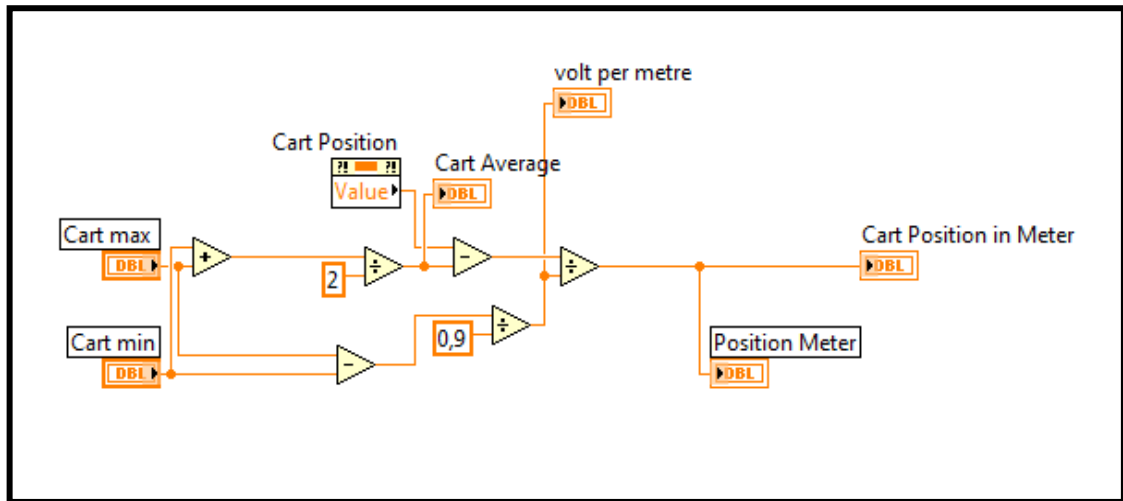


Figure 3.15. Converting the analog input into the meter

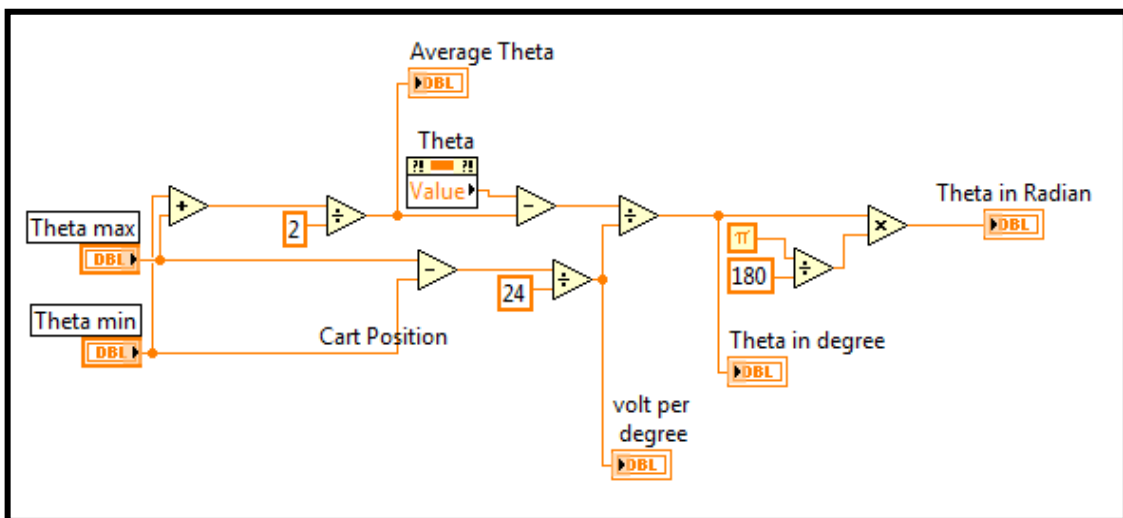


Figure 3.16. Converting the analog input into the angular position of the seesaw (in radians)

Two timers channels of the LabJack are used to send commands to the driver of the cart motor. Reason of using two timers is that H-bridge, L293D, requires two inputs to provide $\pm 10V$ analogue signals. PWM creation for the timer outputs and the output channel selection of timers are shown in Figure 3.17.

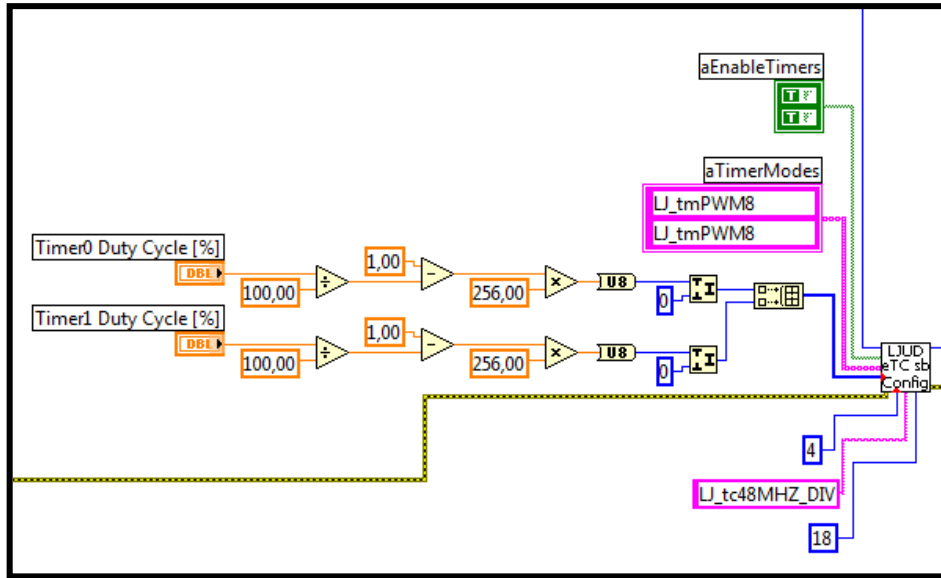


Figure 3.17. Configuration of LabJack timer

Used timers have 8 bits resolution and sampling rate of 1 kHz. Duty cycle of the timers signal is changed with respect to the required voltage output.

3.3. Conclusion

SolidWorks[®] is one of the most popular software used by the design engineers. The analysis capabilities of the program enables the designers to test their systems even before the prototypes are produced. This procedure allows to designer to modify and optimize the design at early stage of the design.

Currently, SolidWorks[©] is limited in the sense of creating controllers and conducting simulation tests. Therefore, a simulation environment is required to perform these studies before the prototyping stage. In MATLAB[®] Simulink environment, designers can observe the virtual representation of the simulated mechanism, developed control algorithms and they can test the developed controllers.

In experimental set-up, seesaw, has single DoF rotation. System has one input, and two outputs. The outputs are cart position and rotation angle of the seesaw. The input is the force applied to the cart. In order to transfer real world sensory data to computer, a DAQ system called LabJack is used. LabVIEW[®] is used as a software to manipulate the acquired data and send output signals to the actuation system, thus, it is the platform the develop the control software of the experimental system.

CHAPTER 4

MECHANISM DESIGN

In this chapter, conceptual designs for Unmanned Underwater Vehicle (UUV) and mechanism designs are proposed.

4.1. Mechanism Designs and Constraints

The designed system needs to be able to hover by making use of moving masses and buoyancy control, and it should be able to move with a single thruster complying with the design criteria set in Chapter 3. Also, the desired system needs to have a bladder for buoyant force control and should tolerate the faults. For the buoyancy control, alternatives are changing the volume of the vehicle or changing the total mass of the vehicle. In this project, changing the vehicle's displaced volume method is selected.

There are different methods to accomplish the dynamic change in the volume. One of them is using the hydraulic pumps (Sherman et al., 2001). This system is usually used for deep water applications where more forces are required to change the volume. Second method is the use of single-stroke piston pumps, which are relying on gearing to obtain a high mechanical advantage to rotate a screw and extend or retract a piston in the cylinder. This method is especially suitable for shallow-water operation since the required force is low. This method also provides quick reaction. Therefore, it is a good fit for two-way buoyancy control and increases the maneuverability.

Another issue to address to perform the desired task is designing the steering control mechanisms. The platform should be able to steer like an airplane or glider by making use of pitch and roll rotations. Typically, pitch angle is controlled by shifting the internal moving mass forward and backward. For some type of gliders, instead of moving central mass, bladder system is located at the nose of the glider and the change of the mass at glider nose creates a change at the center of gravity of the vehicle which changes the pitch angle of the vehicle (Graver et al., 2003). There are two ways to change the roll angle (heading) of the vehicle. One of them is using a rudder. It creates a

rotation in roll direction during the vehicle propulsion. Second alternative is using eccentric mass or moving mass. Rotating the mass around itself or by moving the mass left and right, it causes the glider to roll; producing a spiral motion.

The desired system's hovering mode control and steering capabilities are based on glider underwater vehicle. Therefore, the three main glides models are investigated and a comparison table was created (Bender et al., 2008) (Table 4.1). Design parameters are selected by investigating the gliders given in Table 4.1.

Table 4.1. Comparison of gliders

Attribute	Slocum Electric	Spray	Seaglider
<i>Hull (and Fairing)</i>	1.5 m length, 21.3 cm diameter	2 m length, 20 cm diameter	1.8 m length, 30 cm diameter
<i>Mass</i>	52 kg	51 kg	52 kg
<i>Batteries</i>	260 alkaline C cells, 8 MJ	52 lithium CSC DD cells, 13 MJ	81 Lithium D cells, 10 MJ
<i>Volume Change</i>	520 cc, 90 W single stroke pump, 50% efficiency	900 cc, Motor & reciprocating pump, 20-50% efficiency	840 cc, Motor & reciprocating pump, 8-40% efficiency
<i>Horiz Speed</i>	0.4 m/s	0.45 m/s	0.45 m/s
<i>Range</i>	2300 km, 30 days @ 20° glide, 0.25 m/s horizontally	7000 km, 330 days, @ 18° glide, 0.25 m/s horizontally	4500 km, 220 days @ 18° glide, 0.25 m/s horizontally
<i>Max Depth</i>	200 m	1500 m	1000 m
<i>Wings</i>	98 cm span, 14 cm chord (MAC), 45° sweep	120 cm span, 10 cm chord (MAC)	100 cm span, 16 cm chord (MAC)

4.2. Conceptual Design for UUV

Two conceptual designs are proposed that meet the design specifications. Among these, one of them is inspired from the nature. Other one is based on previous works and resembles a torpedo.

4.2.1. Conceptual Design - 1

The desired UV should to be able to hover. A good example of a sea animal that is able to hover is ray fish (Figure 4.1).



Figure 4.1. Ray fish
(Source: planetanimalzone 2011)

The first conceptual design inspired from Ray fish is shown in Figure 4.2. An advantage of this design is the fact that it provides lots of free space to place control systems, motor drivers and batteries. Thrusters are located at the backside of the vehicle. Reason of using two thrusters is to introduce a joint-level fault tolerance to the vehicle.

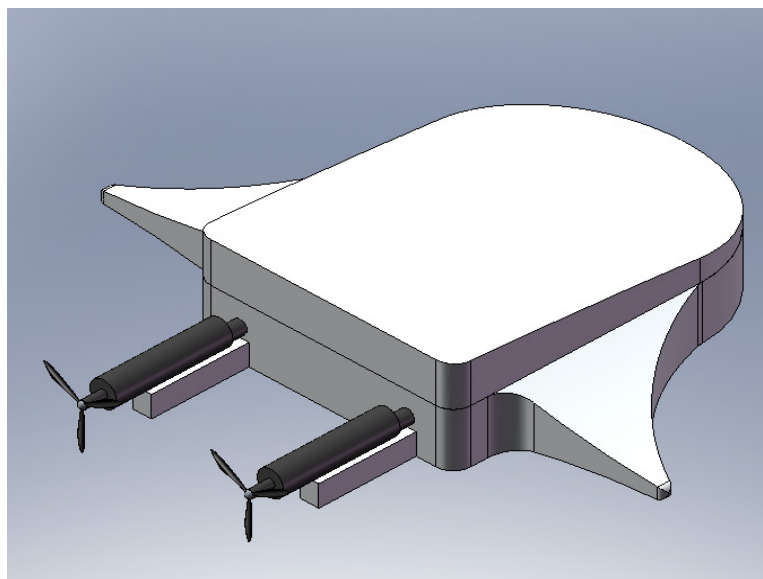


Figure 4.2. SolidWorks[®] drawing of the conceptual design - 1

The internal moving masses are located as seen in Figure 4.3. The proposed internal moving mechanism will be discussed further throughout this chapter.

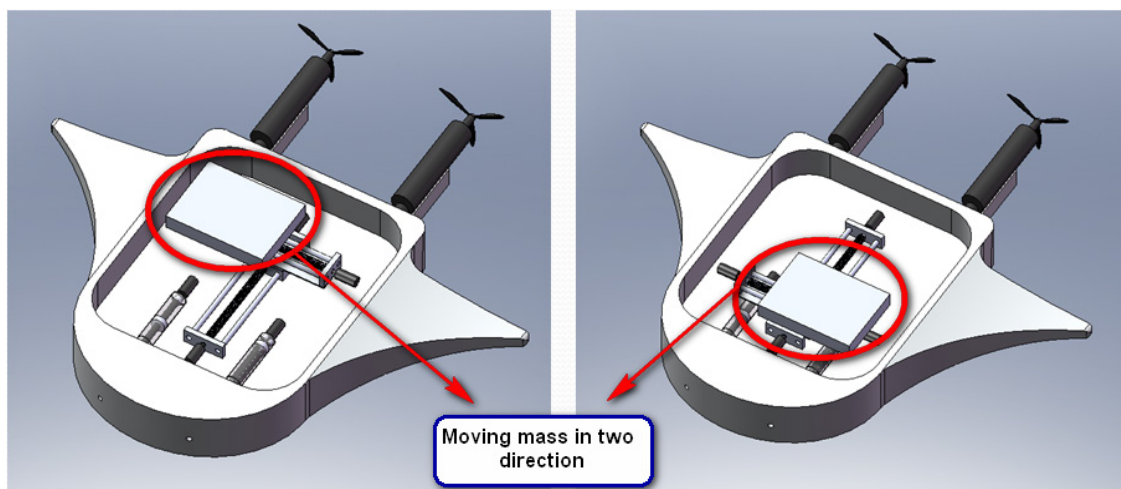


Figure 4.3. Internal moving mass system for conceptual design - 1

Since this vehicle is considered for the shallow water operations, single-stroke pumps can be used. On the other hand, UUV needs to hover at a certain depth. Therefore, single-stroke pump is needed to be modified and have a variable stroke in order to change its buoyancy level by level. These pumps use screw system to move forward and backward (Figure 4.4).

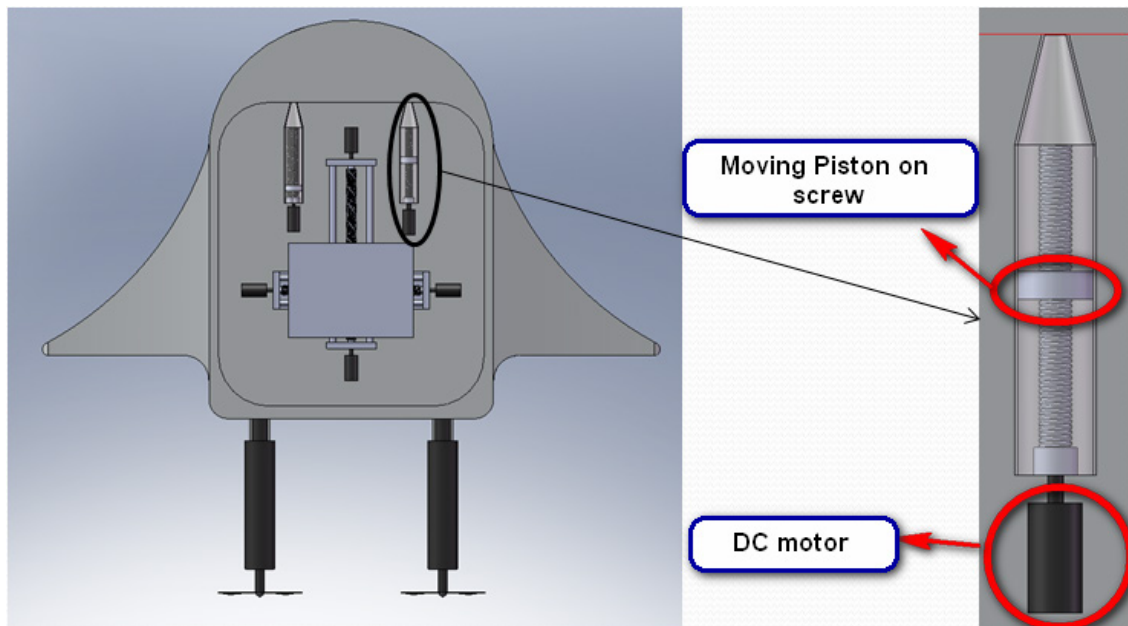


Figure 4.4. Buoyancy control of the conceptual design - 1

This conceptual design provides a well balanced system, as the buoyancy center is designed to be at the top of the mass center that can hover and has large enough space to place equipments. In addition to these, conceptual design – 1 is has enough space for further modifications, such as, adding manipulator to the vehicle.

4.2.2. Conceptual Design - 2

This conceptual design was inspired from previous underwater gliders that offer better hydrodynamics. It resembles a torpedo as seen in Figure 4.5. Speed of the vehicle increases as a result of a better hydrodynamic. Thrusters are located at the two sides of the vehicle.

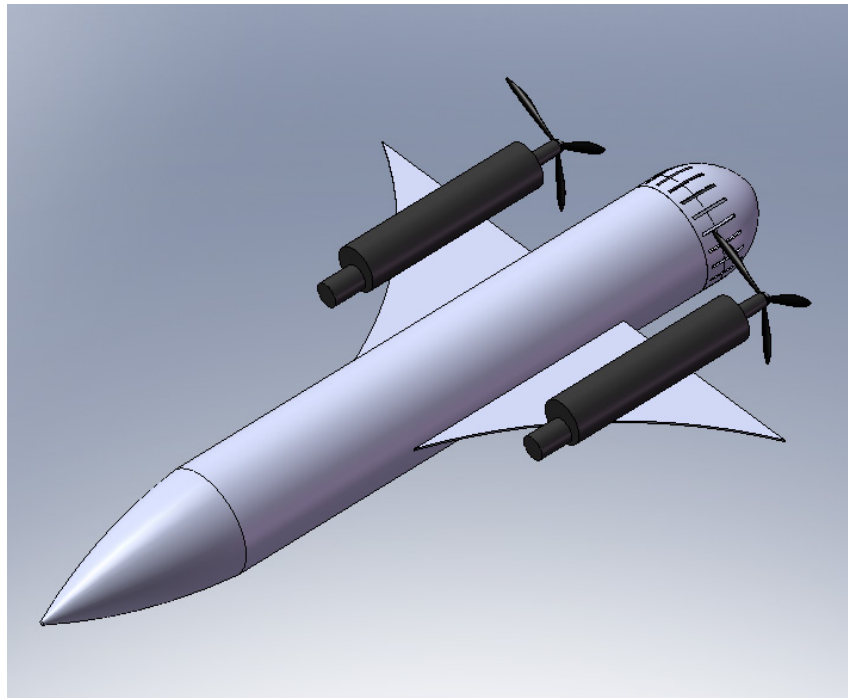


Figure 4.5. SolidWorks[®] drawing of the conceptual design - 2

The internal moving masses can be seen in Figure 4.6. Pitch angle of the vehicle can be changed by the motion of the moving mass.

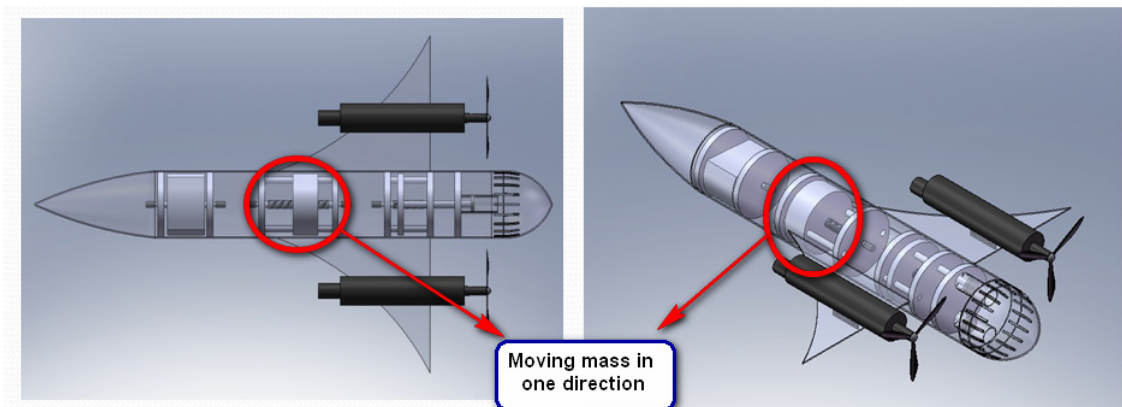


Figure 4.6. Internal moving mass for pitch rotation for conceptual design - 2

As it can be seen in Figure 4.6, the moving mass mechanism provides rotation in only pitch direction. Therefore, a secondary mass is required to rotate the vehicle in roll direction and for this purpose eccentric mass is used (Figure 4.7).

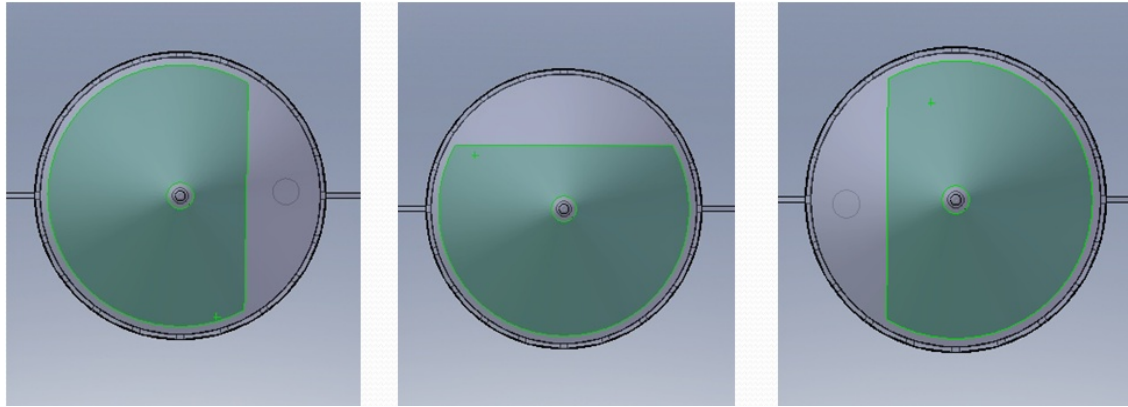


Figure 4.7. Rotary mass for roll rotation for conceptual design - 2

Bladder system is used to change buoyancy of the vehicle in conceptual design – 2. Single stroke pistons are used in bladder system as seen in Figure 4.8.

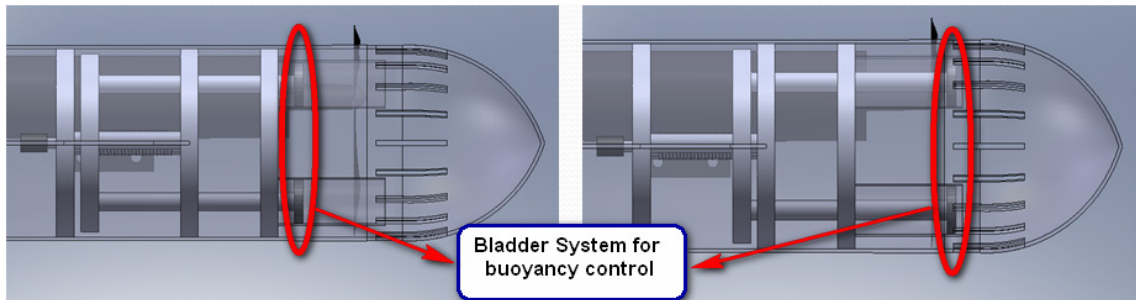
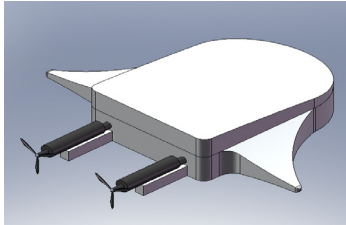
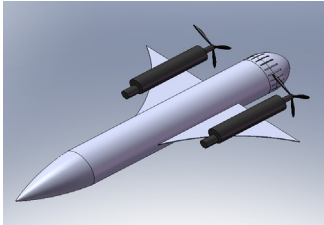


Figure 4.8. Buoyancy control for the conceptual design - 2

The comparison of two conceptual designs is given in the table.4.2.

Table.4.2. Comparison of conceptual designs of UUV

Conceptual Design - 1	Conceptual Design - 2
	
More Space for equipments	Good hydrodynamic design
Low speed	High speed
Open for modification	Limited modification
Suitable for hovering operations	Not good for hovering

Conceptual design - 1 is selected as the final design after studying the comparison table. The reasons to select conceptual design - 1 are that it is more suitable for hovering operations and open for further modifications, and high speed operation is not a requirement of this study.

4.3. Conceptual Designs for Internal Moving Mass System

Conceptual designs studies are conducted for internal moving masses which create the roll and pitch motions. There are four designs concepts proposed for the roll and pitch motions in this study.

4.3.1. Conceptual Design - 1

First conceptual design is based on Gimbal mechanism (Figure 4.9). This system has 2 revolute joints and by changing the rotation angle of these joints, center of gravity of the system changes (Figure 4.10). Two DoFs are uncoupled.

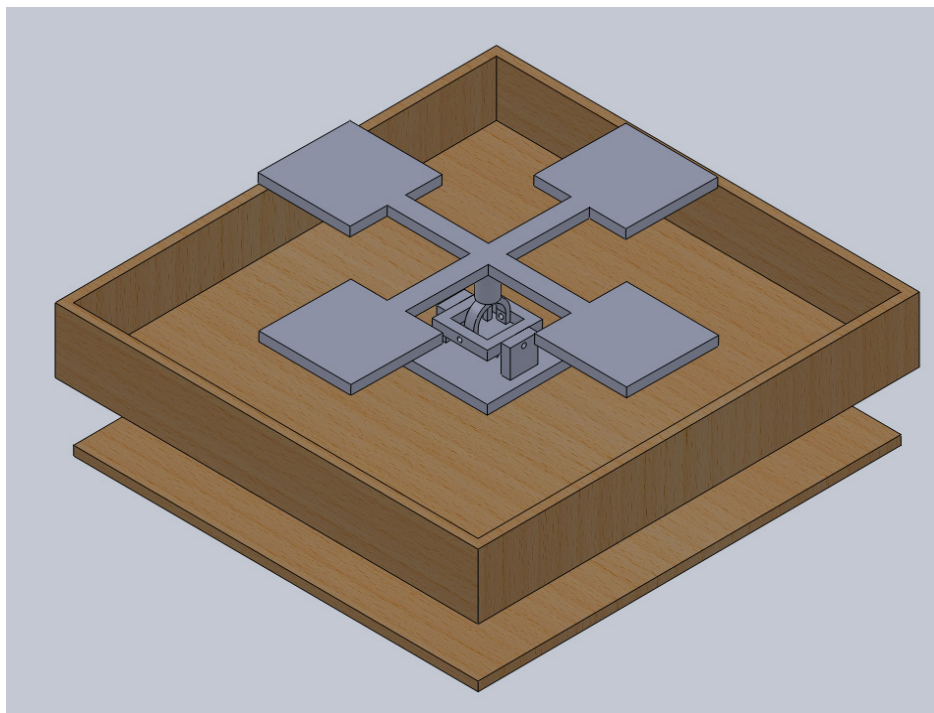


Figure 4.9. Gimbal mechanism for conceptual design - 1

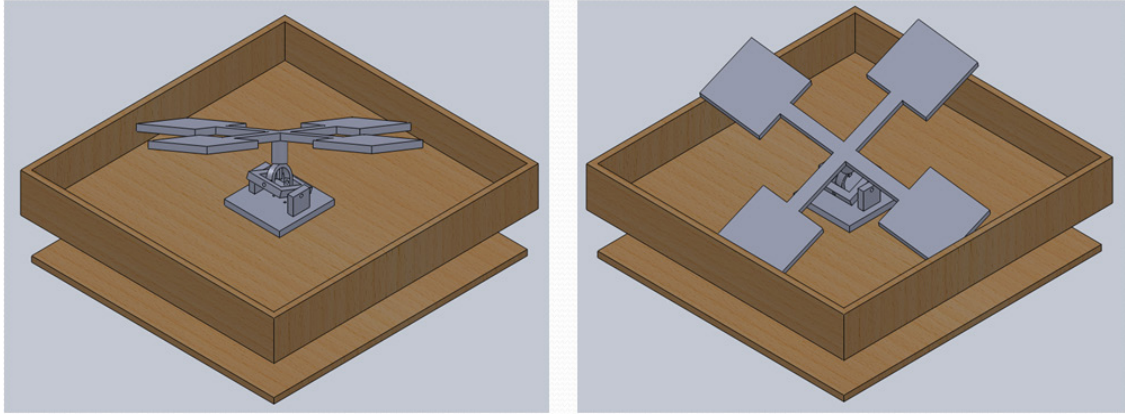


Figure 4.10. Gimbal based mechanism

Advantage of the system is that each DoF can be controlled independently due to the uncoupled architecture of the mechanism. On the other hand, change at the center of gravity is limited with respect to its footprint.

4.3.2. Conceptual Design - 2

In conceptual design - 2, proposed system is based on x - y table. System has 2 prismatic joints and mass can move along the base in both directions in an uncoupled fashion. Conceptual design - 2 can be seen in Figure 4.11.



Figure 4.11. x - y table based system conceptual design - 2

Advantage of using x - y table as internal moving mass system is that it has long range of motion. Therefore, change of the location of the center of gravity is relatively larger with respect to the previous mechanism.

4.3.3. Conceptual Design - 3

In this concept, proposed system is an RR manipulator for changing the center of gravity location as can be seen in Figure 4.12. The two DoF are coupled and both DoF should be actuated in coordination in order to locate the center of gravity for only a rotation in one direction. In Figure 4.13, two cases where the center of gravity is located at different places are shown.

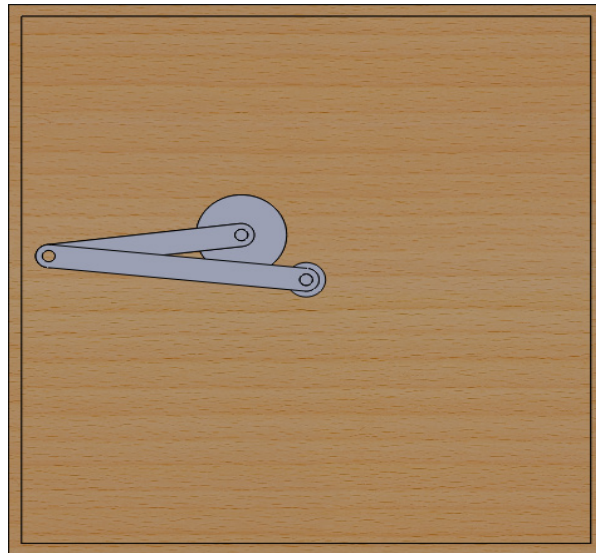


Figure 4.12. RR manipulator based conceptual design – 3

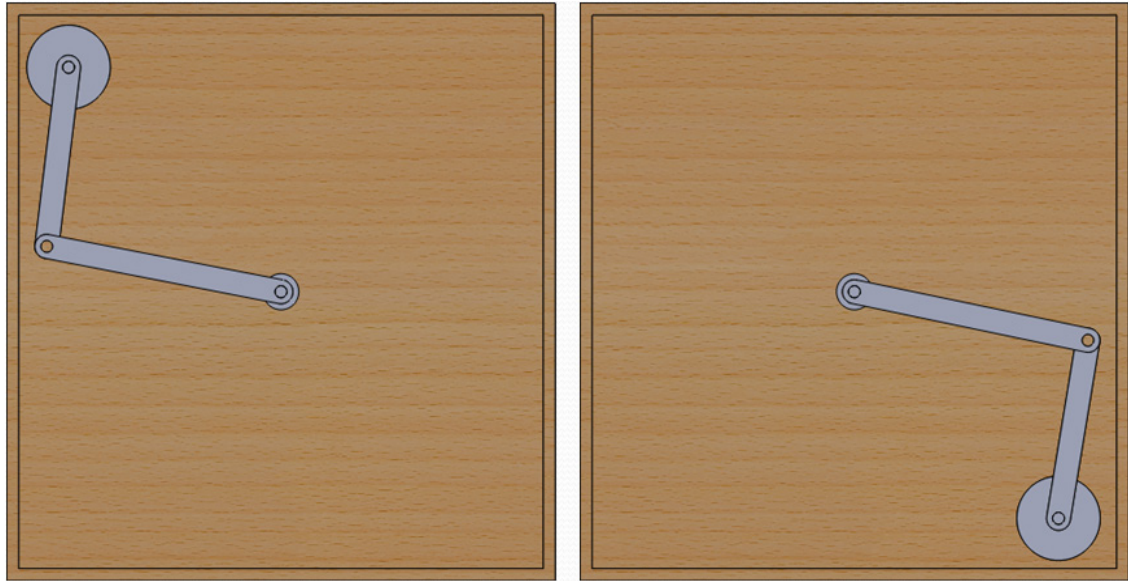


Figure 4.13. Changed center of gravity of the conceptual design - 3

Advantage of the system is that it has a wide range of change of the center of gravity location. However, the control of the roll and pitch rotations are coupled and thus, the control becomes harder. Also, obstacle avoidance algorithms should be employed due to the workspace limitations.

4.3.4. Conceptual Design - 4

The last proposed conceptual design is using a mobile robot as internal moving mass. System can be seen in Figure 4.14. It has four omni-directional wheels and therefore, it can move in any directions on the plane without need of change of direction. Figure 4.15 presents two cases where the mobile platform is located at two corners and thus the location of the center of gravity is changed.

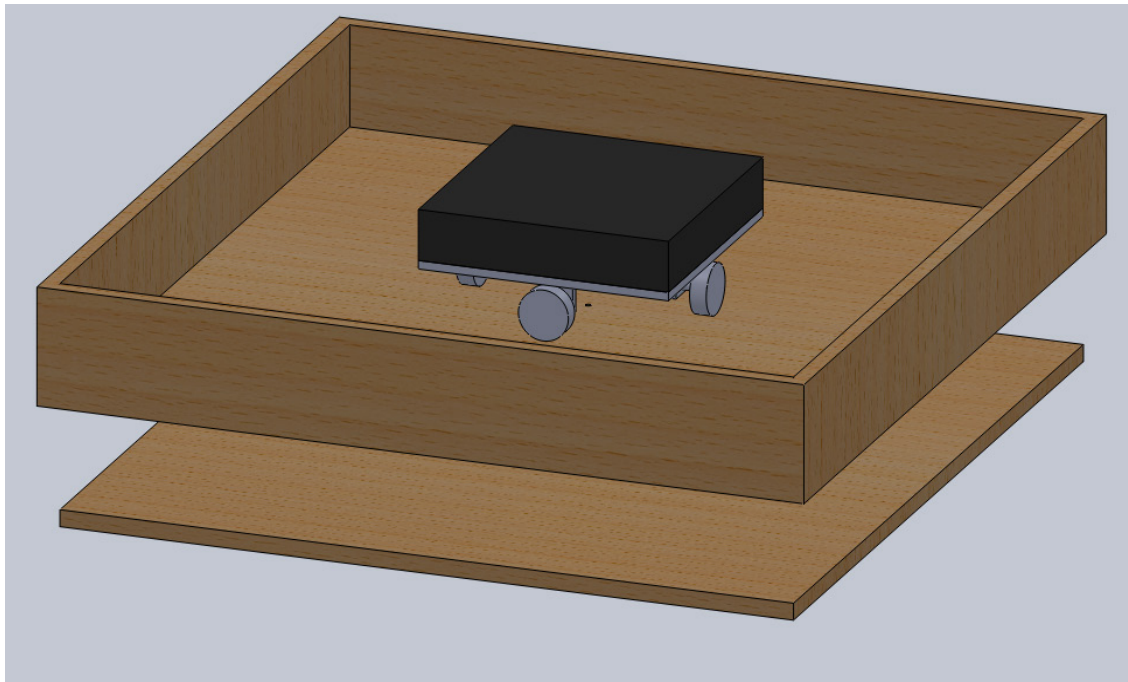


Figure 4.14. Mobile robot based conceptual design - 4



Figure 4.15. Mobile robot based changed center of gravity of conceptual design - 4

The mobile robot concept is similar with x - y table based model. On the other hand, it has some drawbacks such as; when the vehicle experiences dive or surface motions, or some disturbance (underwater currents), it is possible that the mobile robot might slide and lose its position.

After all conceptual designs for internal moving masses are reviewed, the final design selected is concept number 2 which is x - y table. The system allows wide range of change in center of gravity location which is enough to compensate for higher

degrees of roll and pitch motions. It is easier the control, since both DoF are uncoupled and this system does not lose its position like the mobile robot concept.

4.4. Simulation Set-up

After the concept of internal moving mass system is decided, next step is testing this system. In UUVs, rotation center is at the buoyancy center. Therefore, the proposed mechanisms center of rotation acts as the center of buoyancy of the system. In underwater vehicles, center of buoyancy and center of gravity location is important. Normally, center of gravity is kept below the center of buoyancy and that makes the system inherently stable.

Tests of the moving masses to stabilize and control the steering of the vehicle are initiated with an inherently unstable system in order to test the control algorithms at the most extreme conditions. Therefore, in this study, a customary seesaw system is used in simulation and experimental tests. In customary seesaw systems, center of gravity is above the center of rotation and that makes the system highly (inherently) unstable.

Initially, one DoF seesaw is modeled and then the works is extended to a two DoF system that can imitate the rotation of the final design for moving masses. These systems are first modeled in SolidWorks[®] and then transferred to MATLAB[®] Simulink environment for simulation tests.

4.4.1. Seesaw Mechanism

First step is modeling a single DoF seesaw. The modeled system resembles the experimental single DoF seesaw system. Designed system has one rotational joint on the seesaw and one prismatic joint attached to the cart. Proposed seesaw system can be seen in Figure 4.16.

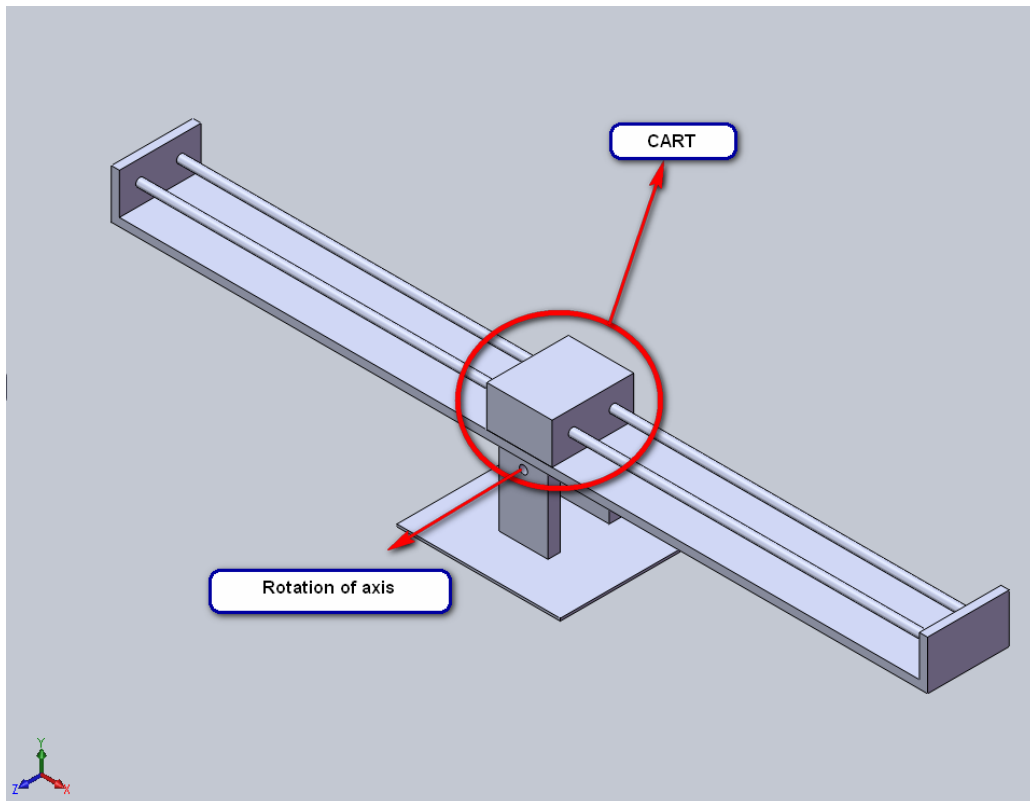


Figure 4.16. Proposed seesaw mechanism

4.4.2. Two Degree of Freedom Mechanism

The proposed conceptual design requires two degrees of rotations for pitch and roll motions. After single DoF seesaw mechanism is controlled, next step is designing a mechanism that can make the system to do these two rotations, and keep the balance by using moving masses. These masses are located over the center of rotation, which resembles the extreme case where the center of gravity is located over the center of buoyancy. Designed system that meets these requirements is shown in Figure 4.17.

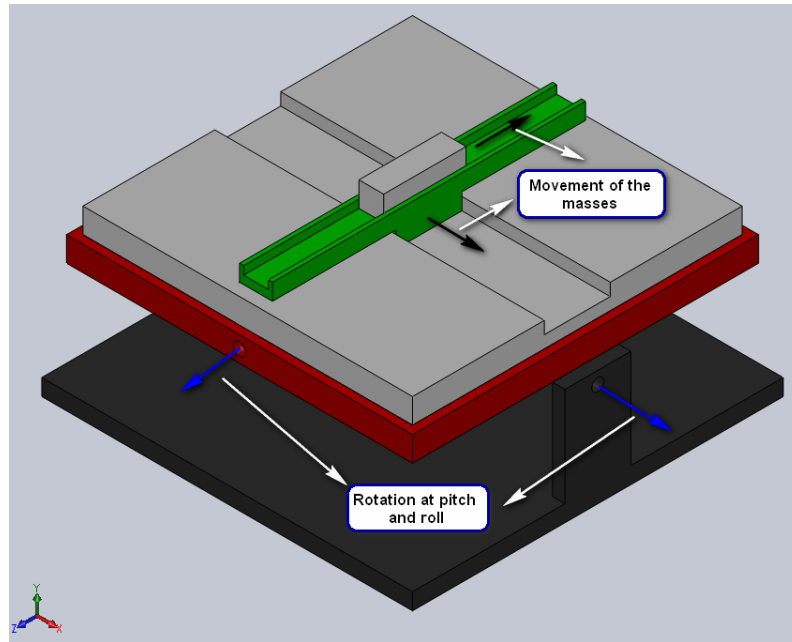


Figure 4.17. Two degree of freedom seesaw system

4.5. Conclusion

Conceptual designs for UUV and moving mass mechanisms are proposed and compared in this chapter. Biologically inspired model is selected as the final design because of it is more suitable for hovering tasks and open to further modifications. In addition to these features, it provides large space to place necessary equipments.

After deciding on the final design of UUV, next step was choosing the internal moving mass system. Four different concepts are investigated. These are based on; Gimbal mechanism, x - y table, RR manipulator, and two DoF omni- directional mobile robot. These concepts were compared against each other, and x - y table was chosen as mechanism. The reason is that it covers a wide range of change of the center of gravity location. Also, it is a decoupled system, thus, it is possible to control each rotation separately.

Subsequently, simulation set-ups are presented making use of the selected internal moving mechanism design. Simulation studies are started with single DoF seesaw system, because of its similarity with proposed internal moving mass design. Then, the study is extended to two DoF seesaw system that can imitate the two rotational motions of the UUV.

CHAPTER 5

SIMULATION AND EXPERIMENTAL STUDIES

In this chapter, the results of the simulation and experimental studies are presented. First part of the chapter includes the solution of the equation of motion of the proposed systems in Chapter 4. Following this, controllers are designed and validity of the controller is tested for various conditions.

Finally, experimental studies are conducted and related results are given. The results are discussed at the end of the chapter.

5.1. Mathematical Modeling

In this part, equation of motion of the systems will be determined for single DoF and two DoF systems.

5.1.1. Single DoF Seesaw System

Control architecture development is initiated on single DoF seesaw system. In this system, a moving mass is used to stabilize the seesaw system. In order to balance the system, seesaw and cart center of gravity has to be aligned along the gravity direction.

There are number of ways to find the equation of motion of a system. One of them is energy-based Lagrangian Method. Lagrangian is the difference between kinematic and potential energy of the system as seen in equation (5.1). In this equation, K represents the kinetic energy of the system and U represents the potential energy of the system. In order to find Lagrangian term for the system, free-body diagram of the single DoF seesaw system is drawn as seen in Figure 5.1. The equation of motion can be derived as

$$L = K - U \quad (5.1)$$

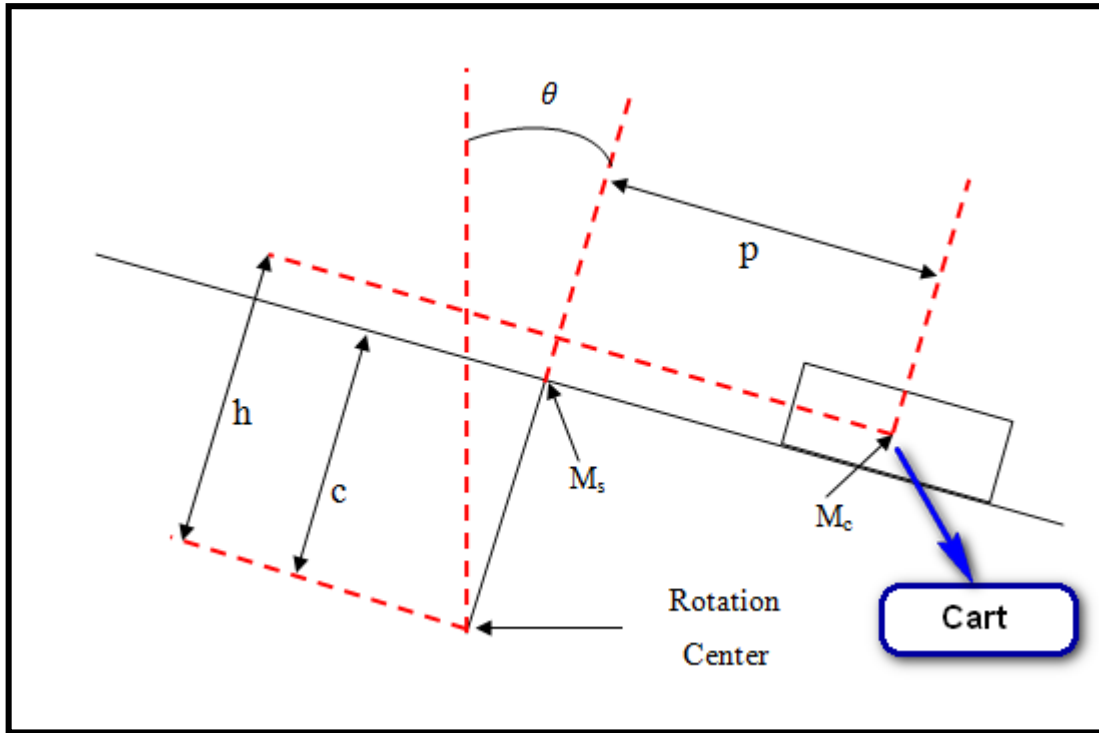


Figure 5.1. Free-body diagram of the Single DoF Seesaw system

- θ is the rotation angle of the seesaw
- p is the cart position from the center
- c is the distance of the center of gravity of the seesaw with respect to the rotation center
- h is the distance of the cart gravity center with respect to the rotation center.
- M_s is the mass of the seesaw.
- M_c is the mass of the cart.
- J is the inertia of the seesaw system including the cart.

Potential energy of the cart and the seesaw are found by using Equations 5.2 and 5.3 respectively.

$$U_c = M_c g (h \cos \theta - p \sin \theta) \quad (5.2)$$

$$U_s = M_s g (c \cos \theta) \quad (5.3)$$

Kinetic energy of the cart and the seesaw are determined by using Equations 5.4 and 5.5 respectively.

$$K_c = \frac{1}{2} M_c [(h \dot{\theta} + \dot{p})^2 + (p \dot{\theta})^2] \quad (5.4)$$

$$K_s = \frac{1}{2} J (\dot{\theta})^2 \quad (5.5)$$

Lagrangian equation of the system is later calculated by using the potential and kinetic energy equations as presented in Equation 5.6.

$$L = K_c + K_s - U_c - U_s \quad (5.6)$$

The equations of the motion for the system are then obtained from Equations 5.7 and 5.8

$$\frac{d}{dt} \frac{\partial L}{\partial \dot{p}} - \frac{\partial L}{\partial p} = F \quad (5.7)$$

$$\frac{d}{dt} \frac{\partial L}{\partial \dot{\theta}} - \frac{\partial L}{\partial \theta} = 0 \quad (5.8)$$

Then equation 5.6 is applied into equation 5.7 and 5.8 and equation of motion found as,

$$M_c \ddot{p} + M_c h \ddot{\theta} - M_c g \sin \theta - M_c p \dot{\theta}^2 = F \quad (5.9)$$

$$\ddot{\theta} [(M_c h^2) + J + (M_c p^2)] + M_c h \ddot{p} + 2 M_c p \dot{p} \dot{\theta} - M_c g p \cos \theta - M_c g h \sin \theta - M_s g c \sin \theta = 0 \quad (5.10)$$

Next step is converting equation 5.9 and 5.10 into matrix form as presented in Equation 5.11.

$$\begin{bmatrix} M_c & M_c h \\ M_c h & (M_c h^2) + J + (M_c p^2) \end{bmatrix} \cdot \begin{bmatrix} \ddot{p} \\ \ddot{\theta} \end{bmatrix} + \begin{bmatrix} 0 & -M_c p \dot{\theta} \\ M_c p \dot{\theta} & M_c p \dot{p} \end{bmatrix} \cdot \begin{bmatrix} \dot{p} \\ \dot{\theta} \end{bmatrix} + \begin{bmatrix} -M_c g \sin \theta \\ -M_c g p \cos \theta - M_c g h \sin \theta - M_s g c \sin \theta \end{bmatrix} = \begin{bmatrix} F \\ 0 \end{bmatrix} \quad (5.11)$$

5.1.2. Two DoF Seesaw System

The proposed mechanism for two DoF seesaw system, in Chapter 4, is a decoupled system. Therefore, its equations of motion can be calculated separately. Single DoF seesaw system is rotating about a single axis and the cart on top of it is able to move in only one direction. Two DoF system can rotate about two axes and the mass on the system is able move in two directions (Figure 4.17). Since the system is decoupled, the determined equation of motion for single DoF system is also valid for two DoF seesaw system.

5.2. Controller Design and Simulation Results

In this section, examined controller designs are explained. During the development of the controller, equation of motion, found in section 5.1.1, is used.

5.2.1. Non-linearity Cancellation

In this controller, non-linearity effects that are calculated in equation of motion are added as inputs to system in order to linearize the system. First of all, for the sake of simplicity, equation 5.11 presented as follow;

$$\hat{M}(x)\ddot{x} + \hat{C}(x, \dot{x})\dot{x} + \hat{G}(x) = \begin{bmatrix} F \\ 0 \end{bmatrix} \quad (5.12)$$

In this equation terms used are represented in matrix form as presented in the equation set 5.13.

$$x = \begin{bmatrix} p \\ \theta \end{bmatrix}$$

$$\widehat{M} = \begin{bmatrix} M_c & M_c h \\ M_c h & (M_c h^2) + J + (M_c p^2) \end{bmatrix}$$

$$\widehat{C} = \begin{bmatrix} 0 & -M_c p \dot{\theta} \\ M_c p \dot{\theta} & M_c p \dot{p} \end{bmatrix} \quad (5.13)$$

$$\overline{G} = \begin{bmatrix} -M_c g p \cos \theta & -M_c g h \sin \theta \\ -M_c g p \cos \theta - M_c g h \sin \theta & -M_s g c \sin \theta \end{bmatrix}$$

In order to leave \ddot{x} alone, both side of the equation are multiplied by inverse of the \widehat{M} matrix. In order to take inverse of a matrix, determinant of the matrix (5.14) has to be greater than zero.

$$\det(\widehat{M}(x)) = M_c J + M_c^2 p^2 \quad (5.14)$$

In equation 5.14, all the units are non-zero, positive terms. Therefore, determinant of this equation is greater than zero and it is possible to take inverse of the matrix. Equation 5.15 is derived by making use of the inverse of the \widehat{M} matrix.

$$\ddot{x} + \widehat{M}^{-1}(x) \widehat{C}(x, \dot{x}) \dot{x} + M^{-1}(x) \overline{G}(x) = \widehat{M}^{-1}(x) \begin{bmatrix} F \\ 0 \end{bmatrix} \quad (5.15)$$

Next step is multiply both side of the equation by $[0 \ 1]$ to solver for $\ddot{\theta}$, as represented in Equation 5.16.

$$\begin{aligned} \ddot{x} [0 \ 1] + [0 \ 1] \widehat{M}^{-1}(x) \widehat{C}(x, \dot{x}) \dot{x} + [0 \ 1] \widehat{M}^{-1}(x) \overline{G}(x) \\ = [0 \ 1] \widehat{M}^{-1}(x) \begin{bmatrix} F \\ 0 \end{bmatrix} \end{aligned} \quad (5.16)$$

And $\ddot{\theta}$ is calculated as shown in Equation 5.17.

$$\ddot{\theta} = [0 \ 1] \widehat{M}^{-1}(x) \begin{bmatrix} F \\ 0 \end{bmatrix} - [0 \ 1] \widehat{M}^{-1}(x) \widehat{C}(x, \dot{x}) \dot{x} - [0 \ 1] \widehat{M}^{-1}(x) \overline{G}(x) \quad (5.17)$$

Inverse of the matrix \widehat{M} is calculated in Equation 5.18

$$\widehat{M}^{-1} = \begin{bmatrix} \frac{J + M_c h^2 + M_c p^2}{JM_c + M_c^2 p^2} & \frac{-h M_c}{JM_c + M_c^2 p^2} \\ \frac{-h M_c}{JM_c + M_c^2 p^2} & \frac{M_c}{JM_c + M_c^2 p^2} \end{bmatrix} \quad (5.18)$$

After inserting the inverse of \widehat{M} matrix into the equation 5.16 into the right-hand side of Equation 5.16, Equation 5.19 is derived.

$$[0 \quad 1] \widehat{M}^{-1}(x) \begin{bmatrix} F \\ 0 \end{bmatrix} = \frac{-h M_c}{JM_c + M_c^2 p^2} F \quad (5.19)$$

The coefficient of the F is found in the equation 5.19. Then, it is possible to design the actuation force, F , as follows;

$$F = \left(\frac{JM_c + M_c^2 p^2}{h M_c} \right) [-[0 \quad 1] \widehat{M}^{-1}(x) \hat{C}(x, \dot{x}) \dot{x} - [0 \quad 1] \widehat{M}^{-1}(x) \bar{G}(x) - F_v] \quad (5.20)$$

In the equation 5.20, F_v represents the control force variable, and the other terms are non-linear factors and need to be calculated and fed into the actuation system along with the control force input to linearize the system.

After inserting the designed F into Equation 5.17, Equation 5.21 is derived.

$$\ddot{\theta} = F_v \quad (5.21)$$

The error signal to be used in the linear control algorithm can be calculated as shown in Equation 5.22.

$$e_\theta = \theta_d - \theta \quad (5.22)$$

In this equation, e_θ represents the error in seesaw angular position and θ_d represents the desired seesaw angular position. Taking the double derivatives of the equation 5.22 yields Equation 5.23.

$$\ddot{e}_\theta = \ddot{\theta}_d - \ddot{\theta} \quad (5.23)$$

Since $\ddot{\theta}$ is found equal to F_v in Equation 5.21, Equation 5.24 is derived.

$$\ddot{e}_\theta = \ddot{\theta}_d - F_v \quad (5.24)$$

Now, it is possible to apply a PD control to the system, and the equation for the control input is designed as shown in Equation 5.25

$$F_v = \ddot{\theta}_d + k_v \dot{e}_\theta + k_p e_\theta \quad (5.25)$$

5.2.1.1. Simulation Results for Single DoF Seesaw

The proposed concepts in Chapter 4 are transferred to the MATLAB[®] Simulink environment, and the simulation studies are initiated with the single DoF seesaw system. First, seesaw system is modeled in SolidWorks[®] as can be seen in Figure 4.16. Then, it is transferred into Simmechanics blocks (Figure 5.2). Transferred system has 2 joints, one prismatic and one rotational, as in the modeled system.

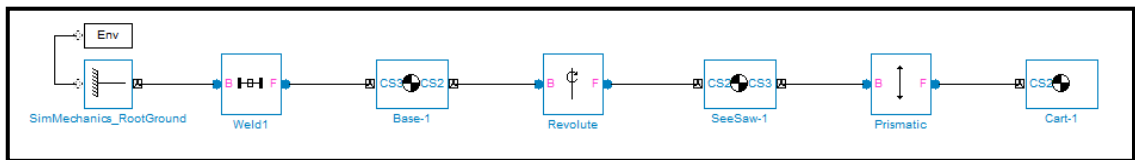


Figure 5.2. Simmechanics blocks of the seesaw system

Next, sensors and actuators are added to the system as can be seen in Figure 5.3.

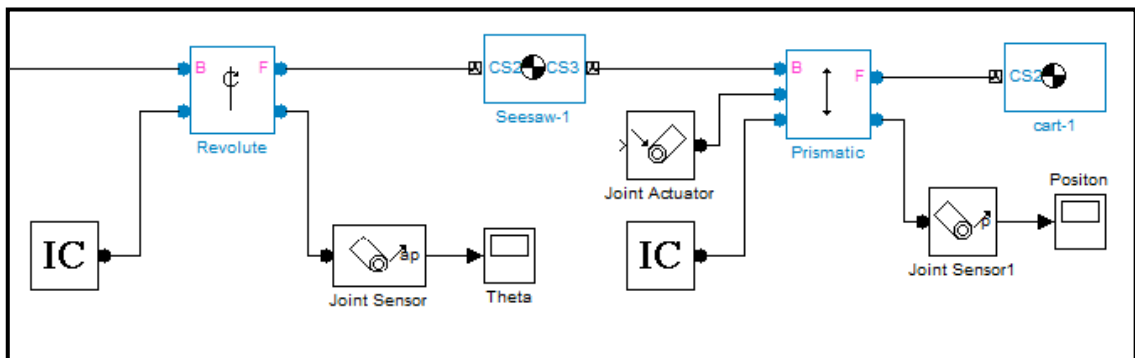


Figure 5.3. Adding sensors and actuator to the system

System has two outputs and one input. Outputs are rotation of the seesaw angle and position of the cart. The only input is sent to the cart via a prismatic joint. Joint actuator is driven by a force input that is calculated by using Equation 5.20.

5.2.1.1.1. Stabilizing the System with Initial Error

In this simulation, initial condition blocks are used to introduce an initial error in the seesaw rotation which results in an unbalanced initial condition. Initial condition for the revolute joint is set to 20 degrees.

Controller is built according to the Equation 5.20. First step is to create e_θ . Since first aim is to stabilize the system, desired angular position of the seesaw system is set to zero as seen in Figure 5.4.

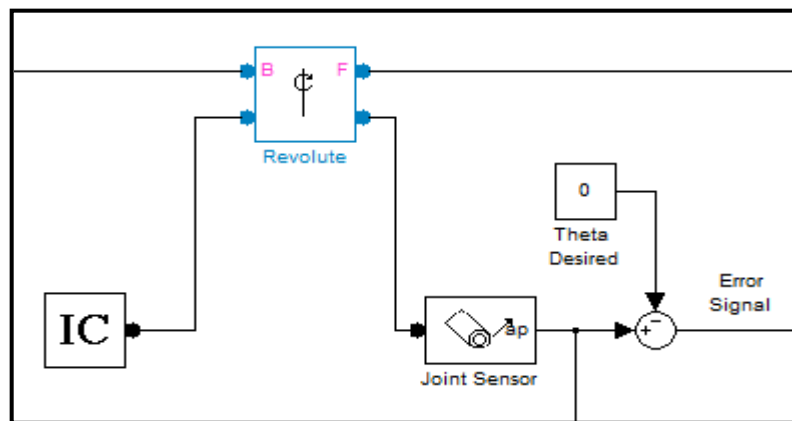


Figure 5.4. Creating the error signal for seesaw rotation

Then control is applied to the e_θ signal. The linear control selected is a Proportional-Derivative (PD) controller. Afterwards, nonlinearities of the system are added to the input signal for the prismatic joint actuation, which drives the cart, as shown in Figure 5.5.

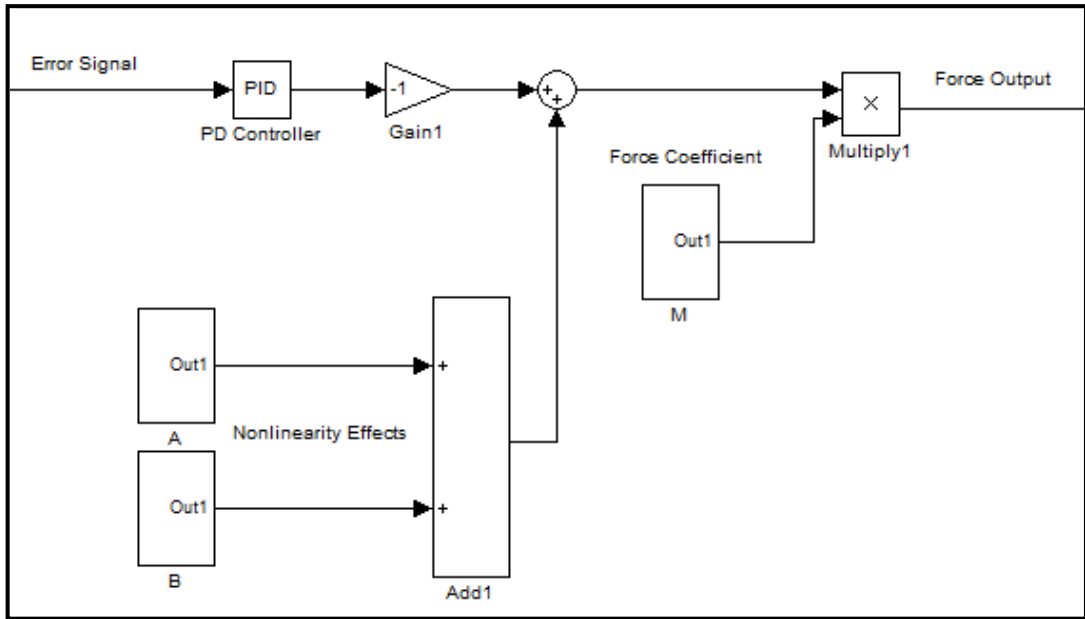


Figure 5.5. Applied controller to the system

In Figure 5.5, A and B boxes are the nonlinearity terms that were determined in equation 5.20 and the M box contains the coefficients in the same equation. A, B, and M matrices are shown in equation 5.26, 5.27, and 5.28 respectively.

$$A = [0 \quad 1] \hat{M}^{-1}(x) \hat{C}(x, \dot{x}) \dot{x} \quad (5.26)$$

$$B = [0 \quad 1] \hat{M}^{-1}(x) \bar{G}(x) \quad (5.27)$$

$$M = \left(\frac{JM_c + M_c^2 p^2}{h M_c} \right) \quad (5.28)$$

Initial condition of the revolute joint is set to 20 degrees and cart initial condition is set to 0 which is the mid-point of the seesaw. In the first trail to set control parameters, K_p parameter is chosen as 10 and K_d parameter is chosen as 0. The result showed that the system tries to balance itself, however, the oscillation on the system remained between ± 30 degrees border, as seen in Figure 5.6.

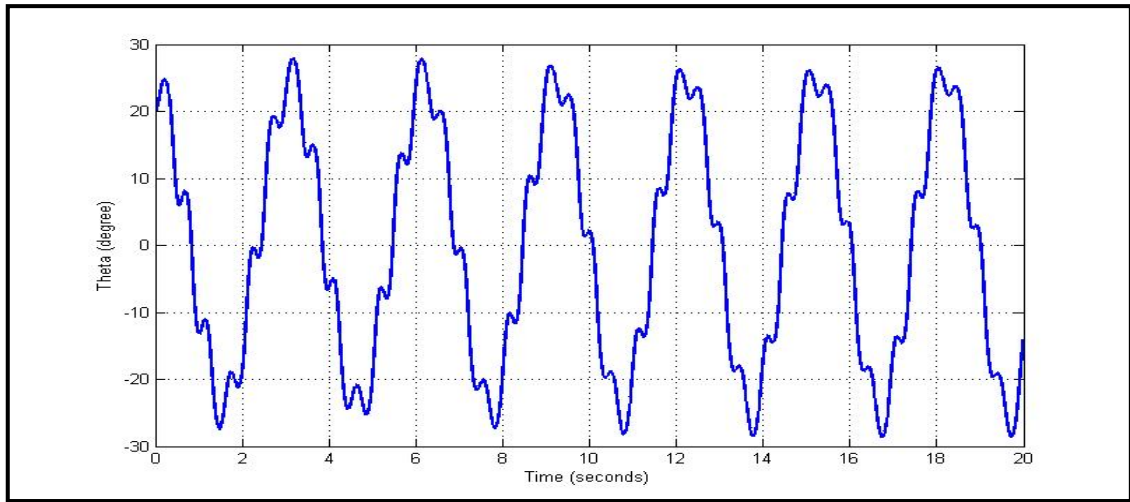


Figure 5.6. $K_p=10$ $K_d=0$, PD controller result

As observed in the figure, system cannot dampen out the response. Therefore, derivative constant of the controller is increased while K_p is held constant. In the first trial, K_d is chosen as 2. Results are shown in Figure 5.7.

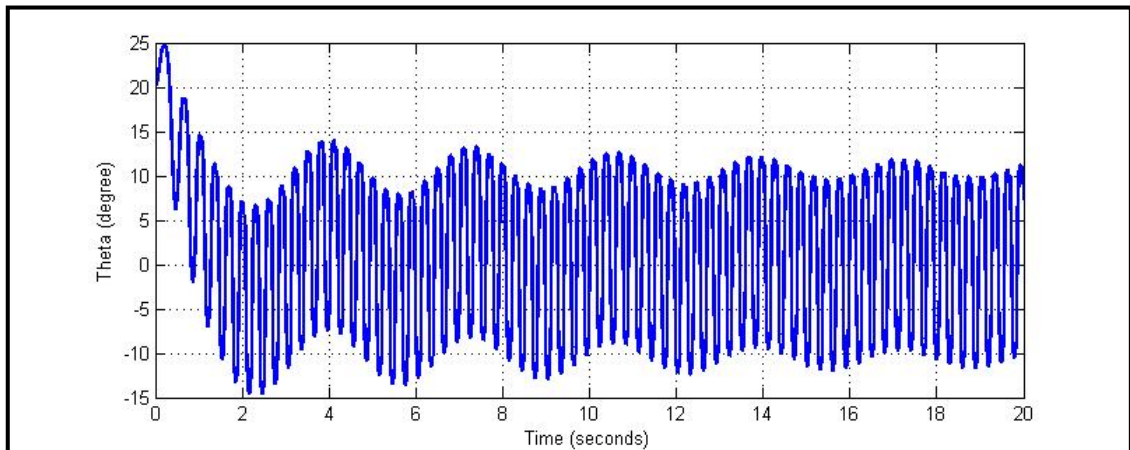


Figure 5.7. $K_p=10$ $K_d=2$, PD controller result

By choosing the K_d parameter as 2, system response is damped to ± 15 degrees border oscillations but still the system response is not acceptable. Therefore, K_d parameter is raised to 8. Results are presented in Figure 5.8.

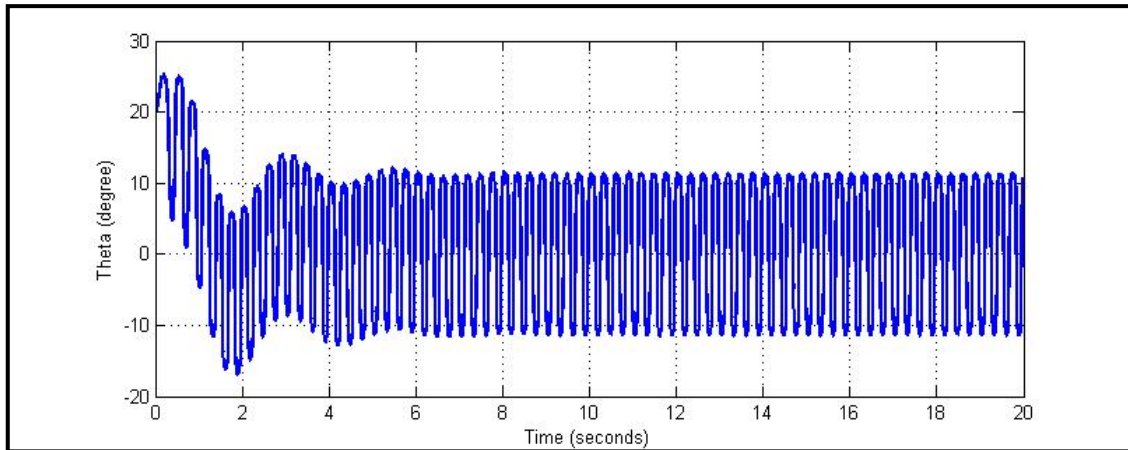


Figure 5.8. $K_p=10$ $K_d=8$, PD controller result

Different K_p and K_d parameters are examined, and best results are obtained when K_p is chosen as 10 and K_d is chosen as 8. As seen in the Figure 5.8, system is not able to stabilize itself but has oscillatory behavior. Seesaw mechanism oscillates around ± 10 degrees. Velocity and acceleration change of the cart is investigated to find the reason of oscillations (Figure 5.9 and 5.10).

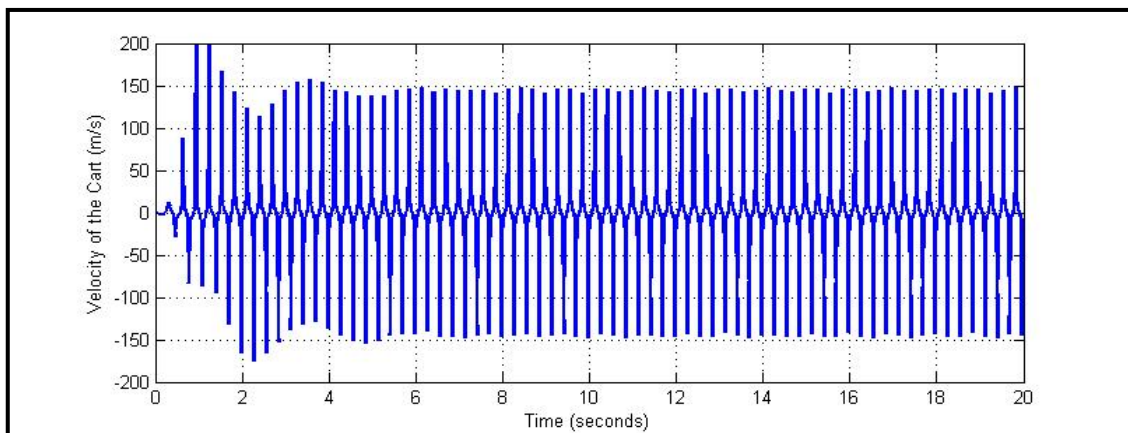


Figure 5.9. Cart velocity change

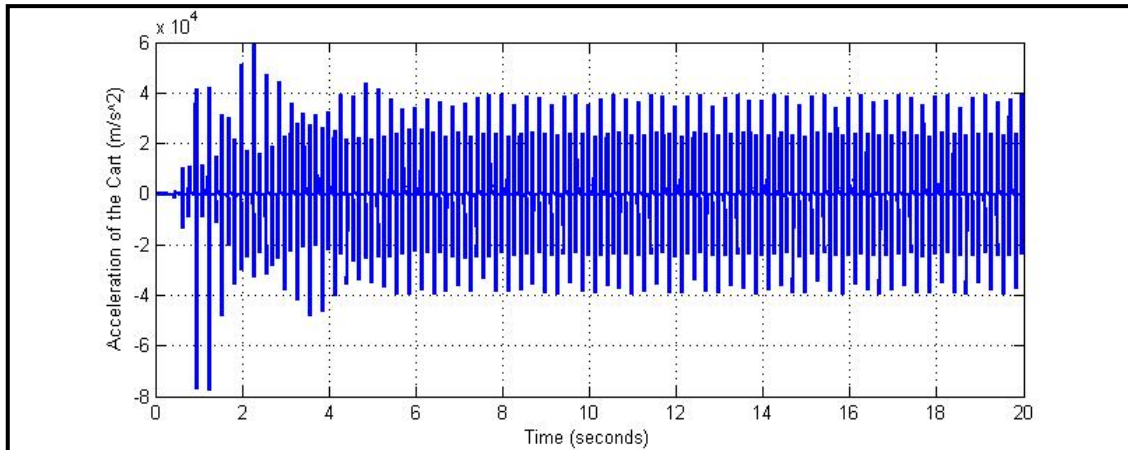


Figure 5.10. Cart acceleration change

As observed in Figures 5.9 and 5.10, acceleration of the cart reaches extreme values. Thus, it creates instability in the system. Acceleration of the cart is provided by the input force, which is shown in Figure 5.11. The only way to control the acceleration of the cart is to apply a saturation to force input. In that case, system is not able to provide enough force return back to the equilibrium point.

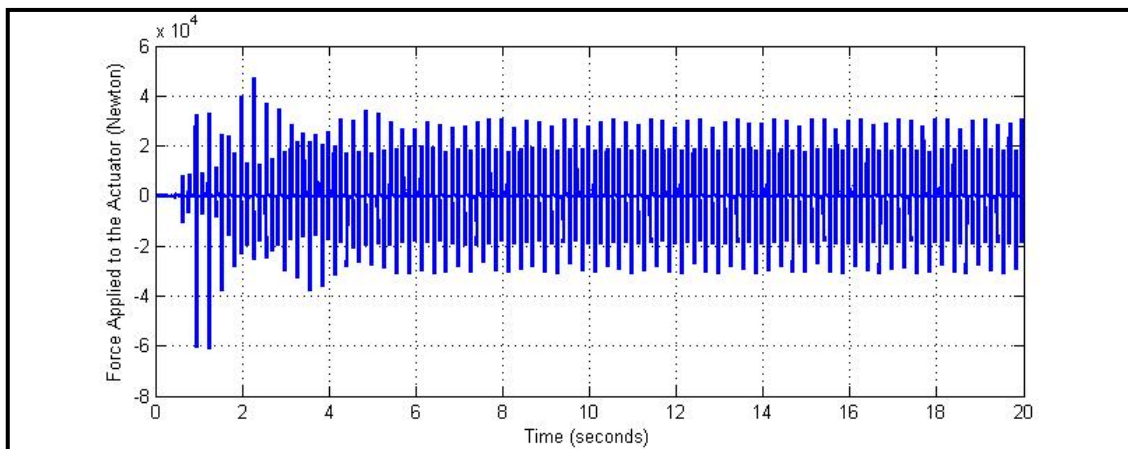


Figure 5.11. Applied force to the cart actuator

The designed controller did not provide satisfactory results. It was not able to stabilize the system at the equilibrium point. The main reason of failure was that developed controller output only depends on the change of the angular position of the seesaw and position data of the cart was only used in the non-linearity cancellation blocks.

Due to the failure of the designed controller, no further tests were conducted and this controller was not tested for 2-DoF seesaw mechanism.

5.2.2. State Feedback Controller (LQR)

In the previous PD controller with non-linearity cancellation, only one variable is controlled, and seesaw angular position and cart position information is only used for the non-linearity cancellation. It is observed that change of the velocity and acceleration of the cart reaches extreme values. It creates instability for the system. Therefore, in the second controller design, the proposed algorithm uses the both feedbacks from the seesaw and the cart.

Linear-quadratic regulator (LQR) is a type of optimal control. In optimal control, a control system (eq. 5.29) and its constraints (eq. 5.30) determine best control strategy for the Equation 5.31 minimize the performance index Equation 5.32.

$$\dot{x} = f(x, u, t) \quad (5.29)$$

$$h(x, u, t) \leq 0 \quad (5.30)$$

$$u = g(x, t) \quad (5.31)$$

$$J = \int_{t_i}^{t_f} L(x, u, t) dt \quad (5.32)$$

In order to apply LQR controller (Figure 5.12), equation of motion is needed to be converted into state space form as seen in Equations 5.33 and 5.34. In order to create state space form, Equation 5.15 is used.

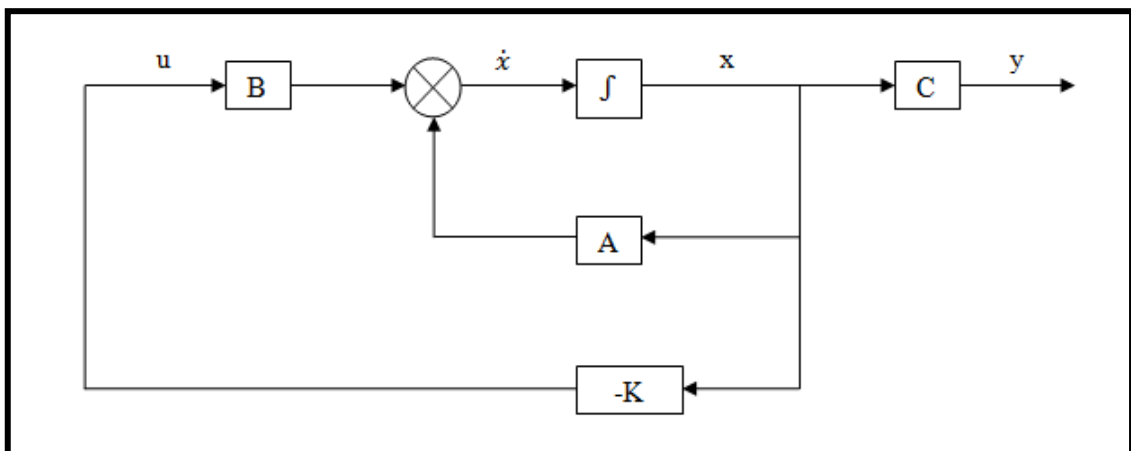


Figure 5.12. LQR feedback configuration

$$\dot{x} = Ax + Bu \quad (5.33)$$

$$y = Cx \quad (5.34)$$

State vector is described as

$$x = \begin{bmatrix} p \\ \dot{p} \\ \theta \\ \dot{\theta} \end{bmatrix} \quad \text{and} \quad \dot{x} = \begin{bmatrix} \dot{p} \\ \ddot{p} \\ \dot{\theta} \\ \ddot{\theta} \end{bmatrix}. \quad (5.35)$$

After the values of \ddot{p} and $\ddot{\theta}$ are found, the system is linearized around the equilibrium point, $p = \dot{p} = \theta = \dot{\theta} = 0$ by using Taylor series expansion. State space matrix is derived for the state vector in equation 5.36. In equation 5.33, u is the control input force, F , and in equation 5.34, y is the output vector $[p \ \theta]$. After the linearization process, A and B matrixes are found as shown in Equation 5.36.

$$\dot{x} = \begin{bmatrix} 0 & 1 & 0 & 0 \\ \left(\frac{-g h M_c}{J}\right) & 0 & \left(\frac{g j - g c h M_s}{J}\right) & 0 \\ 0 & 0 & 0 & 1 \\ \frac{M_c g}{J} & 0 & \frac{M_s g c}{J} & 0 \end{bmatrix} \begin{bmatrix} p \\ \dot{p} \\ \theta \\ \dot{\theta} \end{bmatrix} + \begin{bmatrix} 0 \\ \frac{J+h^2 M_c}{J M_c} \\ 0 \\ \frac{-h}{J} \end{bmatrix} \cdot u \quad (5.36)$$

The Equation 5.36 is in the form of Equation 5.33. And the output matrix is $[p \ \theta]$. By using this information, it is possible to find the C matrix; that satisfies the output as $[p \ \theta]$ as shown in Equation 5.37.

$$C = \begin{bmatrix} 1 & 0 & 0 & 0 \\ 0 & 0 & 1 & 0 \end{bmatrix} \quad (5.37)$$

The result of LQR controller algorithm is a constant gain matrix K which is used as the feedback control parameter (Equation 5.38). In order to close the feedback loop, at the output of the system all states are needed to be available. The resulting closed-loop system is described in Equation 5.38.

$$\dot{x} = (A - BK)x \quad (5.38)$$

K is a constant gain matrix and it is calculated by solving the Algebraic Riccati Equation (5.40) which optimizes the system performance to minimize energy in equation 5.39.

$$J_{LQR} = \int_0^{\infty} x^T(t) Q x(t) + u^T(t) R u(t) dt \quad (5.39)$$

$$A^T S + SA - (SB + N)R^{-1}(B^T S + N^T) + Q = 0 \quad (5.40)$$

In this equation Q and R are symmetric positive-definite matrices which are the controller design parameters. Q matrix is defined in the equation 5.41. Large values of Q penalizes the transients of state values, large values of R penalizes usage of control action (u).

$$Q = C^T \cdot C \quad (5.41)$$

State feedback gain matrix K can be found by using MATLAB[®] software or manually, in equation 5.42 results of the S is derived from the equation 5.40 and result of the equation 5.42 is derived by using this S value. K output depends on the values of Q and R . In this study, R matrix is chosen as a positive number and the Q matrix is formed as seen in Equation 5.43. By changing the parameters of “x” and “y”, the best response for the system is found through simulation tests.

$$K = R^{-1}(B^T S + N^T) \quad (5.42)$$

$$Q = \begin{bmatrix} x & 0 & 0 & 0 \\ 0 & 0 & 0 & 0 \\ 0 & 0 & y & 0 \\ 0 & 0 & 0 & 0 \end{bmatrix} \quad (5.43)$$

5.2.2.1. Simulation Results for Single DoF Seesaw

Seesaw is transferred into the MATLAB[®] Simulink environment as explained in the previous controller design simulations.

In this controller, state variable values of the system are collected and they are multiplied with constant gain matrix K as seen in Figure 5.13.

5.2.2.1.1. Stabilizing the System with Initial Error

In the initial tests, x and y values of Q matrix, and R are chosen as 1. Initial condition for rotational joint is set to 20 degrees. Result of the K constant gain matrix (Equation 5.44) and change in the seesaw angular position are shown in Figure 5.14.

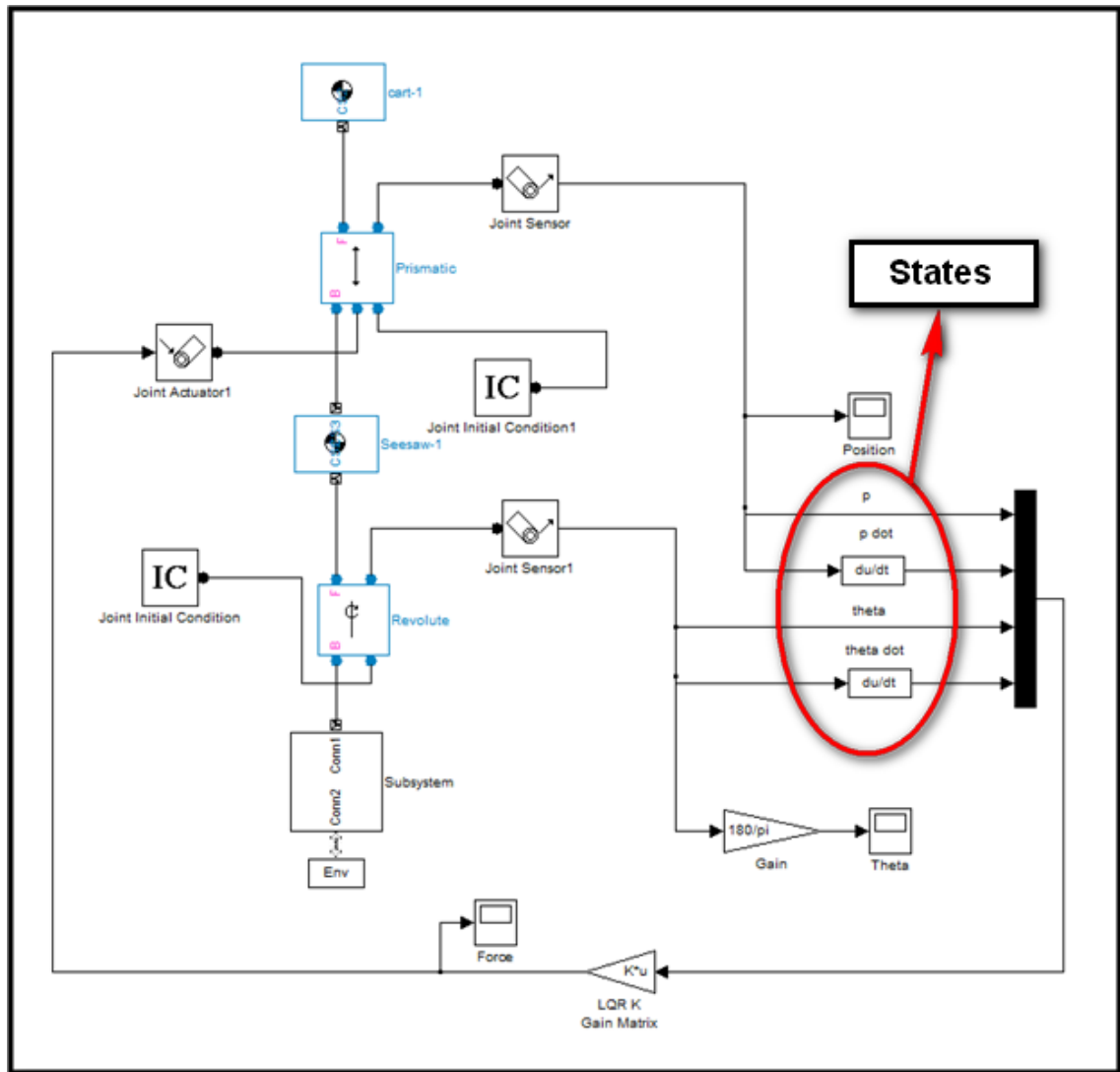


Figure 5.13. LQR control design of the system

$$K = [59.2251 \quad 10.6129 \quad 27.1447 \quad 5.1023] \quad (5.44)$$

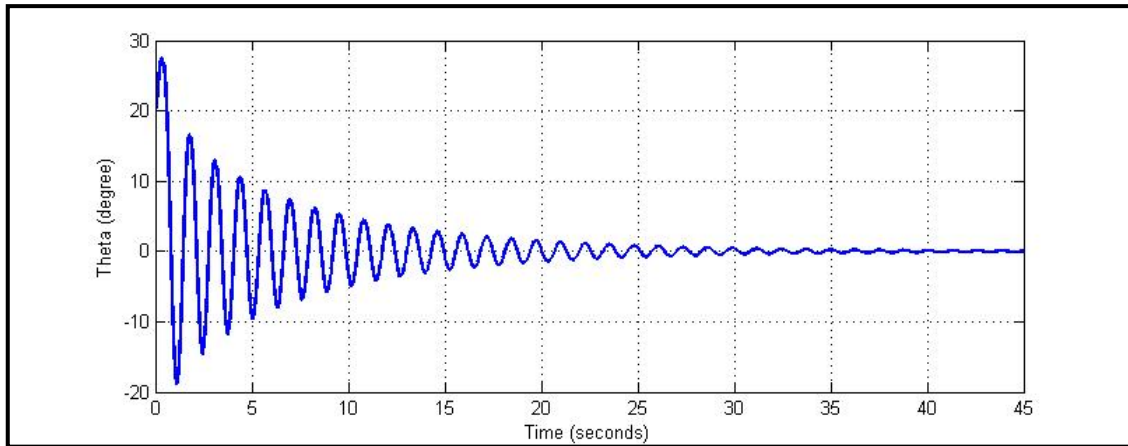


Figure 5.14. LQR controller test for rotation change trial-1

As observed in Figure 5.14, system is able to damp oscillations slowly, and almost in 45 seconds, it reaches the equilibrium point. Angular position of the seesaw reaches nearly 30 degrees. The reason to move away from the equilibrium point at the start of the simulation is because, until the cart initially moves to the location where the moment created by the tilt is balanced, the seesaw starts to rotate more on the tilted direction.

In previous controller, it was observed that applied force to the cart reaches higher values. In this controller method, change in the applied force to the cart can be seen in Figure 5.15.

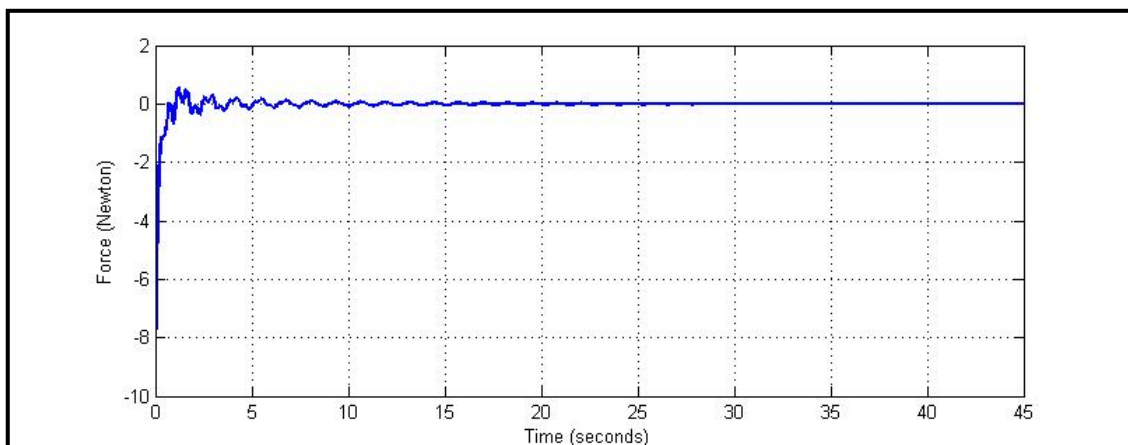


Figure 5.15. Applied force to the cart

LQR controller produces better results in terms of optimized applied force to the cart with respect to the PD controller (Figure 5.11). In contrast with the PD controller,

LQR controller uses both feedback variables as the input parameter for the controller and as a result, it provides better control.

As observed in Figure 5.14, system is able to reach equilibrium in 45 seconds. In order to decrease transition time, weighting matrixes Q and R , are modified. In second trial, R is again selected as 1, and x is chosen as 1000 and y is chosen as 5000. When choosing the control parameters, y was selected to be bigger with respect to the x parameter because y is the control gain applied to the seesaw angular position and our primary aim is to stabilize the seesaw at its equilibrium point. K matrix calculated with these control parameters is presented in Equation 5.45. The result of the trial with the new K is shown in Figure 5.16.

$$K = [284.5118 \quad 29.3717 \quad 133.9345 \quad 29.0764] \quad (5.45)$$

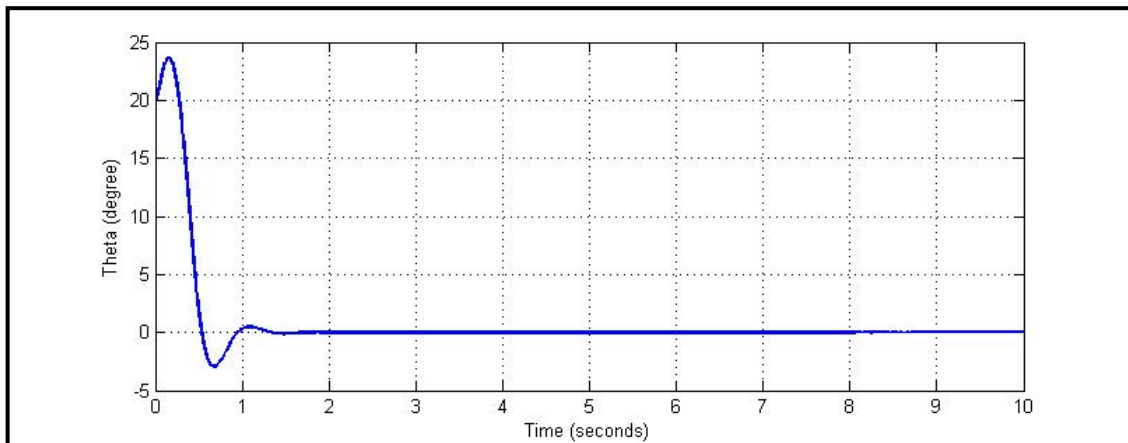


Figure 5.16. LQR controller test for rotation change trial-2

System response is improved with the new values of x and y . System reaches the equilibrium in two seconds and the amount of the overshoot is decreased. As a consequence of increasing the values of x and y , value of the K matrix is increased. Thus, applied force amount is also increased and it almost reaches 40 N (Figure 5.17).

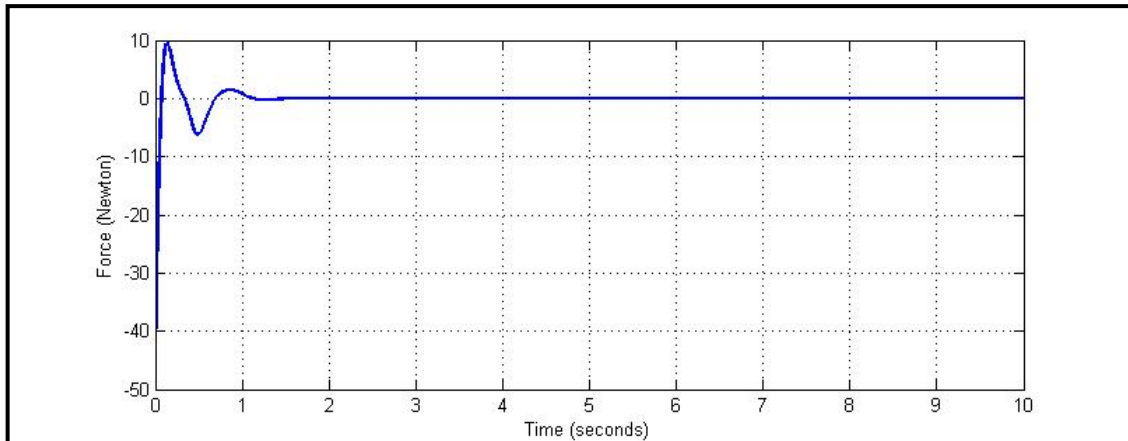


Figure 5.17. Applied force to the cart

In the third trial, x and y values was held constant and value of the R was chosen as 0.001. K matrix is found as presented in Equation 5.46.

$$K = [4.5848 \times 10^3 \quad 0.4155 \times 10^3 \quad 3.2731 \times 10^3 \quad 0.6175 \times 10^3] \quad (5.46)$$

System reaches the equilibrium point quicker with new K matrix values with respect to the previous trials. On the other hand, the amount of applied force to the cart reaches extreme values. As a result of this, cart acceleration reaches very high values with respect to the previous trials. In order to prevent reaching high accelerations, saturation is applied to the force demand for the actuator (limited to ± 100 N which is close to the experimental set-up force limits). Results for both cases where a saturation is applied to the input force (limited force) and no saturation applied to the input force (unlimited force) are shown in Figure 5.18 to 5.20, for rotation angle of the seesaw, force applied to the cart and acceleration change of the cart respectively.

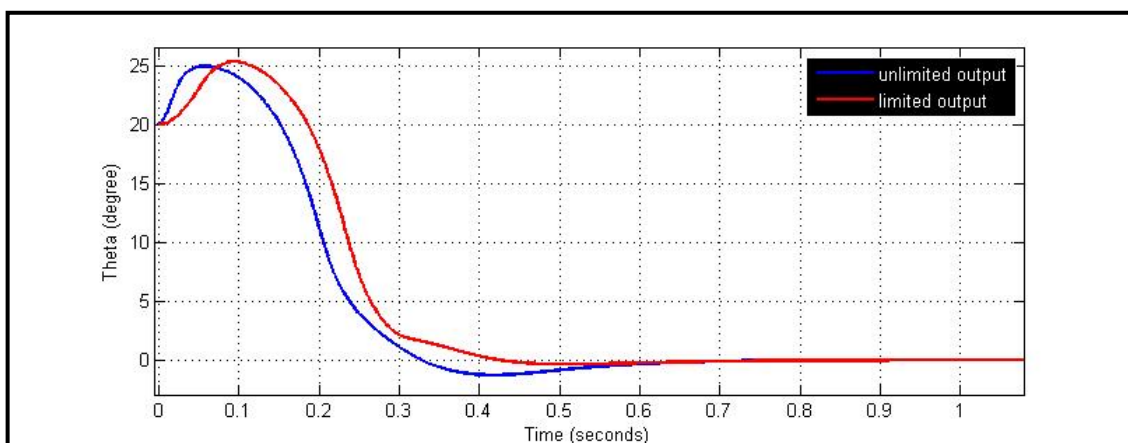


Figure 5.18. LQR controller test for rotation change trial-3 theta change with limited and unlimited force

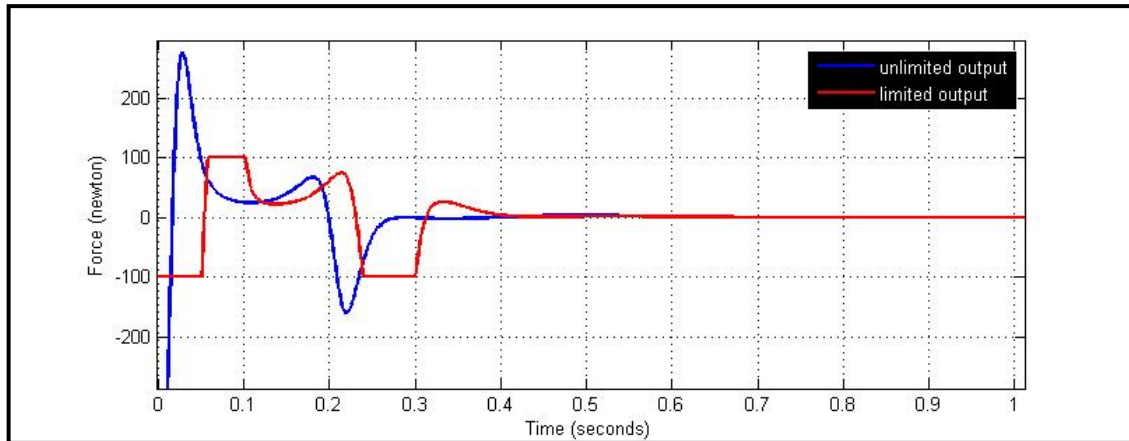


Figure 5.19. Applied force to the cart with limited and unlimited force

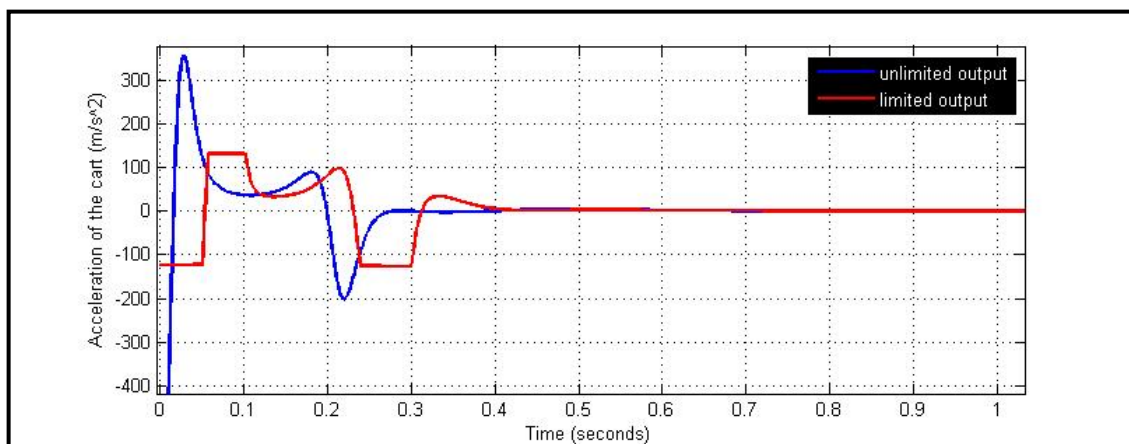


Figure 5.20. Acceleration change of the cart with limited and unlimited force

With the change of the R value, the initial tilt over angle until the cart reaches the first equilibrium point is increased over 25 degrees. On the other hand, steady-state equilibrium is reached in one second. As seen in Figures 5.18 - 5.20, there are two cases examined as limited force (with force saturation) and unlimited force (without force saturation). Force limitation caused a slight increase in the amount of initial tilt over angle as observed in Figure 5.18. However, the system response is improved in the sense of decreasing the overshoot when the system reaches the steady-state equilibrium point.

When the amount of the force applied to the cart is investigated, it is seen that without saturation, amount of the applied force to the cart nearly reaches 1000 N. It results in higher accelerations of the cart. This was an undesired result and it is prevented by using saturation in the actuation forces. With saturation, amount of the

force applied is limited to 100 N and as seen in Figure 5.19 and 5.20. System provides better response with respect to the case where no saturation is applied to the force.

Simulation tests with initial error in seesaw rotation angle indicated that the LQR controller produces satisfactory results. The system is able to stabilize itself in almost one second when an initial error of 20 degrees is present in the system.

5.2.2.1.2. Tracking Control of the System with Set Point

In the second trial, the single DoF seesaw system is stabilized at a certain set-points. In LQR method, the system is linearized at the equilibrium point which was zero for seesaw rotation angle and cart position in the previous sub-section. In order to track a given set point, measured angle information is manipulated to stabilize the system at the desired angular position. In this method, system tries to move the state variables to the equilibrium point. Sensory data manipulation method is shown in the Figure 5.21. A signal generator is added to the system and its set to generate square waves. Magnitude of the waves is limited to 10 degrees and the frequency of the square waves is set to 0.05 Hz. Then, this information is converted into radians to manipulate the sensory data.

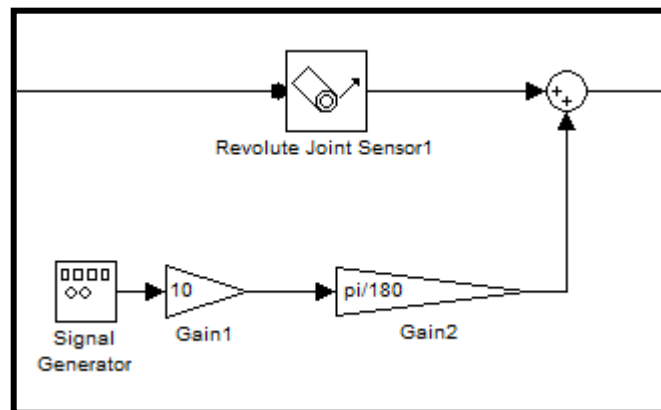


Figure 5.21. Sensory data manipulation method

It is also necessary to manipulate the cart position data after rotation angle data is manipulated. The cart position to balance the system at the given angular position set-point is calculated and is used to manipulate the cart position sensory information. Calculation of the cart position with respect to set angle explained in Figure 5.22 and the following equations.

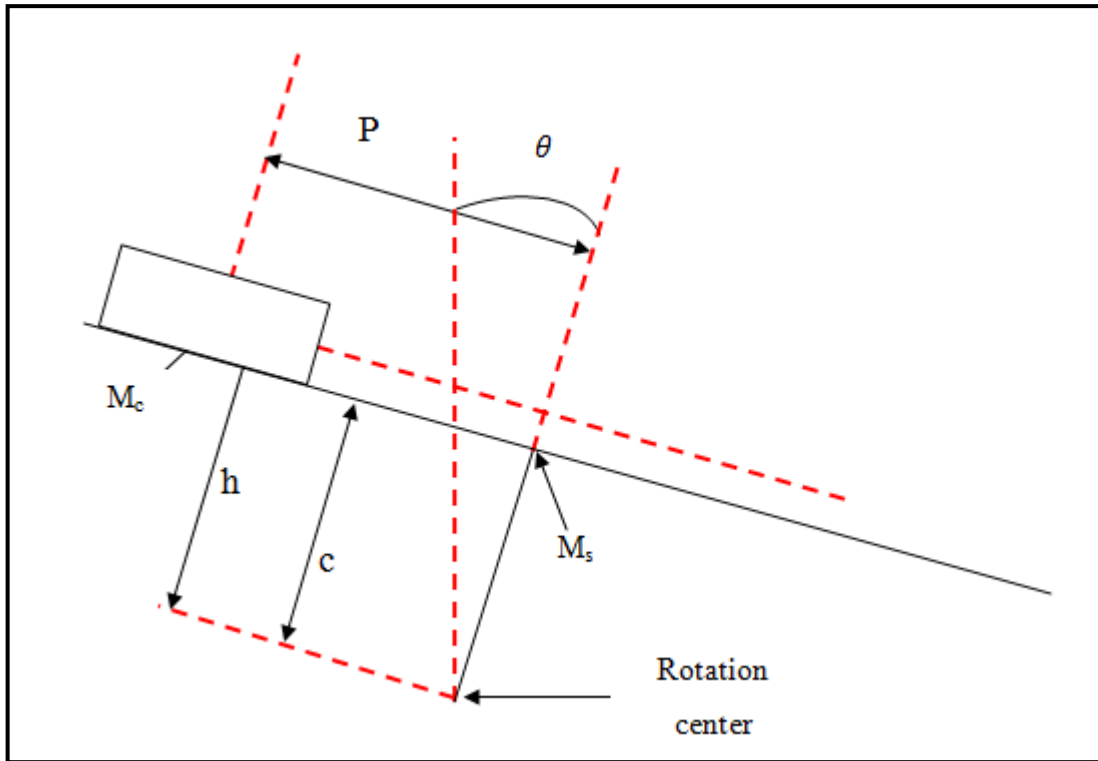


Figure 5.22. Free body diagram of the seesaw system stabilized for a given angular position set-point

Equation derived from Figure 5.22 to stabilize the system at a given angular position set-point is presented in Equation 5.47.

$$M_s c g \sin \theta = M_c g p \cos \theta - M_c g h \sin \theta \quad (5.47)$$

The cart position, p , is then calculated from equation 5.48.

$$p = \frac{M_s c \sin \theta + M_c g h \sin \theta}{M_c \cos \theta} \quad (5.48)$$

The calculated position value with respect to angle change is added to prismatic joint sensor output and tests are conducted for seesaw angular position set-point tracking.

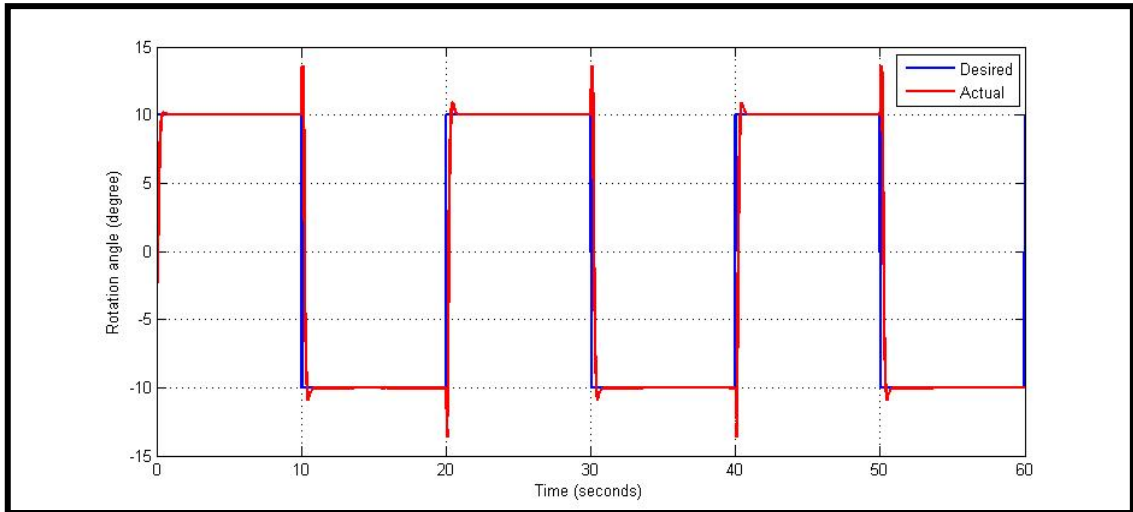


Figure 5.23. Desired and actual orientation of the seesaw

The proposed control method provided satisfactory results for set-point tracking as can be observed in Figure 5.23. A closer look to the response of the system can be seen in Figure 5.24.

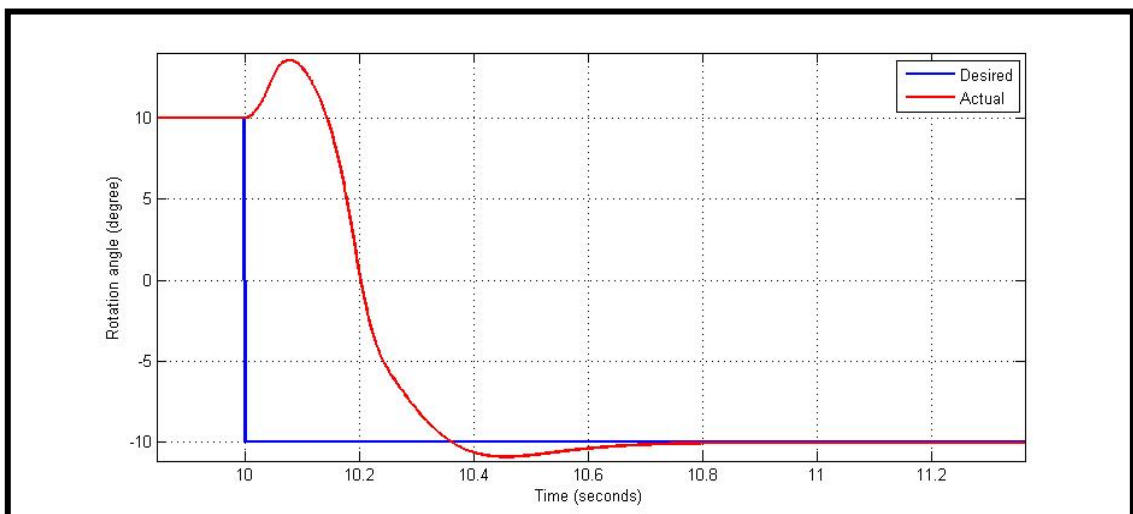


Figure 5.24. Desired and actual orientation of the seesaw (focused view)

As observed in Figure 5.24, system shows a quick response to the demand and reaches the desired position in a second and able to keep its position at the desired angle. Rotation angle information acquired from the joint sensor and modified by the set-point angle, which is sent to the state vector, can be seen in Figure 5.25.

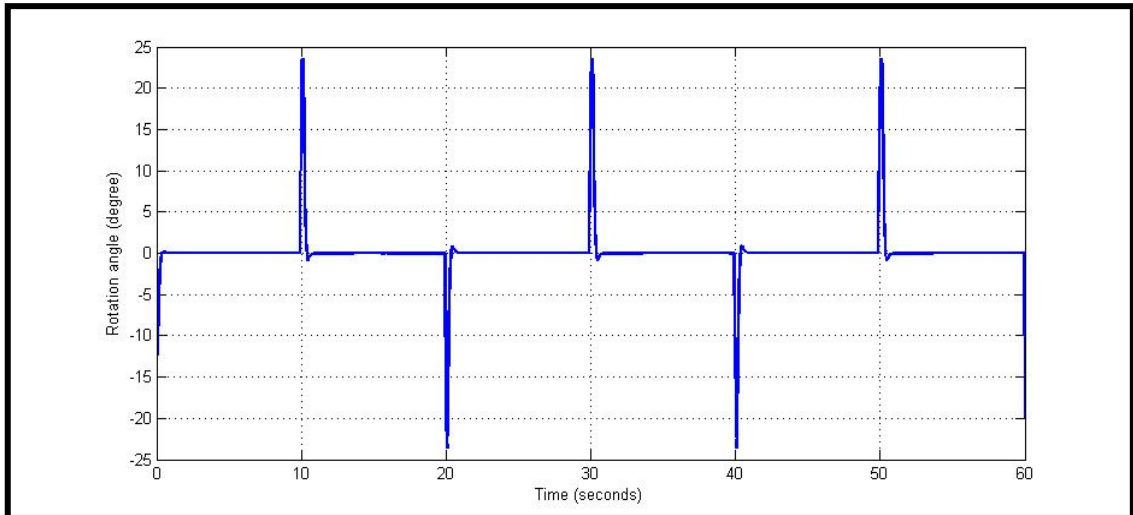


Figure 5.25. State input of the theta with a set point

The equilibrium point of the system is shifted as a result of the square wave demand. When the system reaches the new equilibrium point the seesaw input rotation angle modified as a state vector converges to zero.

5.2.2.1.3. Stabilizing the System under Disturbance

One of the goals of the study is to develop hovering-mode control of the vehicle which experiences external disturbances such as underwater currents. Therefore, the system is tested under disturbance. It is expected that system will absorb the disturbance by changing the center of gravity with respect to direction and magnitude of the disturbance.

In order to create the disturbance in simulation studies, another joint actuator is connected to the revolute joint of the seesaw (Figure 5.26). A signal generator is inserted to the simulation to generate sine waves. The reason to choose sine wave is to imitate the underwater currents. However, the magnitude of the waves is selected so that the moment created by moving the cart can compensate this disturbance. The frequency of the sine wave is limited with the acceleration profile of the cart which is related with the maximum amount of the forces that can be applied to the cart. The frequency of the sine wave also depends on the delays in the response of the electro-mechanical equipment used in the system. However, the delays in the electro-mechanical components are not considered in this thesis.

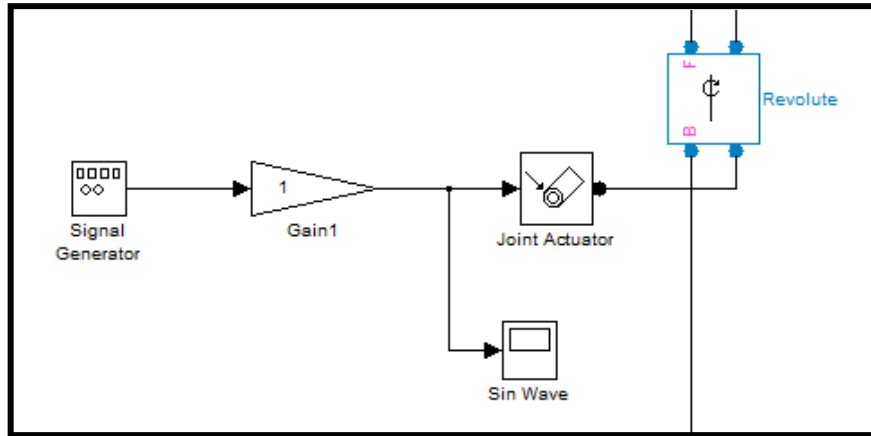


Figure 5.26. Addition of disturbance to the system

Maximum torque amount that can be compensated by the system is calculated to select the magnitude limits of the sine wave. Maximum distance of the cart from the center is measured as 0.45 m in the experimental system. Mass of the cart is 0.8 kg. With these information, maximum torque amount is found as 3,53 N-m. The magnitude of the disturbance is chosen as 1 N-m and frequency is set to 0.1 Hz. Result of the first test is shown in Figure 5.27.

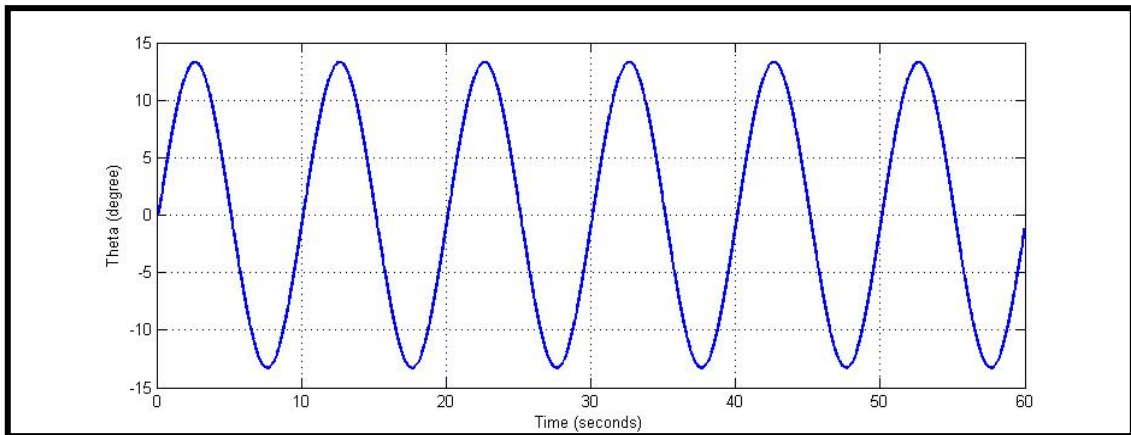


Figure 5.27. Response of the system under disturbance

Figure 5.27 shows system is unable to absorb disturbance with customary LQR controller and it needs to be modified.

Modification starts with the addition of an observer to the system. Observer is a state estimation tool. It is used when the states of the system are not immediately available. Thus, an observer is required to estimate the states of the system accurately.

The state equations of the observer are shown in Equations 5.49 and 5.50. Schematic representation of the system including the observer is shown in Figure 5.28.

$$\hat{x} = A\hat{x} + Bu + L(y - C\hat{x}) \quad (5.49)$$

$$\hat{y} = C\hat{x} \quad (5.50)$$

This is a full order state observer. It has two inputs, u and y and one output \hat{x} . In this system, A , B and u is known as the mathematical model of the system is available. Design of the observer becomes easier as the mathematical model of the system is known and it provides accurate results around the linearized point.

As seen in Figure 5.28, observer is added to the as a mathematical replica of the real system and a correction term is added. Correction term is a constant gain matrix, L . Difference between the output of the real system (plant) and estimated system (observer) is supplied to the system continuously.

The L gain matrix can be found by using the pole placement method by using the place command of the MATLAB[®]. First of all, poles of the system are found by using the Equation 5.51. With respect to these poles, observer gains are found as presented in Equation 5.52 for the system.

$$eig(A - BK) \quad (5.51)$$

$$L = \begin{bmatrix} 163.3 & 11 \\ 6658.8 & 96.7 \\ 9 & 162.7 \\ 138.5 & 6630.5 \end{bmatrix} \quad (5.52)$$

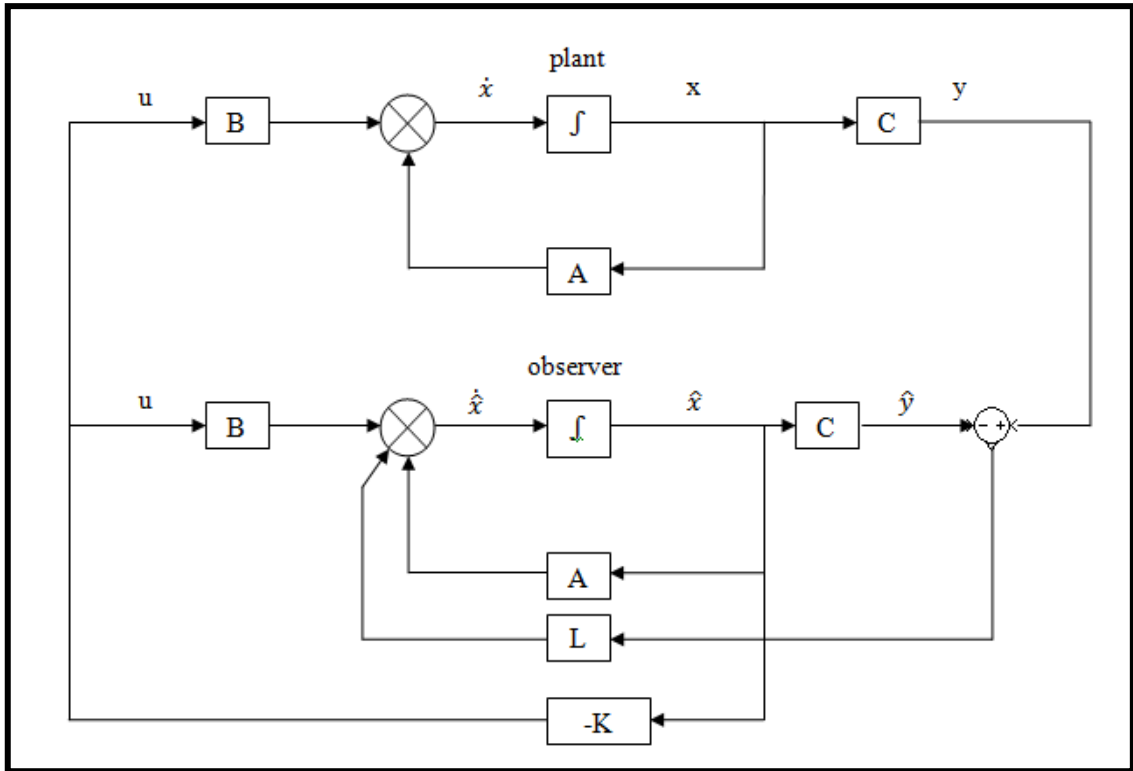


Figure 5.28. Schematic of state space controller using an observer

The transferred system from SolidWorks[®] to MATLAB[®] Simulink consists of the Simmechanics blocks to present the mathematical model of the system (Figure 5.12). In order to add observer to the system, the mathematical model is created by using the standard Simulink blocks. Mathematical (state-space model) model of the system is shown in Figure 5.29

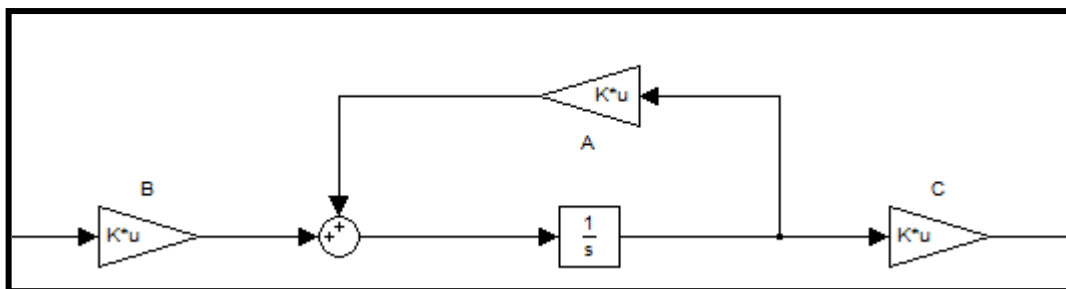


Figure 5.29. Mathematical model of the system

Mathematical model is modified with addition of the observer gain. Model with addition of the observer can be seen in Figure 5.30.

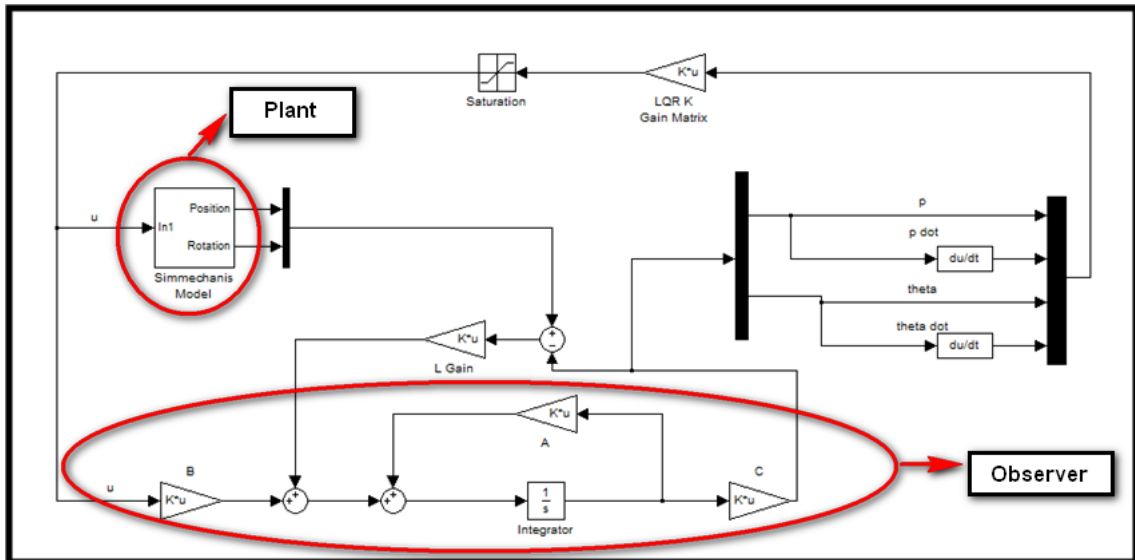


Figure 5.30. Single DoF seesaw with observer

The responses of the LQR with observer controller and the customary LQR controller are compared when initial error is present in the system. In both simulation tests, initial condition is set to 20 degrees. Performances of the controllers are shown in Figure 5.31.

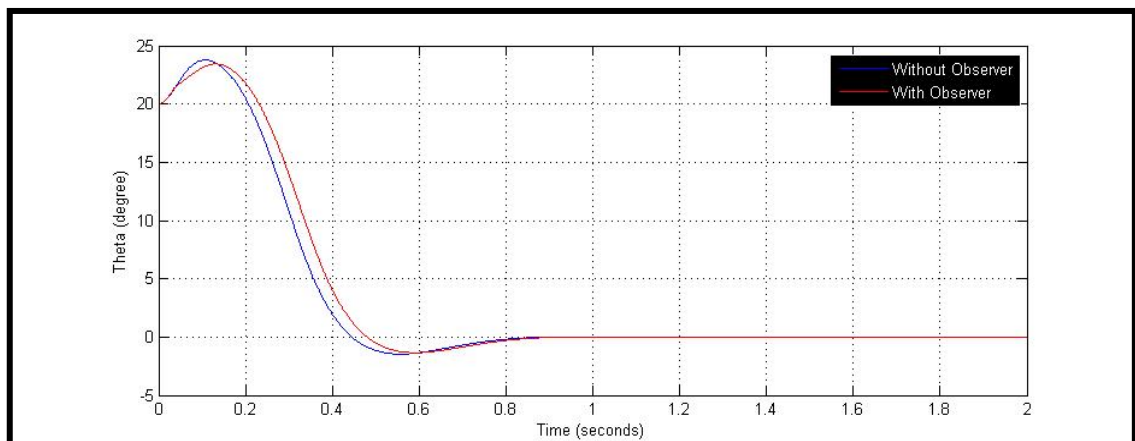


Figure 5.31. Comparison of the system with and without observer

As seen in Figure 5.31, system with observer gain successfully estimates the states of the system. In this controller, it is assumed that all data is noise- and disturbance-free. This is not possible in real life, therefore, it is required to modify the Observer gain as a Kalman gain to reject disturbances. Also, in that condition, it is possible to introduce the underwater currents as disturbance or noise. State equations are re-written as in the Equation 5.53 and 5.54.

$$x = Ax + Bu + Gw \quad (5.53)$$

$$y = Cx + Gw + v \quad (5.54)$$

In equation 5.53 and 5.54, w can be defined as a stationary process noise, and v is the sensor noise. Application of the Kalman filter is similar to the application of the observer. The known inputs and outputs are again used to estimate the states of the system. Connection of Kalman filter to the plant is explained in the Figure 5.32.

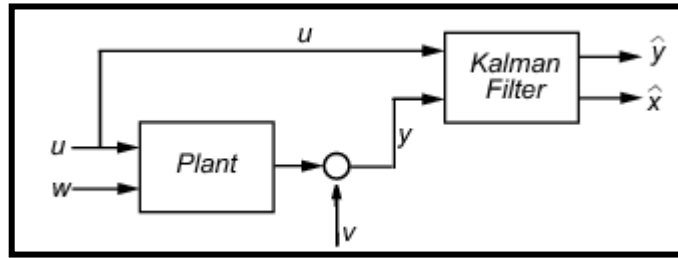


Figure 5.32. Kalman filter implementation to the plant
(Source: MathWorks, 2011)

The Kalman filter is essentially a set of mathematical equations that implement a predictor-corrector type estimator. The mean square estimation error is given by

$$J = E [(x(t) - \hat{x}(t))^T (x(t) - \hat{x}(t))], \quad (5.55)$$

where

$$E [(x(t) - \hat{x}(t))^T y(t)] = 0. \quad (5.56)$$

The optimal Kalman gain is given by

$$L(t) = S_e(t)C^t R^{-1}, \quad (5.57)$$

where $S_e(t)$ is the same as J given in Equation 5.55. The Algebraic Riccati Equation can be written for $\dot{S}_e(t) = 0$ as shown in Equation 5.58.

$$0 = S_e A^T + A S_e + Q_n - S_e C^T R_n^{-1} C S_e \quad (5.58)$$

Where Q_n and R_n are the process and measurement noises respectively. By tuning these parameters, it is possible to change Kalman gain, L . After a number of trials, Q_n and R_n matrices are defined as

$$Q_n = 1 \quad (5.59)$$

$$R_n = \begin{bmatrix} 0.001 & 0 \\ 0 & 0.001 \end{bmatrix}. \quad (5.60)$$

With respect to chosen Q_n and R_n parameters, L gain matrix found as

$$L = \begin{bmatrix} 8.1537 & 3.0668 \\ 37.9442 & 7.3068 \\ 3.0668 & 12.2099 \\ 55.1448 & 79.2433 \end{bmatrix}. \quad (5.61)$$

Equation 5.61 is replaced with observer gain, and system is again initiated with a 20 degree initial error. The result is shown in Figure 5.33.

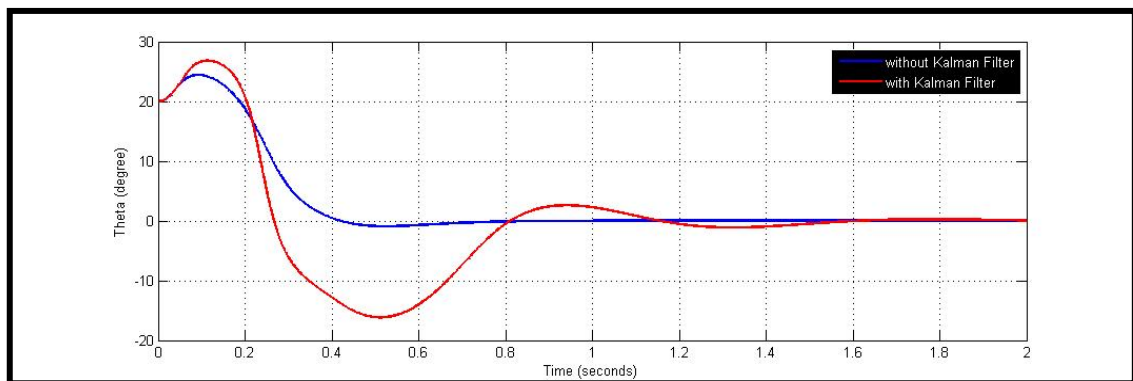


Figure 5.33. Comparison of the system with and without Kalman filter

After Kalman filter is implemented to the noise-free system, transition time of the seesaw system has increased but it is still under two seconds. Next test is conducted for the system with the disturbance. Amount of disturbance is set to 1 N-m and frequency to 0.1 Hz, which is the same disturbance applied to the customary LQR controller (Figure 5.27).

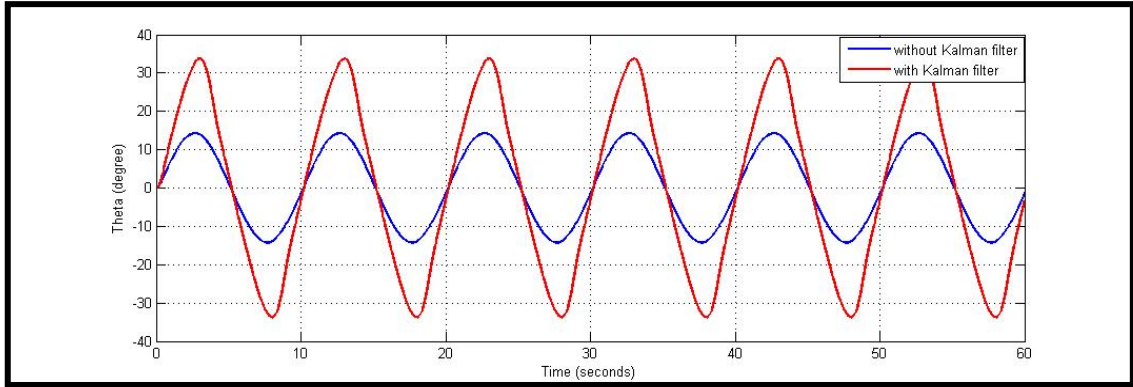


Figure 5.34. Comparison of the system with and without Kalman filter under disturbance - 1

The system response was worse with the chosen Q_n and R_n parameters for the Kalman gain. Therefore, these parameters are tuned and determined as follows after a number of trails.

$$Q_n = 2 \quad (5.62)$$

$$R_n = \begin{bmatrix} 0.6 & 0 \\ 0 & 0.01 \end{bmatrix} \quad (5.63)$$

L gain matrix is found as in Equation 5.64 by using the selected parameters in Equations 5.62 and 5.63. The system is able to absorb the applied disturbance better with respect to the initial selection of the Kalman gain parameters and the Observer controller without the Kalman gain.

$$L = \begin{bmatrix} 0.1551 & 7.5642 \\ 0.4888 & 23.2681 \\ 0.1261 & 15.8078 \\ 1.6247 & 125.420 \end{bmatrix} \quad (5.64)$$

The system response comparison for using the Kalman gain is shown in Figure 5.35.

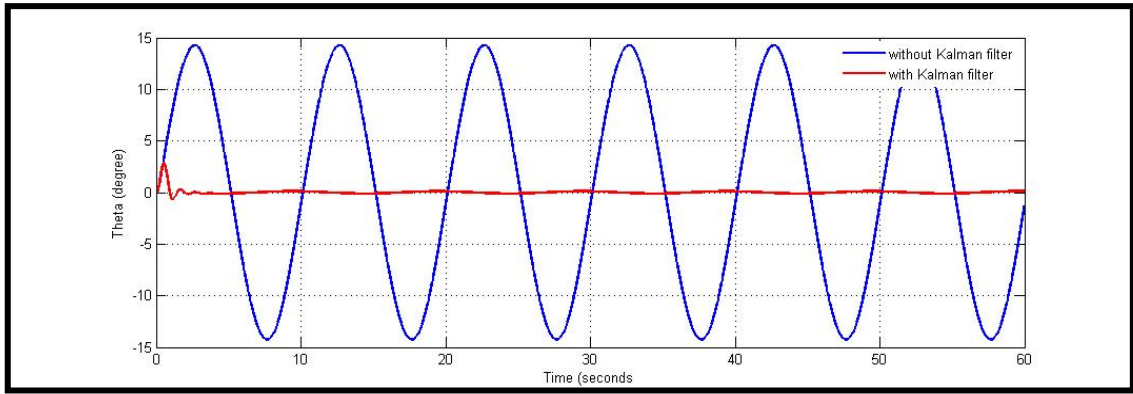


Figure 5.35. Comparison of the system with and without Kalman filter under disturbance - 2

A closer look to the system response for the controller with Kalman filter is shown in Figure 5.36.

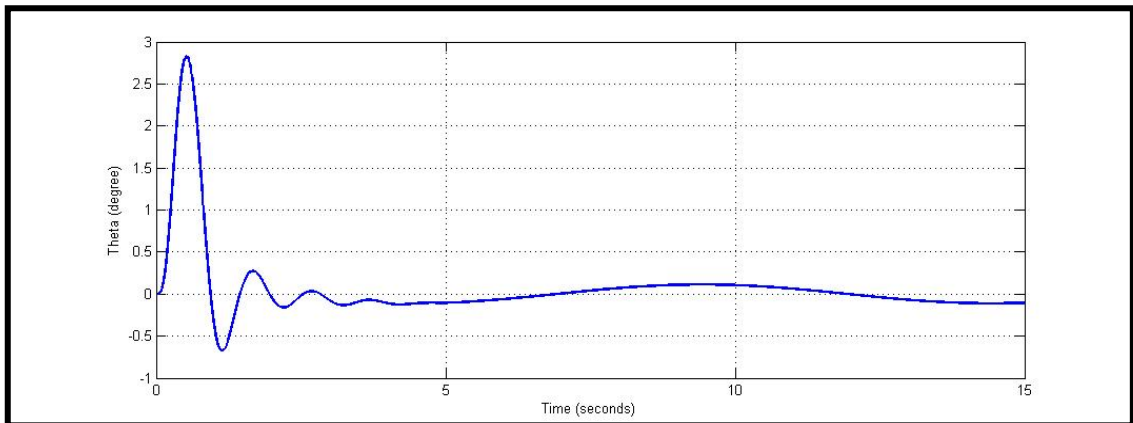


Figure 5.36. Reaction of the controller with Kalman filter under disturbance

As seen in Figure 5.36, system is minimizing the effect of the disturbance in five seconds and the amount of the rotational oscillation of the system is bounded within ± 0.15 degrees band. Position change of the cart is shown in Figure 5.37.

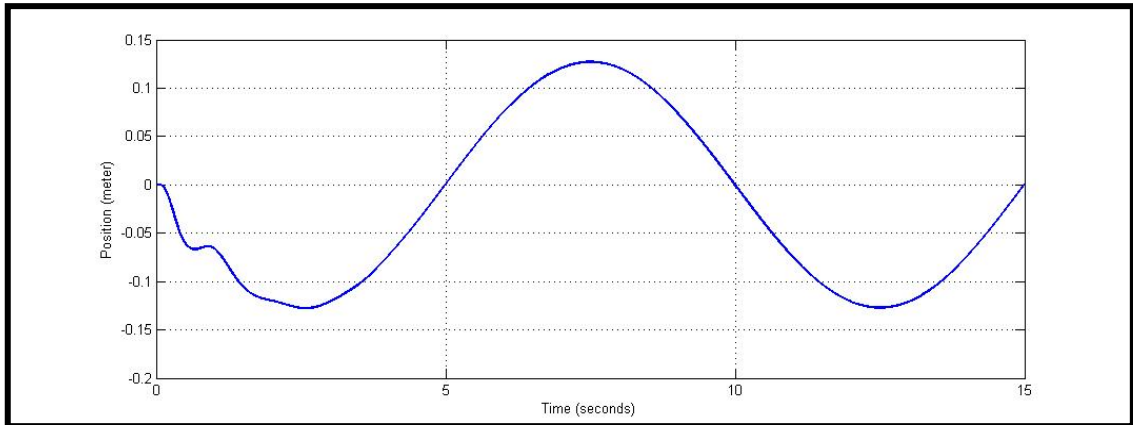


Figure 5.37. Position change of the cart mass under disturbance

Cart position change is a sine wave after five seconds which is expected as it follows the disturbance profile. The maximum distance of the cart from center is 0.1271 m which provides 0.9975 N-m of torque to the system which is almost same as the disturbance magnitude. Overall, the controller with the Kalman gain is able to absorb disturbance and limit its effect within an acceptable tolerance band.

5.2.2.2. Simulation Results for Two DoF Seesaw

The designed LQR controller with modifications for the single DoF seesaw system has shown its robustness through various tests. In this part, this controller is examined for the 2-DoF seesaw system.

5.2.2.2.1. Stabilizing the System with Initial Condition

Simulation studies of the system are initiated with the control of only one rotation axes and other revolute and prismatic joint is position is kept constant.

First, rotation about z-axis is tested. Therefore, the position of revolute joint, which rotates about x-axis, and prismatic axis, which moves along z-axis, are kept constant. In order to do that, joint actuators are connected to these joints as seen in Figure 5.38 that act as breaks for the motion of these joints.

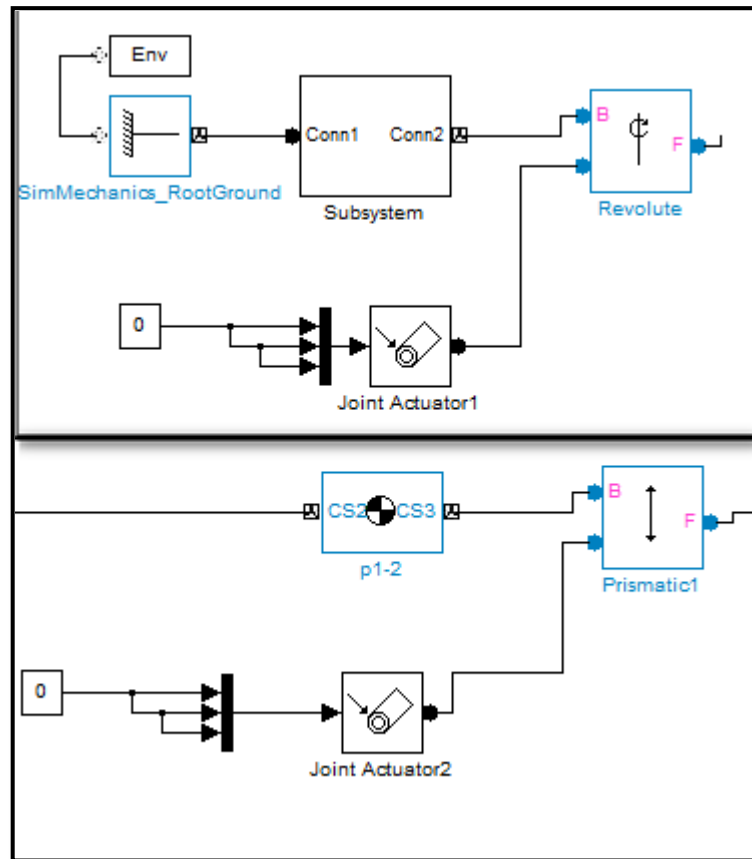


Figure 5.38. Fixed prismatic and revolute joints

After the DoF of the system is reduced to one, it is expected to see a similar reaction to the customary seesaw system. Initial error is set to 10 degrees and the same procedure that was used in customary seesaw tests is applied to this system and result of the simulation test is given in Figure 5.39 to 5.41

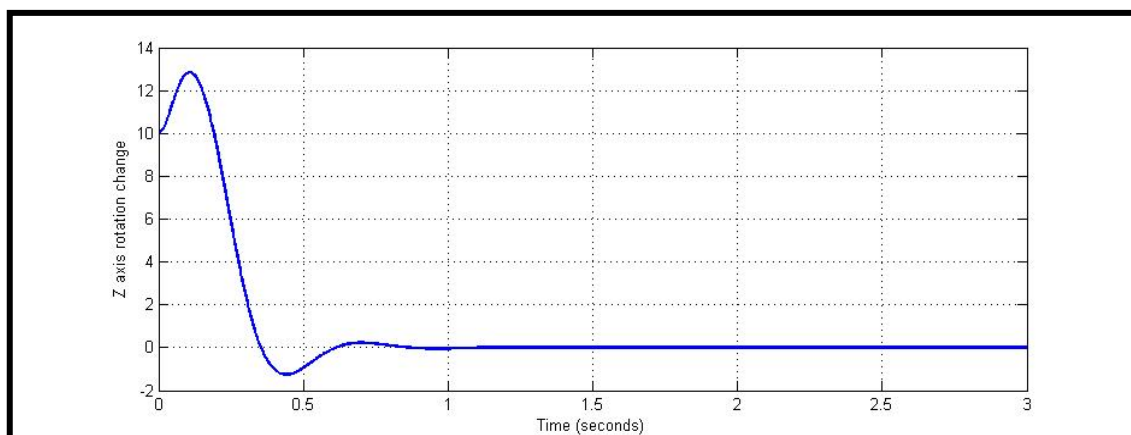


Figure 5.39. Rotation around Z change with a given initial condition

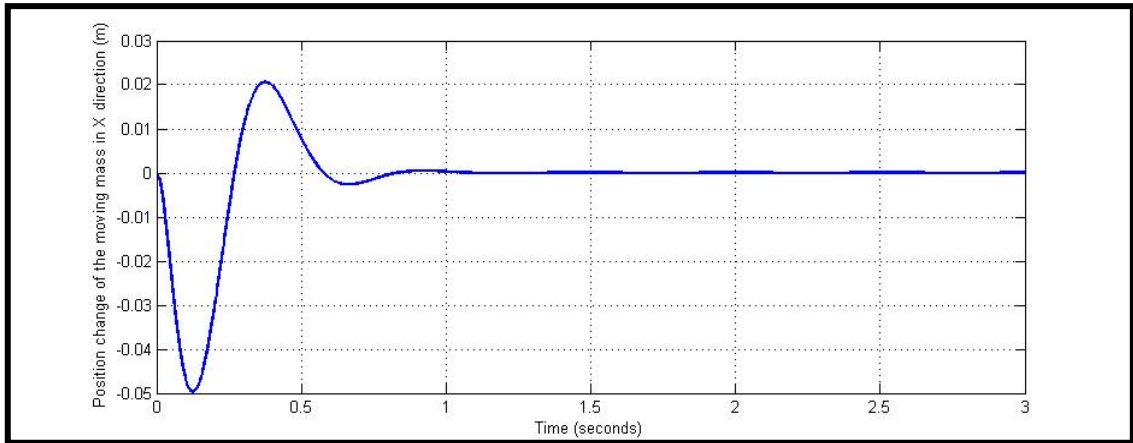


Figure 5.40. Position change of the moving mass in X direction

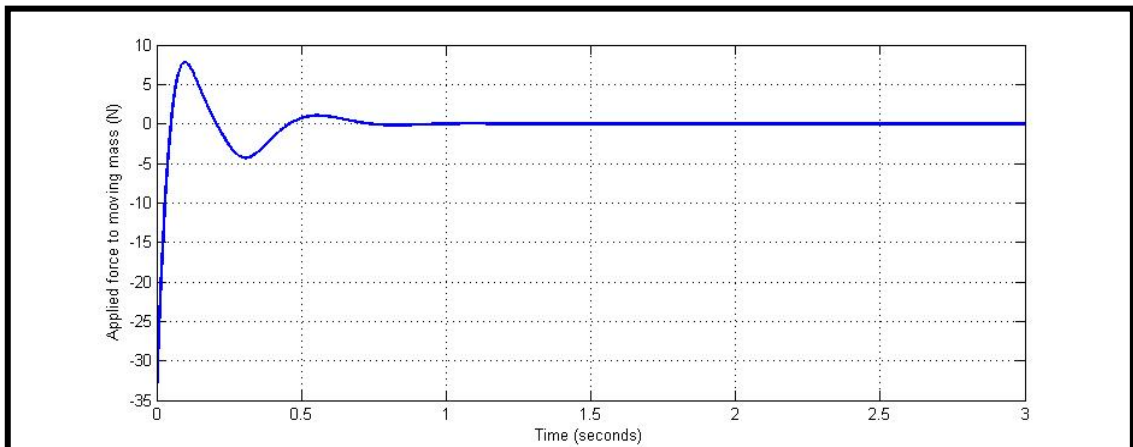


Figure 5.41. Applied force to the system (X)

Figures showed that the system can be stabilized when it experiences initial errors as seen in Figure 5.39. System reaches nearly 13 degrees with a given initial error of 10 degrees until the cart can reach the first equilibrium point. System is able to reach the equilibrium (steady-state) to in one and a half second. Applied force to moving mass does not exceed the 35N.

In the second phase, rotation around x-axis is examined, and similarly z-axis rotation and motion in the x-axis direction is kept constant. Initial error for the system is set to 10 degrees. System response is shown in Figure 5.42 to 5.44.

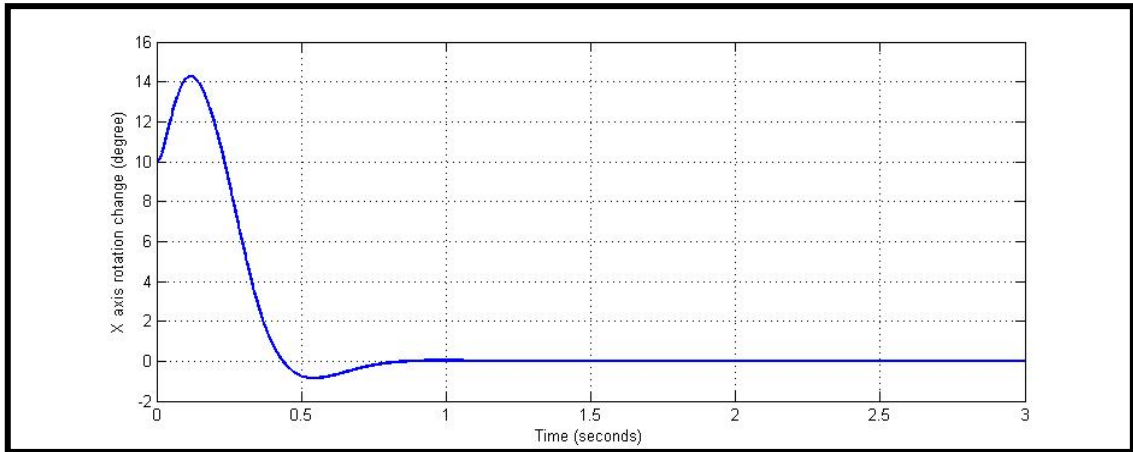


Figure 5.42. Rotation around X change with a given initial condition

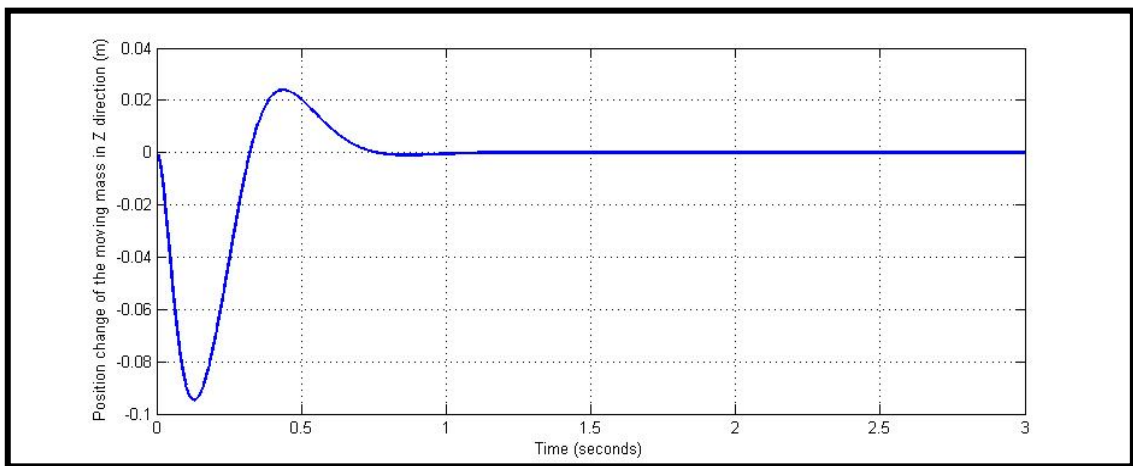


Figure 5.43. Position change of the moving mass in Z direction

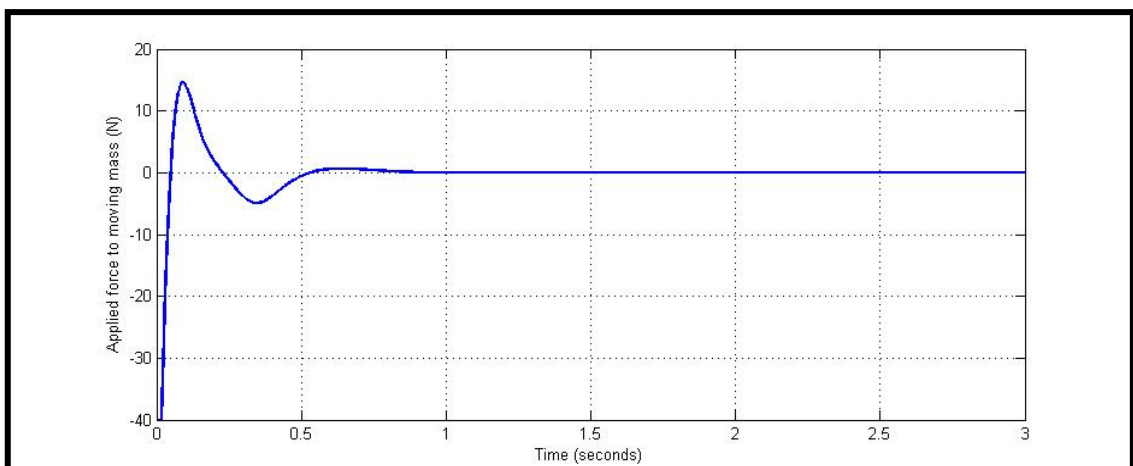


Figure 5.44. Applied force to the system (Z)

The total mass carried by the cart along z-axis direction and the seesaw rotation about x-axis is more than the previous case. Also, center of gravity is located farther

away from the rotation axis with respect to the previous case. This result in the slight decrease in the system performance and until the cart initial equilibrium point, the seesaw rotation angle tilted more to 14 degrees. System reaches the equilibrium in less than one and a half second as seen in Figure 5.42. Applied force to the cart does not exceed 40 N.

In these tests, system is tested for two rotations separately. Initial errors are set to 10 degrees and system is able to reach the equilibrium in less than one and a half seconds for both z-axis rotation and x-axis rotation tests. Designed LQR controller is proved to be successful for both DoF independently.

Since the system has a de-coupled design, proposed LQR controller should be able to stabilize the system when two revolute joints are tested with an initial error. Simulation test when two DoF are active is conducted and the results are shown in Figure 5.45 and 5.46.

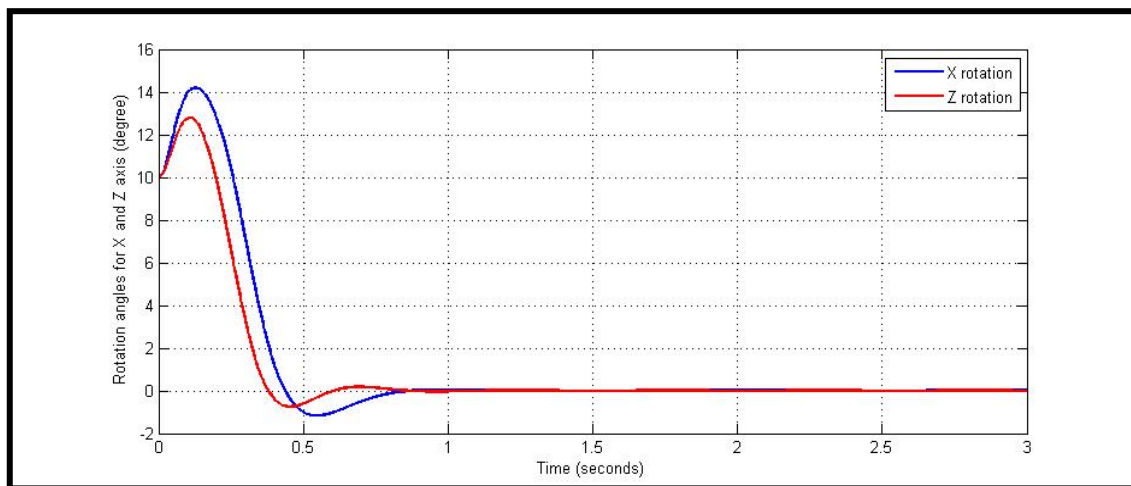


Figure 5.45. Theta change of the system in X and Z direction

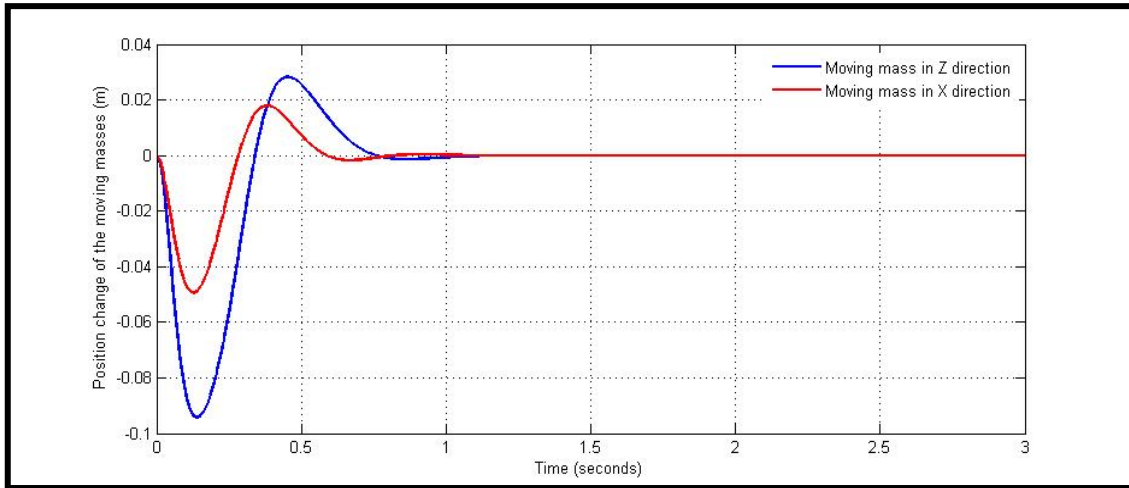


Figure 5.46. Position change of the moving masses in X and Z direction

In Figure 5.45, it is observed that system can reach the equilibrium in one and a half second similar to the test results with single DoF case. This was an expected result since the DoF of the system are uncoupled. Therefore, customary LQR controller is also shown to be successful to stabilize the system with a given initial error in both DoF when no disturbance is present in the system.

5.2.2.2.2. Tracking Control of the System with Set Point

Second set of tests for the 2-DoF seesaw is conducted to evaluate the steering performance of the system. As explained earlier, internal moving masses are not only used for stabilization but also for steering the underwater vehicle. In this experiment, demand for the rotation angle is a square wave in order to observe the system's step response.

Similar to the single DoF seesaw system, by manipulating the sensory data, the equilibrium point of the system is shifted to corresponding steering demand angle. Angle demand is created via signal generator and the magnitude of the wave is set to 5 degrees and frequency to 0.1 Hz. With respect to demand for rotation angle, necessary position of the cart to keep the system in balance is calculated as explained previously for single DoF seesaw system and added to the cart position sensory data. Simulation results for the motion on both joints can be seen in Figures 5.47 and 5.48.

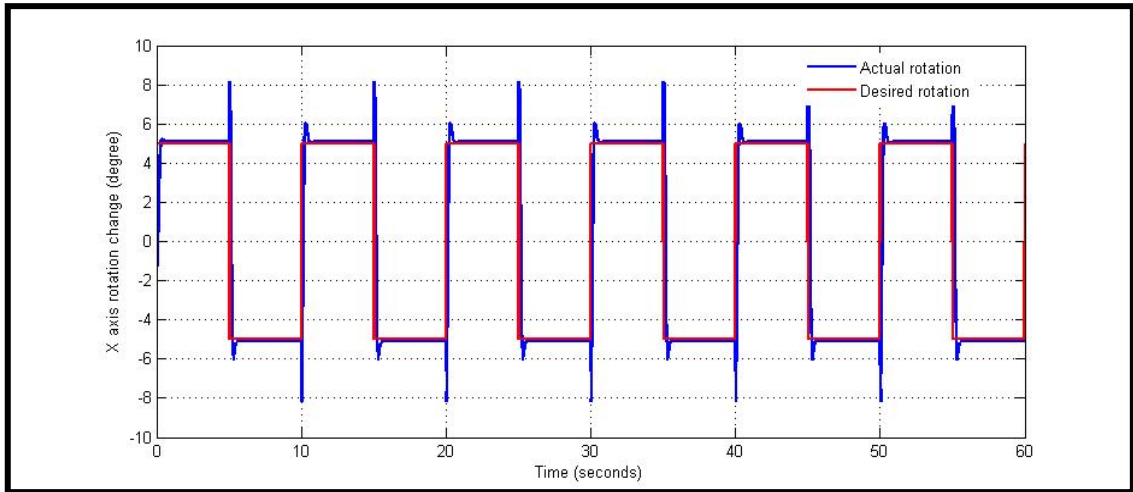


Figure 5.47. Tracking control of the 2-DoF seesaw at x-axis

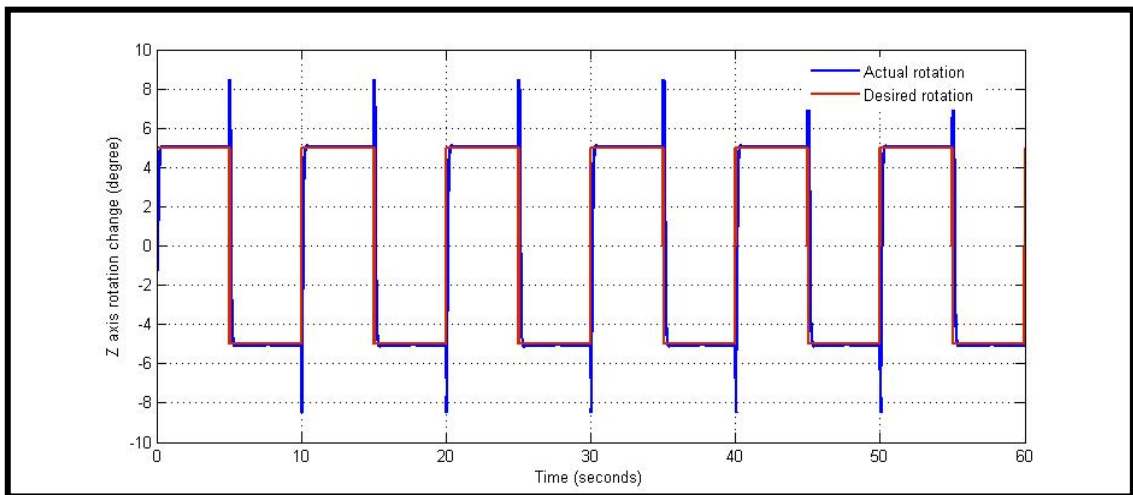


Figure 5.48. Tracking control of the 2-DoF seesaw at z-axis

System is tested when the two DoF are active for its steering performance under step inputs. Performance of the control on both joint showed satisfactory results for tracking the set points. Set-point tracking in z-axis rotation was more successful than x-axis rotation performance which had a slight overshoot. Reason could be that center of gravity location with respect to the z-axis rotation center is closer and that makes the system response in that axis better in terms of overshoot performance.

5.2.2.2.3. Stabilizing the System under Disturbance

Another test for the two DoF seesaw system is stabilization under disturbance. For the single DoF system, LQR controller was modified with the addition of the

Kalman filter and the system was able to keep its balance under the effect of disturbance. Therefore, same controller is applied to the 2-DoF seesaw system.

Dimension of the designed system is a square and distance from the center is 0.2 m. Total mass moving along x-axis direction is 1 kg, and the total mass moving along z-axis direction is 0.8 kg. Therefore, maximum torque amount that can be compensated by the system is found to be 1.6 N-m. The disturbance amount for both axes is chosen as 1 N-m magnitude sine waves and the frequency of the wave is set to 0.1 Hz.

Q_n and R_n parameters are selected as shown in Equation 5.65 and 5.66 for the both controllers after a number of trails.

$$Q_n = 2 \quad (5.65)$$

$$R_n = \begin{bmatrix} 0.5 & 0 \\ 0 & 0.01 \end{bmatrix} \quad (5.66)$$

With the chosen parameters, L gain matrix which controls the x-axis rotation, L_x , is found as shown in equation 5.67 and L gain matrix which controls the z-axis rotation, L_z , is found as shown in equation 5.68.

$$L_x = \begin{bmatrix} 0.1147 & 5.0783 \\ 0.2215 & 10.5224 \\ 0.0846 & 16.0660 \\ 1.1942 & 129.2733 \end{bmatrix} \quad (5.67)$$

$$L_z = \begin{bmatrix} 0.0767 & 5.1753 \\ 0.2261 & 15.1209 \\ 0.0863 & 18.3755 \\ 1.3396 & 169.0525 \end{bmatrix} \quad (5.68)$$

The system responses on both axes under the effect of disturbances are shown in Figures 5.49 to 5.52.

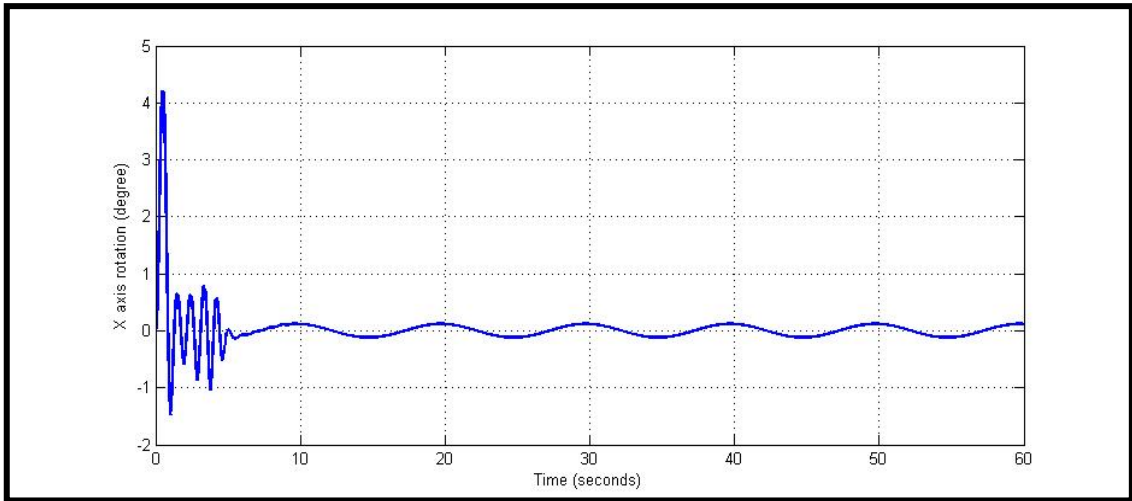


Figure 5.49. x-axis rotation angle change under disturbance

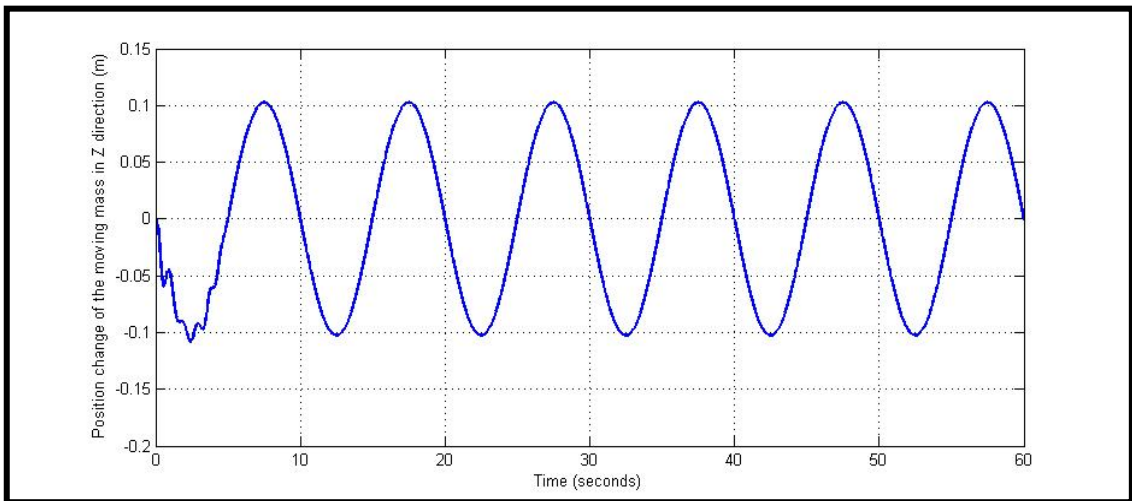


Figure 5.50. Moving mass position change at Z direction under disturbance

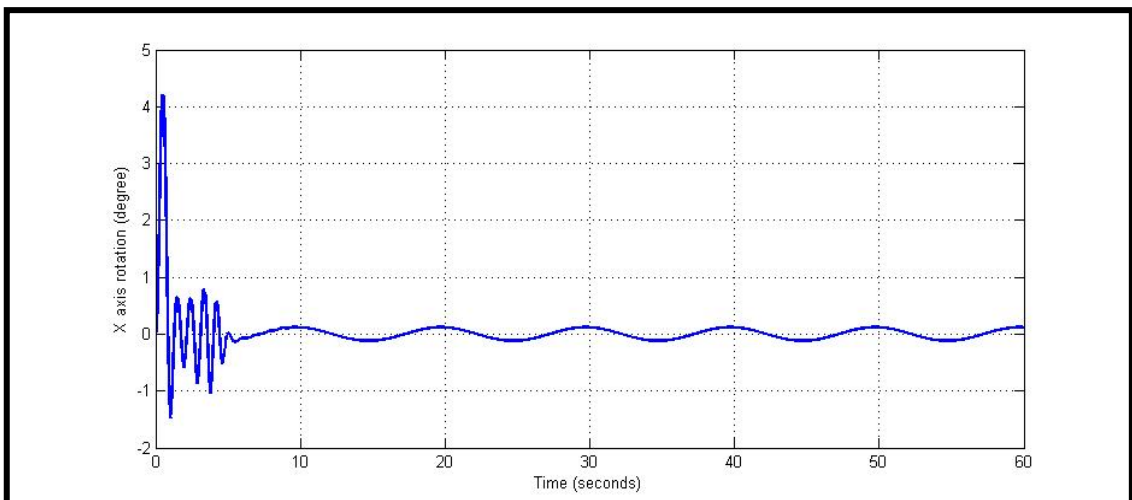


Figure 5.51. z-axis rotation angle change under disturbance

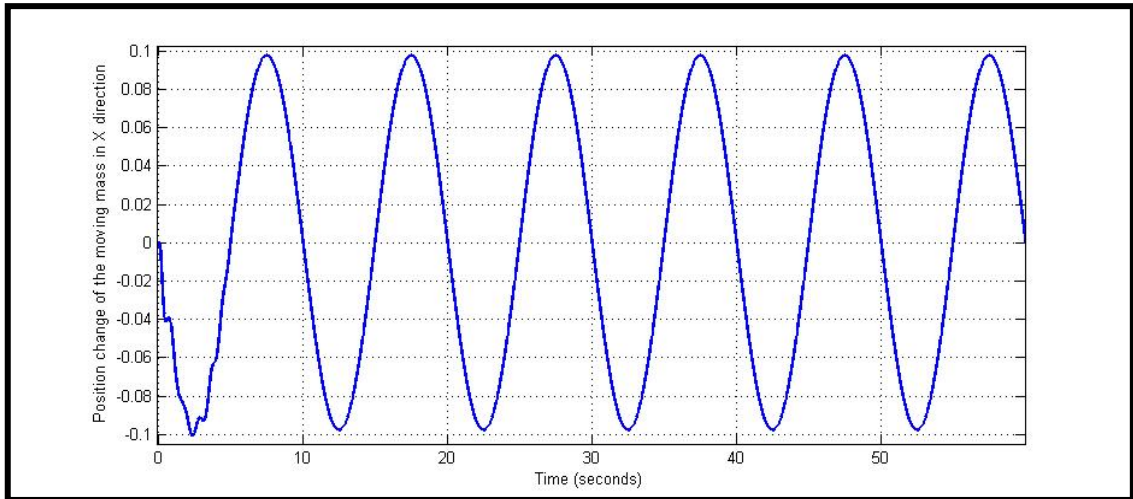


Figure 5.52. Moving mass position change at X direction under disturbance

As it can be observed from Figures 5.49 and 5.51, disturbance is successfully absorbed after 5 seconds. Figure 5.50 and 5.52 shows the position change of the moving masses under disturbance. Figures indicate that the system is able to adapt itself to environmental conditions and keep its balance after transition period. The designed controller proved its robustness under the presence of disturbance for 2-DoF seesaw mechanism.

5.2.2.2.4. Set-Point Tracking Test of the System under Disturbance

In this test, desired rotation angle to the system is sent via a signal generator and demands are square waves with 3 degrees magnitude at a frequency of 0.01 Hz for both axes. Amount of the disturbance applied to the system is in the form of a sine wave with a magnitude of 0.5 N-m at a frequency of 0.1 Hz. The controller used is LQR with the Kalman gain and set-point tracking is achieved through manipulating the sensory data for the seesaw rotation and cart positions as explained earlier. Response of the system is shown in Figures 5.53 and 5.54.

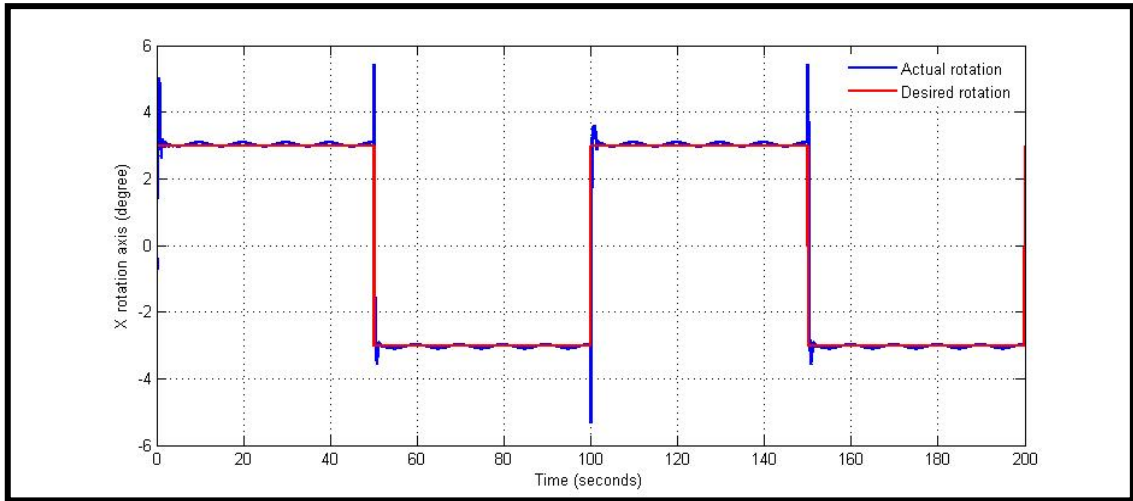


Figure 5.53. Set point tracking of the system around X axis

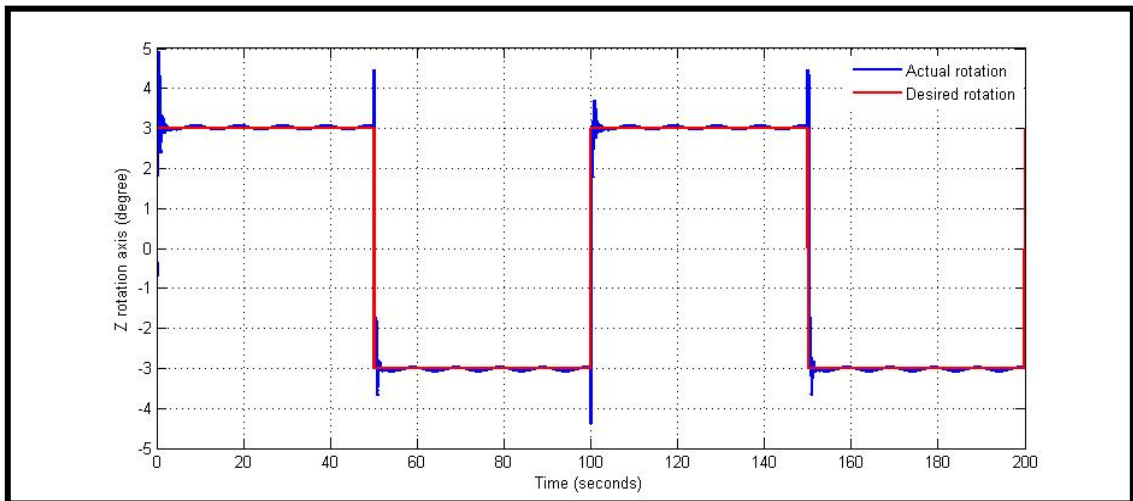


Figure 5.54. Set point tracking of the system around Z axis

As observed from the figures, the system is able to track the demand under the effect of disturbances in both DoF. Controller is able to absorb the disturbance in 5 seconds. Then, system oscillates within the ± 0.05 degrees band.

5.3. Experimental Results

The cart on the seesaw experimental system is driven by a DC motor. The equation of motion is equivalent to force (N) in Equation 5.9. The force applied to the cart is related to the voltage supplied to the DC motor as seen in Equation 5.69.

$$F = \frac{K_m K_g}{Rr} V - \frac{K_m^2 K_g^2}{Rr^2} \dot{p} \quad (5.69)$$

In this equation;

- K_m is the motor torque constant
- K_g is the gear box ratio
- R is the armature resistance
- r is the radius of the motor pinion.

F equability in Equation 5.9 is placed in the Equation 5.69 and Equation 5.70 is derived.

$$M_c \ddot{p} + M_c h \ddot{\theta} + \frac{K_m^2 K_g^2}{Rr^2} \dot{p} - M_c g \sin \theta - M_c p \dot{\theta}^2 = \frac{K_m K_g}{Rr} V \quad (5.70)$$

Then, the equations are again converted to the matrix form (state space form). After linearizing the system at its equilibrium point the linearized state-space representation of the system is found as shown in Equation 5.71.

$$\dot{x} = \begin{bmatrix} 0 & 1 & 0 \\ \left(\frac{-g h M_c r^2 R J}{r^2 R J^2} \right) & \left(\frac{K_g^2 K_m^2 J + K_g^2 K_m^2 M_c h^2}{M_s r R J} \right) & \left(\frac{g j - g c h M_s}{J} \right) \\ 0 & 0 & 0 \\ g & \frac{-h K_g^2 K_m^2}{r^2 R J} & \frac{M_s g c}{J} \end{bmatrix} \begin{bmatrix} p \\ \dot{p} \\ \theta \\ \dot{\theta} \end{bmatrix} + \begin{bmatrix} 0 \\ \frac{K_m K_g J + K_m K_g h^2 M_c}{J M_c r R} \\ 0 \\ \frac{-h K_g K_m}{J r R} \end{bmatrix} \cdot u \quad (5.71)$$

Customary LQR controller is used to stabilize the system with the initial error at its equilibrium point. Parameters in the Q matrix to calculate for the feedback gain, K , which are x and y values in the equation 5.40, are chosen as 1000 and 5000. As a result, constant K gain is found as

$$K = [746.0548 \quad 191.4199 \quad 996.8504 \quad 312.7352]. \quad (5.72)$$

After K constant gain is found, state vector of the system is created as seen in Figure 5.56.

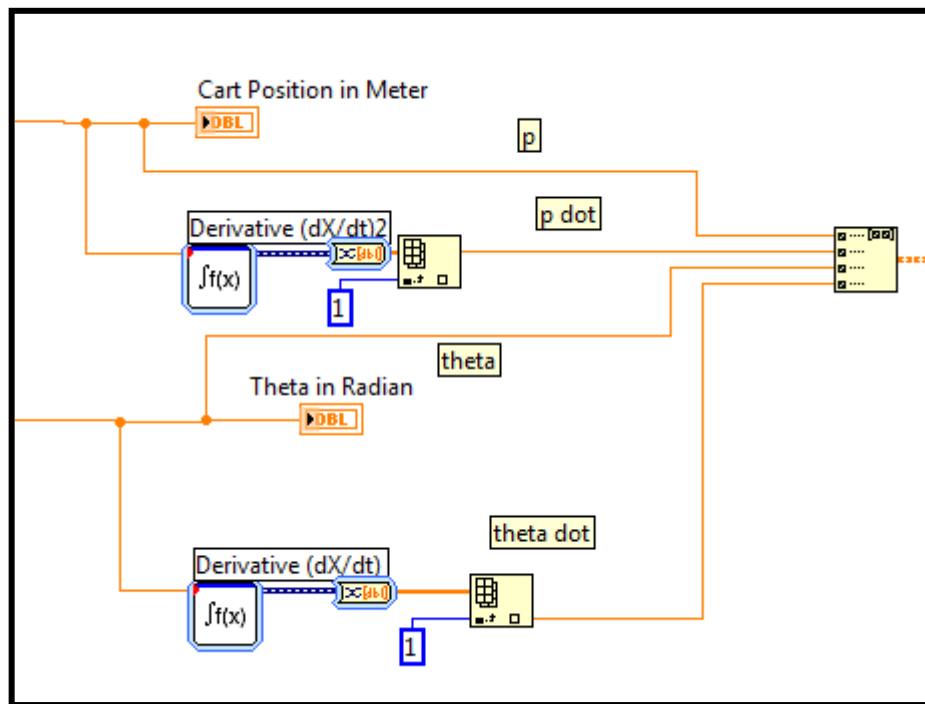


Figure 5.55. Creating the state vector of the system

State vector is multiplied with the constant K gain matrix. Then, output voltage is converted into the duty cycle percentage proportionally to produce control signals to drive the cart motor.

Experimental trial is initiated with 9 degrees of error. Response of the system is shown in Figure 5.56 and 5.57.

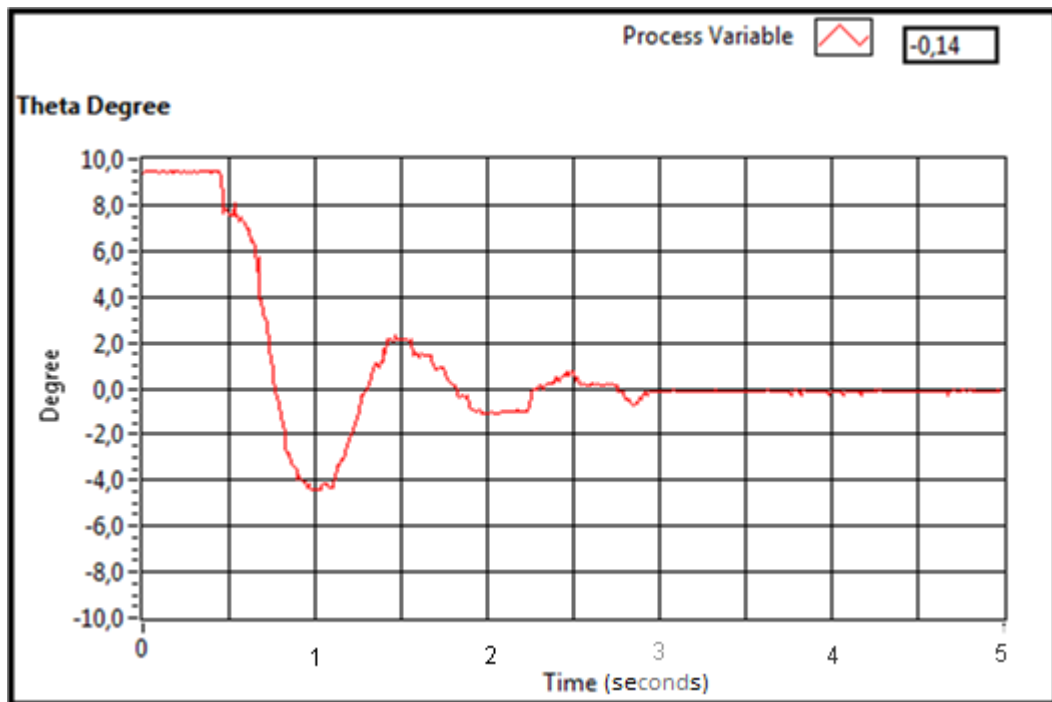


Figure 5.56. Rotation change of the system

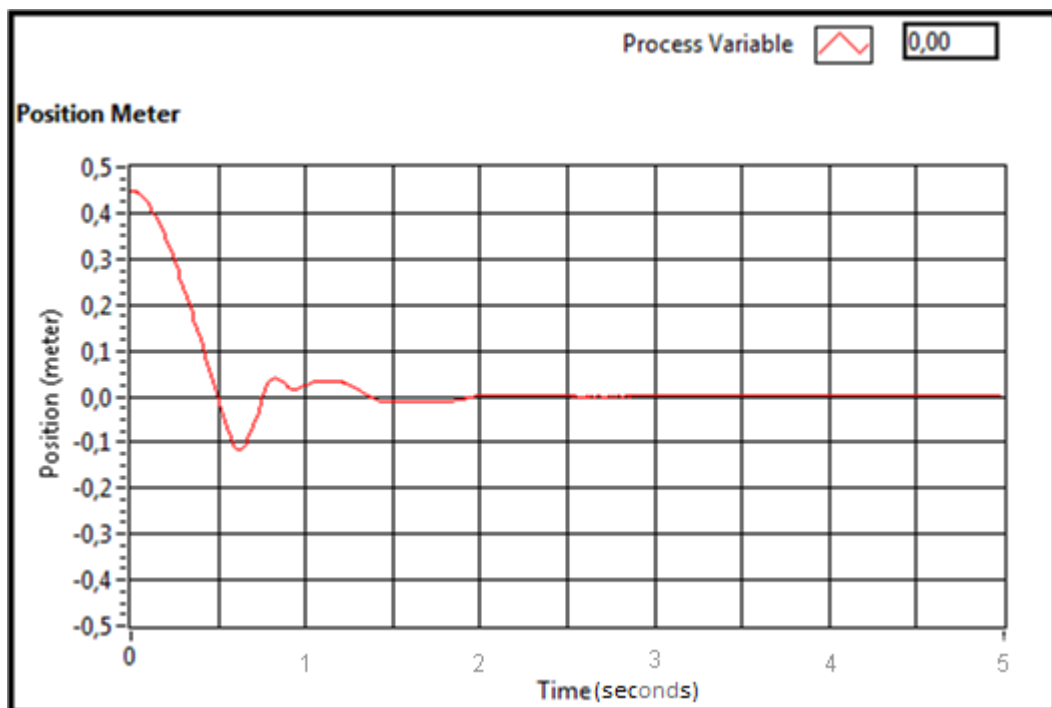


Figure 5.57. Cart position change of the system

Figure 5.56 shows the rotation angle change of the seesaw system. In three seconds, system reaches the equilibrium point. The seesaw does not move in the first half a second, because during that time, system has reached the mechanical limit and cannot tilt over anymore. Therefore, the excessive amount of tilt, which is observed in

simulation tests before the cart reaches the first equilibrium point, is not observed in experimental tests. As it can be seen in Figure 5.57, during the first half of a second, cart moves to the other side of the seesaw system to tilt the seesaw system on the other direction. In almost half of a second, the cart reaches the mid-point of the seesaw. After that point, seesaw starts to bend over to the other side and after two swings, system gets to the equilibrium point and keeps its balance at the equilibrium point.

5.4. Conclusion

In this chapter, equation of motion of the system is found by using the energy-based Lagrangian method. Equation of motion is used for designing controllers. First controller examined uses non-linearity cancellation to linearize the system. Thus, non-linear terms are found and these terms are added to the control input of the cart actuator. The linearized system is then controlled with a PD control to stabilize the system at its equilibrium point. Controller is tested to balance an initially unstable system. Even though a number of PD parameters tried, system was not able to reach the equilibrium. Since, in this controller only rotation angle is controlled, acceleration amount of the cart reaches extreme values. Therefore, a new controller is designed that controls both rotation angle of the seesaw and position of the cart.

Second control method is a state feedback controller (LQR). In this controller, state space of the system is formulated and the system equations are linearized around the equilibrium point. Then, by using the MATLAB[®] LQR command, K constant gain is found after a various trials of for better system response. System successfully reaches the equilibrium point. Second test for the control is for set-point tracking, which will be used for steering the vehicle. In order to create set-point demand, sensory data information is manipulated and the equilibrium point is shifted in both rotation angle of seesaw and position of the cart. Demand is created by sending square waves and system response is observed. System is able to reach desired angle in one second and keep its balance. Next, system is tested for stability under the disturbance. In these tests, disturbance set as sine waves to imitate underwater currents. During the tests, it is seen that the customary LQR controller was not able to absorb the disturbance. Therefore, LQR controller is modified with the addition of Kalman filter. After tuning the parameters, LQR with Kalman filter was able to absorb the disturbance. Tests are

extended to 2-DoF seesaw system. Since, the designed system is de-coupled, proposed controller can directly be applied to the system. Ultimately, 2-DoF system performance is examined for set-point tracking under the influence of disturbances. The LQR controller modified with the Kalman filter produced satisfactory results for the final simulation tests.

In the last part of the chapter, seesaw experimental system is tested. In this part, equation of motion of the system is changed to include the dynamics of the DC motor in the cart. Equation of motion of the system is re-calculated and linearized around the equilibrium point. LQR feedback gain, K , is optimized after a number trials for better response in terms of transition time and overshoot. System was able to be stabilize at the equilibrium point in three seconds with the selected feedback gain.

CHAPTER 6

CONCLUSIONS

6.1. Conclusions

The aim of the thesis is to design a novel energy-efficient and fault-tolerant underwater vehicle than can hover in shallow water. For that purpose, literature is reviewed and earlier works are analyzed. Internal moving masses are selected to be used for stabilization in hovering-mode operation and steering of the vehicle after the review of the literature. It was possible to reduce number of thrusters on the vehicle by the use of internal masses.

It is proposed to use changing mass method to be able to hover at a certain depth without the need of vertical thrusters. The center of buoyancy location varies with the adjustments made in the mass of the vehicle to meet the buoyancy requirements at certain depths. Center of gravity of the vehicle is altered as the buoyancy center of the vehicle is at a fixed location with respect to the vehicle coordinate system (when the system is at a certain depth) for stabilization and steering of the vehicle.

Underwater currents are a source of disturbance in the hovering performance of the underwater vehicles. Internal moving masses are also suitable for the hovering-mode control of the vehicle to absorb these disturbances.

Usually, underwater vehicles are built to have positive buoyancy to surface itself in case of communication loss or control problem. However, the proposed vehicle has variable buoyancy and it might not surface in case of a failure. Therefore, a fault tolerant system is required. In all active sub-systems of the vehicle, which are thrusters, moving mass actuators, and vehicle mass changing mechanisms, redundancy is introduced to provide fault tolerance to the vehicle.

Proposed underwater vehicle uses internal moving mass mechanism for stability and steering of the vehicle instead of thrusters. Thus, energy consumption due to thruster usage is minimized. Another advantage of using internal moving mass mechanism is that it is placed in the dry-box of the vehicle. Therefore, they do not experience the corrosion or biological fouling since they are not exposed to sea water.

After setting the design criteria, a number of conceptual designs are developed. An x-y table for moving masses is selected as the final design after comparing the conceptual designs on the basis of controllability and robustness. The final design for the moving mass mechanism is based on a seesaw system, except, it has 2 DoF. Usually, in UUVs buoyancy center is placed above the mass center. The buoyancy center acts as the rotation center and thus this configuration makes the system inherently stable. However, in the simulation models and experimental system of this work the mass center is placed over the rotation center and the system becomes inherently unstable. The controllers used for stabilization and steering are tested at the most extreme conditions as a result of this configuration.

Trials for the system are started with single DoF seesaw system. The reason for initiating the tests with single DoF system is that the final design of the moving mass mechanism has 2 decoupled DoF which can be controlled independently.

Two controllers are studied for the moving mass system. The first control method includes non-linearity cancellation. In this method, PD controller is applied to the rotational position change of the system and non-linear terms of the system are added to the system input to linearize the system. This controller was not able to reach equilibrium, because, it only monitors the change in the orientation. Therefore, a second controller is proposed.

The second controller is a state feedback controller called LQR. State space vector of the system is created and it is linearized around the equilibrium point and constant feedback gain K is found. States are multiplied with the constant feedback gain and fed into the actuator of the system. LQR successfully stabilized the system with an initial error in seesaw rotation which makes the system initially unbalanced. Then, system is examined for set-point tracking to evaluate the steering mechanism of the performance of the system. Test results indicated that the system is able to reach the desired seesaw angular position with an acceptable transition performance and keep its balance at a chosen set point. Last test of the system is conducted when the system is exposed to external disturbances. The customary LQR controller was not able to absorb the disturbance. Therefore, Kalman filter is implemented in the controller. After several trials, Kalman filter gain is selected to provide acceptable transition and steady-state performance thus absorbed the disturbance effects. Developed controller is tested for the 2-DoF system after the controller is proven to be successful in single DoF system tests. In 2-DoF system, ultimately, the controller is examined for set-point tracking in

both DoF synchronously under the effect of external disturbances. The LQR controller modified with the Kalman filter produced satisfactory results for this last simulation tests as well.

After the developed controllers proved their success in various simulation environments, experimental studies are initiated for the single DoF experimental system. In this system, LabJack is used as DAQ system and for programming LabVIEW is utilized. The experimental system does not include any subsystem to create external disturbance that imitates the underwater currents. Therefore, the customary LQR controller is selected to be used for the experimental tests. Similar to simulation configuration, state vector of the system is created and it is multiplied with constant feedback gain matrix. The system was able to reach equilibrium point in three seconds after tuning the control parameters.

The control methods are developed for hovering-mode control of an underwater vehicle in this thesis. Center of gravity of the underwater vehicles is commonly located below the center of buoyancy. However, in this thesis, the center of gravity of the tested systems is located above the rotation center, which is the buoyancy center in underwater vehicles, in order to test the controller in extreme conditions. The developed controllers proved to be successful in these inherently unstable test systems. The vehicle built having the center of gravity below the center of buoyancy is an inherently stable system. Therefore, it can be concluded that this vehicle, having the controllers developed in this thesis, can be stabilized in conditions where it is initially unbalanced and exposed to underwater currents, and it can be steered with the use of moving mass mechanism.

6.2. Future Works

In the future, the controller can be experimentally tested for all the cases examined in simulation studies. The experimental set-up should be improved and modified in order to conduct these tests. Analog sensors on the system can be replaced with digital encoders for more accurate and noise-free measurements of the rotation angle of the seesaw and the position of the cart. The translation motion mechanism of the cart can be replaced with a ball screw system for precise and smooth motion.

The mass changing mechanism to adjust the buoyancy of the vehicle can be included in the simulation studies for heave motion. It is expected that will produce

instability in the system that should be compensated by the moving mass mechanism. Studies can be conducted to address this issue. Also, the control of the heave motion with the help of the changing mass mechanism can be studied in the future.

Ultimately, an underwater vehicle that includes the moving mass and changing mass mechanisms can be designed and produced. The controllers developed in this thesis then can be tested for the operation of this developed UUV.

REFERENCES

- Alessandri, A., Caccia, M., Indiveri, G., and Veruggio, G. 2002. Application of LS and EKF techniques to the identification of underwater vehicles. *Control Applications*, 1998. Proceedings of the 1998 IEEE International Conference on Vol. 2, p. 1084–1088.
- Alvarez, a, Caffaz, A., Caiti, A., Casalino, G., Gualdesi, L., Turetta, A., et al. 2009. Fòlaga: A low-cost autonomous underwater vehicle combining glider and AUV capabilities. *Ocean Engineering*, 36(1), 24-38.
- Antonelli, G., Chiaverini, S., Sarkar, N., and West, M. 2001. Adaptive control of an autonomous underwater vehicle: experimental results on ODIN. *IEEE Transactions on Control Systems Technology*, 9(5), 756-765.
- Arstech, Radar Sonar Teknolojileri Ltd. Şti, Inc Official WEB site. <http://arstech.de/> (accessed Jan, 2011)
- Aytar, E. B. and Dede, M. İ. C. 2009. A Survey on Uninhabited Underwater Vehicles (UUV). *ASME Early Career Technical Journal*, Volume 8, Number 1, 35.1-35.8.
- Barnett, D., McClaran, S., Nelson, E., McDermott, M., and Williams, G. 2002. Architecture of the Texas A&M autonomous underwater vehicle controller. *Autonomous Underwater Vehicle Technology, 1996. AUV'96.*, Proceedings of the 1996 Symposium on p. 231–237.
- Bender, A., Steinberg, D. M., Friedman, A. L., and Williams, S. B. 2008. Analysis of an autonomous underwater glider. *Proceedings of the Australasian Conference on Robotics and Automation*.
- Bhatta, P., and Leonard, N.E. 2002. Stabilization and coordination of underwater gliders. *Proceedings of the 41st IEEE Conference on Decision and Control, 2002.*, 2081-2086.
- De Angelis, C. M., and Whitney, J. 2000. Adaptive calibration of an autonomous underwater vehicle navigation system. *OCEANS 2000 MTS/IEEE Conference and Exhibition Vol. 2*, p. 1273–1275.
- Dede, M. İ. C. 2010. Virtual Prototyping of Robot Controllers. *International Journal of Design Engineering*, Volume 3, Number 3, 276 - 288.
- Detweiler, C., Sosnowski, S., Vasilescu, I., and Rus, D. 2009. Saving energy with buoyancy and balance control for underwater robots with dynamic payloads. *Experimental Robotics: The Eleventh International Symposium* (p. 429).
- Eriksen, C. C., Osse, T. J., Light, R. D., Wen, T., Lehman, T. W., Sabin, P. L., et al. 2001. Seaglider: a long-range autonomous underwater vehicle for oceanographic research. *IEEE Journal of Oceanic Engineering*, 26(4), 424-436.

- Goheen, K. R., and Jefferys, E. R. 1990. Multivariable self-tuning autopilots for autonomous and remotely operated underwater vehicles. *IEEE Journal of Oceanic Engineering*, 15(3), 144-151.
- Grenon, G., An, P. E., Smith, S. M., and Healey, A. J. 2001. Enhancement of the inertial navigation system for the Morpheus autonomous underwater vehicles. *IEEE Journal of Oceanic Engineering*, 26(4), 548-560.
- Grever, J. G., Bachmayer, R., Leonard, N. E. 2003. Underwater Glider Model Parameter Identification. Proc. 13th Int. Symp. on Unmanned Untethered Submersible Technology, xx-xx.
- LabJack, Labjack Company, Inc Official WEB site. www.labjack.com (accessed April, 2011)
- Laine, J. L., Nichols, S. A., Novick, D. K., O'Malley, P. D., Copeland, D., and Nechyba, M. C. 1999. Subjugator: a highly maneuverable, intelligent underwater vehicle. *Electronics*, 1-9.
- Lee, C. S. G. 2003. Self-adaptive recurrent neuro-fuzzy control of an autonomous underwater vehicle. *IEEE Transactions on Robotics and Automation*, 19(2), 283-295.
- Leonard, N.E., and Graver, J. G. 2001. Model-based feedback control of autonomous underwater gliders. *IEEE Journal of Oceanic Engineering*, 26(4), 633-645.
- Li, J. W., Song, B. W., and Shao, C. 2008. Tracking control of autonomous underwater vehicles with internal moving mass. *Acta Automatica Sinica*, 34(10), 1319–1323.
- Linklater, A. 2005. Design and simulation of a towed underwater vehicle. MS Thesis, Virginia Polytechnic Institute and State University, Virginia
- Maki, T., Kondo, H., Ura, T., and Sakamaki, T. 2006. Navigation of an autonomous underwater vehicle for photo mosaicing of shallow vent areas. *OCEANS 2006-Asia Pacific*, 1–7.
- MathWorks, The MathWorks Company, Inc Official WEB site: <http://www.mathworks.com> (accessed June, 2011)
- McLain, T. W., and Rock, S. M. 1998. Development and Experimental Validation of an Underwater Manipulator Hydrodynamic Model. *The International Journal of Robotics Research*, 17(7),
- Nakamura, Y.; Savant, S. 1992. Nonlinear tracking control of autonomous underwater vehicles. *Robotics and Automation*, 1992., 3, 4-9.
- Novick, D. K., Pitzer, R., Wilkers, B., Crane, C. D., Iglesia, E. de la, and Doty, K. L. 1998. The development of a highly maneuverable underwater vehicle. *Robotics*, 98(April), 168–173.

- Oliveira, P., and Pascoal, A. 1998. Navigation systems design: an application of multi-rate filtering theory. OCEANS'98 Conference Proceedings Vol. 3, 1348–1353.
- Seaeeye, Saab Underwater Systems, Inc Official WEB site. <http://www.seaeeye.com> (accessed May, 2011)
- Sherman, J., Davis, R. E., Owens, W. B., and Valdes, J. 2001. The autonomous underwater glider “Spray.” IEEE Journal of Oceanic Engineering, 26(4), 437-446.
- Smallwood, D. A., and Whitcomb, L. L. 2003. Adaptive identification of dynamically positioned underwater robotic vehicles. Control Systems Technology, IEEE Transactions on, 11(4), 505–515.
- Special Information Animal, <http://planetanimalzone.blogspot.com/> (accessed April, 2011)
- Stommel, H. (1989). The slocum mission. Oceanography, 22-25.
- T. J. Tarn, and G. A. Shoults, 1996. A dynamic model of an underwater vehicle with a robotic manipulator using Kane. Autonomous Robots, 20(3), 269-283.
- Tangirala, S., and Dzielski, J. 2007. A variable buoyancy control system for a large AUV. Oceanic Engineering, IEEE Journal of, 32(4), 762–771.
- UNCW, University of North Carolina Wilmington WEB site. <http://www.uncw.edu/> (accessed Dec, 2010)
- Podder, T.K., and Sarkar, N. 2001. An experimental investigation into the fault-tolerant control of an autonomous underwater vehicle. Advanced Robotics, 15(5), 501-520.
- Webb, D. C., Simonetti, P. J., and Jones, C. P. 2001. SLOCUM: an underwater glider propelled by environmental energy. IEEE Journal of Oceanic Engineering, 26(4), 447-452.
- Woolsey and Leonard. 2002a. Stabilizing underwater vehicle motion using internal rotors. Automatica, 38(12), 2053-2062.
- Woolsey and Leonard. 2002b. Moving mass control for underwater vehicles. Proceedings of the 2002 American Control Conference, 2824-2829
- Yang, K. C., Yuh, J., and Choi, S. K. 1998. Experimental Study of Fault-Tolerant System Design for Underwater Robots. Robotics, 1051-1056.
- Yuh, J., Nie, J., and Lee, C. S. G. 1999. Experimental study on adaptive control of underwater robots. Robotics and Automation, 1999. Vol. 1, 393–398.
- Yuh, J. 1990. Modeling and control of underwater robotic vehicles. IEEE Transactions on Systems, Man, and Cybernetics, 20(6), 1475-1483.

Zhou, Z., Peng, Z., Cui, J. H., Shi, Z., and Bagtzoglou, A. 2010. Scalable localization with mobility prediction for underwater sensor networks. *IEEE Transactions on Mobile Computing*, 211-215.

APPENDIX A

EQUIPMENTS USED IN EXPERIMENTAL SET-UP

A.1. DAQ System

LabJack U3-HV model is used during the experiments (Figure A.1). Specifications of the DAQ system are;



Figure A.1 LabJack[®] U3HV
(source: labjack 2011)

- First 4 Flexible I/O are Changed to Dedicated HV Analog Inputs.
- 4 HV Inputs have ± 10 Volt or $-10/+20$ Volt Range.
- 12 LV Inputs (Flexible I/O) Still Available, for 16 Total Analog Inputs.
- Up to 2 Timers (Pulse Timing, PWM Output, Quadrature Input, ...)
- Up to 2 Counters (32-Bits Each)
- 2 Analog Outputs (10-Bit, 0-5 volts)
- Supports SPI, I2C, and Asynchronous Serial Protocols (Master Only)
- Supports Software or Hardware Timed Acquisition
- Maximum Input Stream Rate of 2.5-50 kHz (Depending on Resolution)
- Capable of Command/Response Times Less Than 1 Millisecond

- Built-In Screw Terminals for Some Signals
- OEM Version Available
- USB 2.0/1.1 Full Speed Interface
- Powered by USB Cable

A.2. Motor Driver

Maxon servoamplifier is used in this study. Model of the amplifier is 4-Q-DC Servoamplifier LSC 30/2 (Figure A.2). Specifications of the motor amplifier are;

- IxR compensation.
- Regulator operation.
- Encoder regulator.
- DC tacho regulator and current regulator with DIP switch.
- Operating voltage 12 – 30 VDC.
- Controlled operation for acceleration and braking in both directions.
- External set value or using internal potentiometer to set the speed.
- Maximum and continues output current 2 A



Figure A.2 Motor Driver